Smartglove : a multi-finger sensing system based on optical linear encoder

Li, Kang

2009

Li, K. (2009). Smartglove : a multi-finger sensing system based on optical linear encoder. Master’ s thesis, Nanyang Technological University, Singapore.

https://hdl.handle.net/10356/19317

https://doi.org/10.32657/10356/19317

NANYANG TECHNOLOGICAL UNIVERSITY

MASTER OF ENGINEERING

SMARTGLOVE – A MULTI-FINGER SENSING SYSTEM BASED ON OPTICAL LINEAR ENCODER

LI KANG

LI KANG

SCHOOL OF MECHANICAL AND AEROSPACE ENGINEERING

2009

2009

SMARTGLOVE – A MULTI-FINGER SENSING SYSTEM BASED ON OPTICAL LINEAR ENCODER

LI KANG

School of Mechanical and Aerospace Engineering

A thesis submitted to the Nanyang Technological University in partial fulfillment of the requirement for the degree of Master of Engineering

2009

ACKNOWLEDGEMENT

The author would like to express his heartfelt thanks and gratitude to the following people and organization for their efforts and support to the successful completion of the project.

Associate Professors Chen I-Ming and Yeo Song Huat for their ever encouraging support, guidance, patience and valuable advices. Their expertise in technical background of this research have immensely contributed to the completion of this thesis.

Mr. Nguyen Kim Doang, Mr. Luo Zhiqiang, Mr. Lim Kwang Yong, Mr. Dong Wei, Mr. Goh Young Koon, and Mr. Lim Wenbin, for their beneficial studies and research work on the optical liner encoder and programming. Their roles are important in guiding me in the fulfillment of this research project.

Staff of Robotics Research Centre: Mr Lim Eng Cheng, Technician-in-charge, for his coordination of the available resources. Ms Agnes Tan for her guidance, support and valuable advice. Mr You Kim San and Miss Toh Yen Mei for their valuable advices and assistance in the test process.

My parents and my girlfriend, for their unwavering support, encouragement, and understanding in all my works. They are always there for me.

Finally, to friends who have contributed in one way or another, thank you for your continuous support and endless encouragement during this time.

.

TABLE OF CONTENTS

Page

ABSTRACT

Objective measures of human hands as individuals participate in everyday activities are needed in order to expand the dexterous use of the hand or to evaluate the hand functions in rehabilitation or skill training. Data gloves for measurements of finger movements are a promising tool for this purpose. The requirements for the data glove include easy and comfortable to wear and remove, durability, cost-effectiveness and measurement repeatability and reliability. This thesis presents the design of a wearable glove-based multi-finger motion capture device (SmartGlove) with a specific focus on the development of a new optical linear encoder (OLE) with novel sensing technology. Modelling of the full hand kinematics and constraints are introduced, working principles of the OLE and the multi-point sensing method are illustrated. The OLE development and the SmartGlove construction are also presented. The OLE specially designed for this project has a compact size, light weight and low power consumption. The characterization tests also show that the OLE's digital output has good linearity and accuracy. The first prototype of SmartGlove which uses ten OLEs to capture the flexion/extension motion of the 14 finger joints is constructed based on the multi-point sensing method. A case study for the evaluation of SmartGlove using a standard protocol shows high repeatability and reliability in both the gripped and flat hand positions compared with another four evaluated data gloves using the same protocol. Conclusively, measuring outcomes in a portable manner can provide important information for the utilization and evaluation of the hand's motion data. Results demonstrated that SmartGlove is an important improvement in this direction as both a research and an evaluation tool for widespread use of hand motion capture.

Keywords:

Low cost, Wearable, Glove Based Hand Motion Capture, Hand Kinematic Model, Optical Linear Encoder, Calibration.

LIST OF FIGURES

LIST OF TABLES

LIST OF ABBREVIATIONS

Mocap	Motion Capture
DOF	Degree Of Freedom
ROM	Range Of Motion
DIP	Distal Interphalangeal
PIP	Proximal Interphalangeal
MCP	Metacarpophalangeal
TM	Trapeziometacarpal
HM	Humate-Metacarpal
CMC	Carpometacarpal
IP	Interphalangeal
FE	Flexion/Extension motion
AA	Abduction/Adduction motion
SD	Standard Deviation
ICC	Intraclass Correlation Coefficient
OLE	Optical Linear Encoder
SCLK	Serial Clock
MOSI	Master Output, Slave Input
MISO	Master Input, Slave Output
CS	Chip Select

CHAPTER 1. INTRODUCTION

1.1. Motivation

As the intricate and prehensile parts in the body, human hands are our primary physical interaction with the world. We use our hands in varies of aspects to perform our everyday activities, such as grasping, manipulating, drawing, writing and sculpting. Sometimes, we even use our hands as a communication tool in sign language or finger spelling.

With the rapid development of computer technology, we gradually tend to use computers to work, learn and entertain. However, we always found it unnatural when we work with a computer or use computer-based applications because we are constrained by clumsy input devices such as keyboards and mice. In order to be free from the limitations of the input devices, researchers have been studying and developing methods of getting computers able to “read” and “understand” user’s hand gestures or motions directly. The development of hand motion capture device has been a significant move in this direction that expands the natural use of our hands from physical world to the virtual world.

Motion capture or motion tracking technology started in the 1970s as a photogrammetric analysis method in biomechanics research. Later, with the matureness of the technology, it was expanded into other areas like rehabilitation, training and entertainment. Motion capture is the process of capturing the posture, location and motion information of a subject over a certain period of time. The subject can varies from a whole human body to a single finger joint based on different applications. From the motion capture it is able to obtain the posture and motion data of the subject. Other parameters of the motion (such as displacement, angle, velocity, acceleration) can be calculated from these captured raw motion data later. The captured and calculated data can be used in certain theoretical analyses of the human’s motion. Also, these data can be utilized in either virtual or physical environment to control or drive some objects.

For different applications, there are different requirements for the motion capture device and the captured motion data. In case the applications are animation, gesture recognition, rehabilitation and interactive games which do not require high accuracy in motion capture, the captured data should be stable and the device should be low-cost, comfortable to wear, and easy to use. In case the applications are motion analysis, biomechanics and biodynamics analysis, virtual training which have higher requirements for data in order to get accurate and precise results, the data should be high in both accuracy and resolution, and is better to have other sensors working together to get extra information such as forces or orientations. Also the device should be small and light so that the movements of the subject will not be affected. In case the applications are tele-operation, motion feedback control, besides the stability and accuracy, the data should also have high data rate in order to be real-time. The device should also contain force feedback to increase the intuition of use.

For the last few decades, several motion capture methods have been developed with different characteristics. [1]

1) Mechanical sensing

In the typical mechanical sensing, several rigid mechanical pieces and electromechanical transducers (potentiometers or shaft encoders) are placed on the object. When the object moves, the mechanical pieces change shape and the electromechanical transducers move accordingly. Using the previous knowledge about the rigid mechanical pieces and the measurements of the transducers, the object's position can be estimated with respect to the environment. Mechanical sensing approach can provide very precise posture estimation for a single object, but only over a relatively small range of motion due to the restriction of the mechanical structure. Mechanical motion capture systems are usually real-time, relatively low-cost and non-occlusion.

2) Inertial sensing

Inertial motion capture technology is an effective way for full-body motion capture which is based on the combination of inertial sensing unit, kinematical models and sensor fusion algorithms. The motion data of the inertial sensors is usually transmitted wirelessly to a computer. Specially designed software in the computer can save these

data and replay the motion in a 3D virtual environment. Inertial motion capture systems are capable of capturing the full six degree of freedom (DOF) in real-time without external cameras or markers. Inertial sensors are completely self-contained and have low latency and high rates. They are also not sensitive to the electromagnetic fields or ambient noise interferences. The weakness that prevents inertial trackers from being an ideal choice is drift.

3) Acoustic sensing

The working principle of acoustic sensing device is using high-frequency sound to triangulate a source within the work area. There cannot be hard obstacles or other acoustically reflective surface between the source and the surrounding microphones because the acoustic sensing systems can suffer from acoustic reflections. Acoustic sensing systems work well with large motions, but tend to have difficulties with fingers, faces, wrist rotations or small motions because of the system's resolution.

4) Magnetic sensing

Magnetic sensing systems measure the local magnetic field vector at the sensor. When a changing magnetic field passes through a coil, the system can measure the current induced in the electromagnetic coil. In a single inertial sensing unit there are three orthogonally oriented magnetic sensors. The 3D vector indication of the unit's orientation can be determined by the three sensors with respect to the excitation source. The magnetic sensing has the advantages of compact size, penetrable magnetic fields, and only a single source needed for multiple sensors. It also has the disadvantages of the distortion and strength reduction of the magnetic field.

5) Optical sensing

Optical sensing systems are usually comprised with two components: light source and optical sensors. The light sources can either be the active devices that emit internally generated light (LED) or the passive objects that reflect ambient light (marker). The optical sensors can detect the light from the source and determine the position and motion of the light source. The main disadvantage of optical systems is that there should not be other light source or reflective obstacles between the source and the sensor. However, the optical systems, especially the marker-based camera systems can produce the most realistic motions with enough markers on the object.

The five sensing technologies mentioned above are mainly focus on the whole body motion capture. However, when it comes to the hand motion capture, it is another different scenario. In the field of hand motion capture, there are several long standing problems and difficulties need to be addressed.

The primary difficulty is that the hand is relatively smaller but more articulated than the whole body. There are totally 27 bones and 23 DOFs (excluding the wrist) within one hand which offers dexterity for the hand to perform most of our everyday tasks. In order to cope with the multi-DOF structure, kinematic modeling becomes an important factor, especially the modeling of the palm. The way of modeling determines the placement of sensors, and eventually determines the naturalness and integrity of the whole hand motion capture.

Another problem is the method for hand motion capture. Because the hand's bones and joints are relatively smaller than other parts of the body (such as arm, leg and trunk), several body motion capture technologies may not be suitable for the hand. The sensor for hand motion capture should be small and light so that it can be placed on the palm and fingers easily. Meanwhile, it should not occlude the natural movement of the hand.

Given the importance and variety potential application areas of hand motion capture, as well as the existing problems and difficulties, the purpose of this research is to develop a low cost, high performance, glove-based, un-tethered wearable human hand motion capture device with novel sensing technology and ergonomics, as well as the processing system for real-time sensing and processing of the hand's anatomical motion data. The captured motion data can be further processed to be used in numerous areas such as rehabilitation, virtual input, interactive media and games, real-time tele-control and manipulation.

1.2. Objectives

In order to fulfill the requirements of multi-finger motion capture, several objectives need to be accomplished in the thesis project.

(1) Kinematic modeling of realistic human hand anatomy.

The kinematic model should be a realistic model of the hand, including the fingers and the palm. Anatomical studies on human hand show that the hand is a highly articulated part with 27 bones and up to 23 DOFs. Meanwhile, it is also highly constrained with constraints of the joint's motion range and coupling between joint motions. Based on the structure and constraints, mathematical formulations can be developed using a systematic method for representing constrained large DOF models of human hand. With the kinematic model, the layout of OLEs and the construction of a realistic 3D hand model can be obtained.

(2) Development of a new encoder with novel sensing technology suitable for hand motion capture.

Several sensing technologies used for human body motion capture are mentioned above. However, because of the small size of hand joints, some of the sensing technologies may not be able to implement in the hand motion capture. Consequently, a new encoder with novel sensing technology needs to be developed in this project. The encoder should meet the requirements of hand motion capture with small size, light weight, high resolution, high rate and low cost.

(3) Modeling the encoders on each finger based on the hand's kinematic model.

With the hand's kinematic model and the working principle of the encoder, it is possible to arrange the encoders on each finger to capture each joint's motion. The layout of encoders should be able to capture every joints' movements efficiently, and do not affect the natural movement of the hand at the same time. This model can be used to match the encoder's digital reading with the real joint's angle.

(4) Calibration methods and verification.

Calibration is critical to the hand motion capture system because different people have different hand biometric data. In order to get accurate motion data, calibration process is necessary before capture the hand motion on different subjects. Based on the tradeoff between the accuracy and time, two calibration protocols will be adopted (one is gesture-based protocol for rough calibration with less time; the

other one is tool-based protocol for accurate calibration with more time, a calibration tool will be designed to assist the accurate calibration).

(5) Experimental tests and analysis.

A set of experimental tests will be carried out based on the standard protocols to characterize the encoder and evaluate the performance of and the whole hand motion capture system. The results will be analyzed with comparison to those from other hand motion capture devices using the same test protocols.

1.3. Scope

The scope the research project will cover the following:

- Analyses of the human hand bio-mechatronics.
- Development of a new linear encoder using novel multi-point sensing method to detect the motions of finger joints.
- Modeling of the sensors on each finger and thumb on the human hand.
- System development, including hardware, software and application design.
- Calibration methods design.
- Experimental verification and validation of the characteristics of the encoders, as well as the performance of the SmartGlove.

1.4. Report Organization

This thesis presents the setup of the full hand kinematic model, the flow of the development of a multi-finger sensing device (both hardware and software), and also some experimental tests and results.

Chapter 2 is the literature review of existing hand motion capture devices and their applications. Because of the different requirements between the body motion capture and the hand motion capture, the sensing technologies are also different. In the literature review, three major sensing technologies for hand motion capture are introduced and illustrated with several commercialized hand motion capture devices. Also, some other experimental prototypes with different novel sensing technologies are also presented. In

the application part, five typical applications of the hand motion capture device are introduced. Some applications are applied in the physical world such as rehabilitation, training and tele-operation, and others are applied in the virtual world such as computer animation and interpreting sign language. All of the applications show the benefits that hand motion capture device brings.

Chapter 3 introduces the skeleton, constraints, and kinematic modeling of the human hand. Twenty three major DOFs are derived from the skeleton model, including five DOFs in the thumb, four DOFs for each of the four fingers and another two DOFs in the palm. An effective full hand kinematic model based on these twenty three DOFs is defined using Denavit-Hartenberg (D-H) transformation to illustrate the realistic motions of the hand. The proposed kinematic model is able to represent the transverse deformation of the palm arch, which brings a significant improvement of hand posture and motion representation with comparison to the normal kinematic models without palm arch. Based on the different structures, three different kinematic models are setup respectively for the thumb, the index and middle finger, and the ring and little finger, in which the joints and links are defined by D-H notation. Three kinds of constraints are also studied in this chapter which is able to reduce the 23 DOFs to 17 DOFs in order to reduce the number of OLEs used.

Chapter 4 describes the sensing principle of the OLE. Different from any of the sensing technologies introduced in the literature review, a new sensing principle using optical mouse sensor to measure a finger joint's flexion is illustrated. It is an improved OLE sensing method which is able to use multiple OLEs to capture the displacement of different points on the same strip. The advantage of multi-point sensing method is that it can be used in the situation where the bend angles of several joints in a line need to be captured (such as fingers or even the spine), and the number of joints is not limited as long as they are located in the same straight line.

Chapter 5 illustrates the development of the SmartGlove. Ten OLEs are used to capture the FE motion of ten joints based on the multi-sensing method. The OLE has a very compact design and use Velcro to achieve easily attachable to or de-attachable from the glove. Two OLEs are chained by a strip with rough surface to measure one finger's flexion/extension motion using the multi-sensing method and five such multi-OLE

chains are placed on the hand's five natural longitudinal arches. The OLEs communicate with the microcontroller (Arduino Diecimila) using Serial Peripheral Interface (SPI) protocol and the digital data from the ten OLEs are arranged in a certain defined format. In order to be intuitive, a software application is designed in the OpenGL environment where a 3D virtual hand is displayed and controlled by the SmartGlove directly. A Graphical User Interface (GUI) with basic control functions, as well as real-time data display and store, is also designed to provide easy-of-use for the users.

Chapter 6 focuses on the calibration methods of the SmartGlove. Two calibration methods are proposed based on this demand. For fast calibration, a protocol with four standard postures is able to calibrate all of the ten OLEs roughly. For precise calibration, a special calibration block is designed to calibrate each OLE one by one. The linear regression method is adopted to calibrate the OLE's reading to joint angle. The results of the calibration tests proved that both methods can improve the accuracy, especially the second method.

Chapter 7 presents the experimental tests and results. Three tests are carried out to characterize the OLE, including the linearity of the OLE's reading in both flat and bending conditions, and the accuracy of the OLE comparing to an accelerometer. Two tests based on the standard protocols are also conducted to evaluate the performance of the SmartGlove, including the repeatability, reliability. The evaluation is done by comparing the result of the SmartGlove with the results from the previous four studies using the same standard protocols.

Chapter 8 states the conclusion and recommendation for further improvement. Four major contributions of this project are concluded, including the full hand kinematic model, the development of a new OLE, the design of the novel multi-sensing method, and the tool-based effective calibration method. However, the works done so far are only the preliminary in this project, more efforts need to be done in several aspects in the future work in order to develop a full hand motion capture device.

Additionally, the dimensions of mechanical design, the specifications of sensors, and the layout of PCB boards are attracted as Appendix at the end of the report.

CHAPTER 2. LITERATURE REVIEW

Based on the different methods, hand motion capture systems fall into two categories: Outside-In method and Inside-In method. [2]

Outside-In method employs external sensors that sense sources or markers on the object (such as a video camera based system that tracks the markers on the body). Based on the different sources, Outside-In systems can be classified as the optical tracking system, the magnetic tracking system, and the acoustic tracking system.

Optical tracking, as the Vicon 6-camero passive motion capture system [3] in Figure 2-1, is to attach small markers on the hand. A series of six cameras are setup surrounding the hand and pick out the markers in their visual field. Software correlates the marker's position in the multiple viewpoints and uses the data from different cameras to calculate the 3D coordinate for each marker.

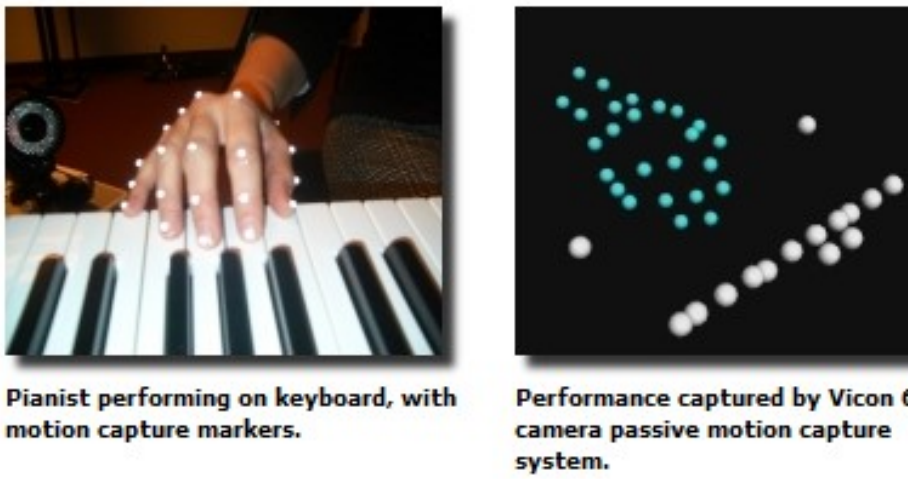

Pianist performing on keyboard, with motion capture markers.

Performance captured by Vicon camera passive motion capture system.

Figure 2-1 Optical Tracking [3]

Magnetic tracking method uses a source element radiating a magnetic field and a series of small sensors that report their positions and orientations with respect to the source. One example is the hand motion capture system using magnetic 3D position sensor to capture the hand movements when playing a piano, as shown in Figure 2-2. [4]

Figure 2-2 Hand Mocap System Using Magnetic Sensor [4]

Similarly, acoustic tracking method uses high-frequency sound to triangulate a source within the work area. Most systems, like the one used in the Mattel Power Glove (see Figure 2-3), send out high-frequency sound from the source (mounted on the hand, for instance) and received by a series of surrounding microphones. [5]

Figure 2-3 Power Glove [5]

These systems can provide 3D information about the hand and finger's gesture and motion, but they suffer from some general disadvantages:

- Because of the small and complex structure of the hand, the resolution is quite low.
- User's activities are limited within the preset work area.
- Fingers are difficult to track, as they occlude each other and are occluded by hand. It is also difficult to put enough markers on hand and fingers appropriately.
- The cost for a whole system is too high to be commonly used.
- The equipment setup, data collection and analysis demands users with high standards.

For these reasons, researchers have turned to the Inside-In method, which place both the sensors and the sources on the object for practical monitoring of the hand motion. The sensors are usually small and easy to wear. Also, it will not be restrained in the preset work area and relatively cheaper than the above mentioned Outside-In systems. Because the Inside-In method always attaches sensors and sources on gloves, systems based on this method are also known as glove-based hand mocap systems.

2.1. Glove-based Hand Mocap Technologies

Glove-based hand Mocap devices measure the shape of the hand as the fingers bend. Over the past few decades, many researchers have built hand movement and gesture measuring devices for computer input. Based on the sensing technology, these existing products can be mainly classified into four categories: fiber-optic sensing glove, strain gauge sensing glove, Hall-Effect sensing glove and other sensing glove.

2.1.1. Fiber-optic Sensing Technology

A light source (such as the LED) and a light detector are required for the fiber-optic sensing. The amount of bending angle is proportional to the attenuation of the detected light in specially treated sections of glass fiber that passes over the top of the knuckle. The advantage of fiber-optic sensing is that the number of the sensing component can be minimized because a bunch of specially designed optical fibers are able to tracking the whole finger's motion. However, complexity of the optical fiber's sectional design and glove construction, as well as the high price becomes its disadvantages.

There are several popular products based on fibre-optic sensing. For example, Fifth Dimension Technologies developed a 5-sensor and a 16-sensor version wireless data glove which transmits data to a nearby computer [6]. As shown in Figure 2-4, two joints per finger (PIP and MCP) are captured by fibre optical sensors. Optical fibers and wires are sewed into the glove which makes the glove looks not so bulky; however, it also adds difficulty to replace the sensor. Besides, the glove is not easy to wear because of the tightness.

Figure 2-4 5DT Data Glove [6]

Figure 2-5 Wrist, Finger and Thumb Motion Capture by ShapeHand [7]

Another popular product, Shape Hand, from Measurand (uses five flex optical fiber ribbons to capture whole hand motion (Figure 2-5). [7]

Different from the 5DT Data Glove's embedded design, the unique design of the easily attachable/de-attachable flexible sensor makes the Shape Hand very easy to use (Figure 2-6). One set of ribbon sensors can fit to gloves with different sizes for both hands. However, the cost is too high to be commonly used.

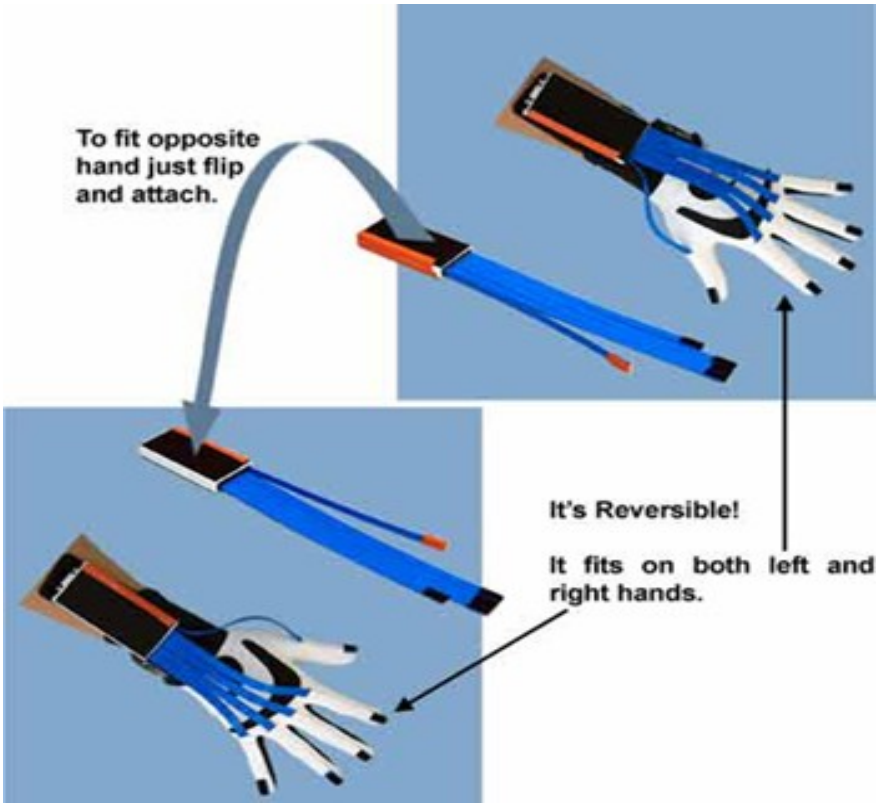

Figure 2-6 Measurand ShapeHand [7]

2.1.2. Strain Gauge Sensing Technology

Strain gauge is also known as resistive bend sensor. Because of its light weight and low cost, strain gauge becomes another choice for hand motion capture. Bend sensors are thin flexible foils that changes resistance when bent. The change of the bend angle is generally associated with the change of measured resistance of the strain gauge. Resistive bend sensor is popular for measuring small changes in shape which makes it suitable for accurate measurement of finger posture. However, it is easily to have a time-varying creep behavior when held in a fixed bend position which could reduce the accuracy of measurement. Also, it is very sensitive to the change of temperature.

Figure 2-7 CyberGlove II [8]

Figure 2-8 DG5 Vhand Data Glove [9]

One famous example using strain gauge sensing method is CyberGlove from Immersion Corporation (Figure 2-7) which contains 5 to 22 strain gauges to measure human finger movements [8]. This glove can interface with computer via Bluetooth. CyberGlove is one of the most successful glove products on market because of its good design as well as satisfactory performance. However, because the resistive sensor is extremely thin, it is also quite delicate and irreplaceable. What's more, the high cost will also be a disadvantage for more widely usage.

Similar to CyberGlove, the DG5 Vhand data glove from DGTech (Figure 2-8) uses five embedded bend sensors to measure the finger movements, with additional 3-axis accelerometer senses both the hand movement and the hand orientation (roll and pitch). The glove communicates with external devices via RS-232 and wireless [9].

Because of the combination use of bend sensors and accelerometers, the DG5 Vhand data glove can be used in different applications like robotics, motion capture, virtual reality, innovative games, rehabilitation, and also as an innovative aid for disabled

people. However, the resolution and accuracy is not satisfactory because it uses only five bend sensors to capture five fingers' motion.

2.1.3. Hall-Effect Sensing Technology

Hall-Effect sensors can be configured as proximity sensors to produce a linear output by detecting the magnetic fields. The output is proportional to the distance from a magnetic source. Several sensors are placed on the back of a glove in a predefined pattern. The finger joint angle can be computed from the changing field strengths measured by these sensors. Though the Hall-Effect sensors are small, the whole glove system can be bulky because an additional magnetic source is needed. Another disadvantage is the interference from other electromagnetic sources.

Figure 2-9 Humanglove [10]

The Humanglove™ (Humanware S.R.L., Pisa, Italy) is a flexible glove with 20 Hall-Effect sensors to measure finger joints' bend angles (Figure 2-9). [10] Hall Effect sensors can provide linear response and an excellent degree of reliability and robustness. However, as mentioned in the working principle of the Hall-Effect sensor, the additional external source and the electromagnetic interference will be the major disadvantages.

Table 2-1 is a comparison of the specifications of the above introduced five popular glove-based hand Mocap products:

Table 2-1 Products' Comparison Chart

Comparisons	*5DT Data Glove 14 Ultra*	*Measurand ShapeHand III*	*CyberGlove II 22 sensor model*	*DG Tech Vhand*	*Humanware Humanglove*
Price(US$)	9,000	11,000	10,000	5,000	7,000
Interface	USB	USB	USB	USB	USB
Number of sensors	14	5	22	6	22
Operating system	Cross platform SDK for Windows, Linux and UNIX operating systems	Windows	Windows	Windows	Windows
Sensor data rate(Hz)	75	n/a	90	25	100
Sensor resolution (°)	0.11	0.5	0.5	0.5	0.2
Type of sensor	Fibre optic	Fibre optic	Strain Gauge	Strain Gauge & Accelerometer	Hall Effect Sensor
Sensor removable	No	Yes	No	No	No
Wireless	Ethernet	Ethernet	Bluetooth	Bluetooth	Bluetooth
Operation range(m)	20	20	9	9	9
Software	Alias MOCAP, XSI, Motion Builder, Character Studio, etc	Alias MOCAP, XSI, Motion Builder, Character Studio, etc	Motion Builder, CATIA V5, VirtualHand SDK	3D Studio MAX, MAYA	n/a

2.1.4. Other Sensing Technologies

Beside the glove products above, there are also several research glove prototypes which are reported with no detailed experimental results.

Pressure sensing electronics are used to track finger flexion by measuring the pressure changes in airtight PVC tubes that are mounted along the fingers (as in Figure 2-10) [11]. Similar trial has been done by using the air tube and pressure sensor which are tiny, light, and easy to attach to glove [12], however, the resolution and accuracy is not satisfactory.

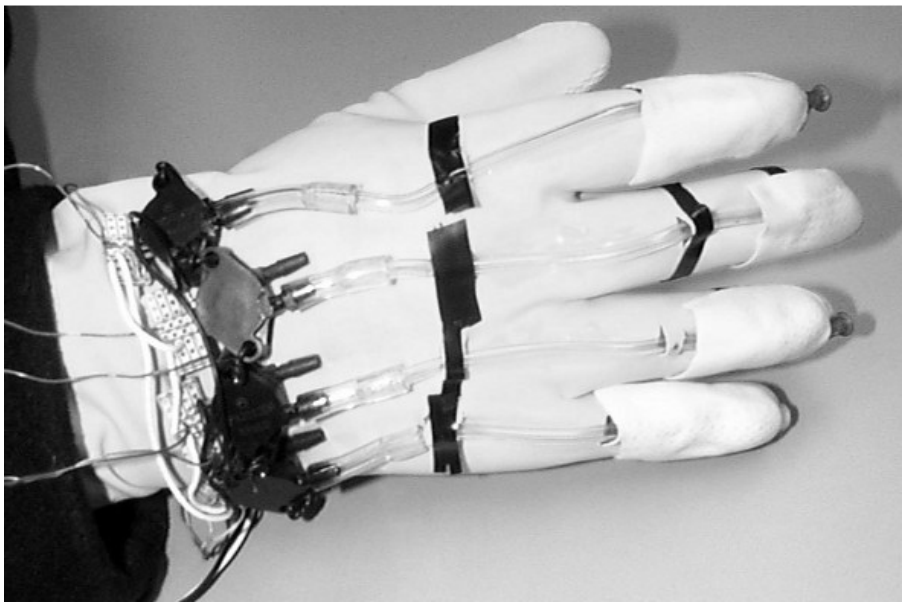

Figure 2-10 Air Tube Glove [11]

Another example adopts six dual-axis accelerometers to report their positions with respect to the gravitational vector [13]. As shown in Figure 2-11, accelerometers are placed on the back of the middle phalanges of the four fingers, on the back of the distal phalange of the thumb, and on the back of the palm. The aim of this research is to use the AcceleGlove as a virtual ASL keyboard because the performance, both accuracy and response, is not good enough for hand motion tracking. However, adopting accelerometers is a good idea for 3D-space hand position and gesture tracking.

Figure 2-11 AcceleGlove [13]

Figure 2-12 Textile Integrated Sensing Glove [14]

The Textile Integrated Sensing Glove is realized by directly printing Electrically Conductive Elastomer (CE) material on a Lycra/cotton fabric glove (Figure 2-12) [14]. The CE composites showed piezoresistive properties when a deformation is applied. This material represented the possibility of integration in textiles which could minimize the size of the glove, although disadvantages include extreme sensitivity to small changes in temperature, and a moderately slow response time.

Variable resistors sensors are also used to design and implement the DHM Glove [15]. Different from Strain Gauge Sensing, the DHM Glove had a mechanical exoskeleton structure which made it robust, but not easy to wear and remove (Figure 2-13).

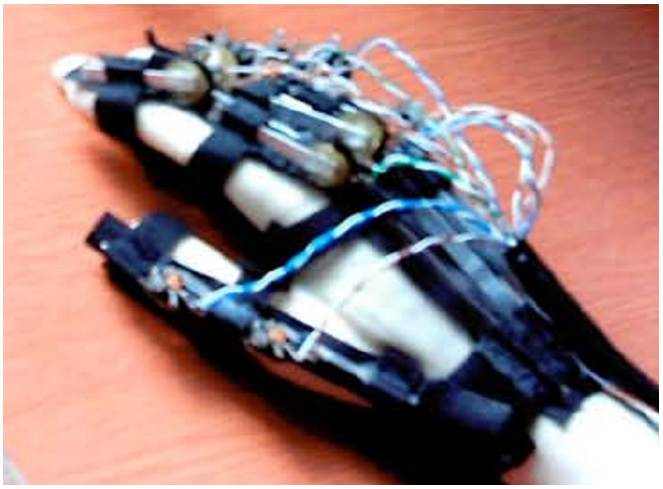

Figure 2-13 Textile Integrated Sensing Glove [15]

2.2. Applications

With the availability of commercialized glove-based hand mocap devices and various research prototypes described above, researches using the hand for computer input, as well as other relevant applications, have blossomed. These projects can be categorized into five different application areas as 1) natural interfaces, 2) systems for understanding signed languages, 3) tele-operation and robotic control, 4) rehabilitation, and 5) computer animation.

2.2.1. Natural Human Computer Interface

Since human interact with the physical world mostly and naturally by hands, there is a great desire to transfer the skills, dexterity, and intuition of the hand directly to the human-computer interface. [16] Many research projects have dealt with this subject and most of the work has been done in the area of virtual reality. In the following application, the hand Mocap glove is used as a master device for a 3D graphical hand in the virtual environment. The user could grab and move objects with the 3D virtual hand (Figure 2-14 [8]) in the virtual environment. Also, the users can use finger postures and motions to select from the on-screen menus. The advantage of this kind of interaction over the interaction with a 3D joystick is the intuition – user's actions correlate with those that might be performed on physical objects.

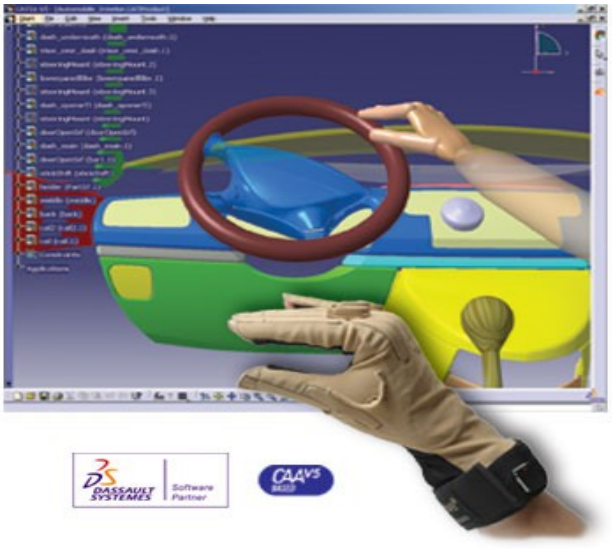

Figure 2-14 VirtualHand for V5 (CATIA) [8]

2.2.2. Interpreting Sign Language

Another interesting application of glove-based devices is the interpretation of sigh languages for human communication, as well as computer input and control. Many researchers have investigated different way of recognizing hand signs from simple finger spelling to analysis of the sign language. The basic concept of hand sign language is to analyze the hand-space-DOF vector for each posture or gesture and to match it with a landmark hand-space vector representing the target posture or gesture within error tolerances weighted by the significance of each degree of freedom. [17] One example called StrainGlove is shown in Figure 2-15. [18]

Figure 2-15 Interpreting Sign Language Using StrainGlove [18]

2.2.3. Tele-operation and Control

Glove-based devices used in tele-operation and robotic control are important for dexterous control of the remote end device. Researchers constructed algebraic transformation matrices to map the human hand poses to the robot hand poses. The kinematic differences between the human hand (as measured by the data glove) and the robot hand are compensated by the transformation matrices. The user can control the robot hand by mimicking the desired poses. Figure 2-16 is an example of using CyberGlove II as a master device to manipulate the slave robotic hand [19].

Figure 2-16 Robotic Hand Manipulation Using CyberGlove II [19]

2.2.4. Rehabilitation and Training

Virtual Reality technology showed its potential benefit as a therapeutic tool for rehabilitation in the past few decades. This technology provides the capability to create a virtual environment where the rehabilitation and training can be systematically monitored, manipulated and enhanced in order to create the most appropriate, individualized motor learning paradigm. Similar to the computer games, VR rehabilitation exercises can be designed to be intuitive and engaging which are important to the patient motivation. The systems can also be used to monitor, record and fully quantify the progress made by the patient, especially in terms of motor learning improvement. [16] The Poared Hand Exoskeleton, as shown in Figure 2-17, is a practical device for hand rehabilitation purpose [20]. The actuation is performed

by motors which transmit forces to the joints through cables. A real-time microcontroller calculates the appropriate control signals for the motor controllers based on the measured forces and joint angles. An interface computer allows the therapist to monitor the progress, change the control modes, define new exercises, and supervise the rehabilitation.

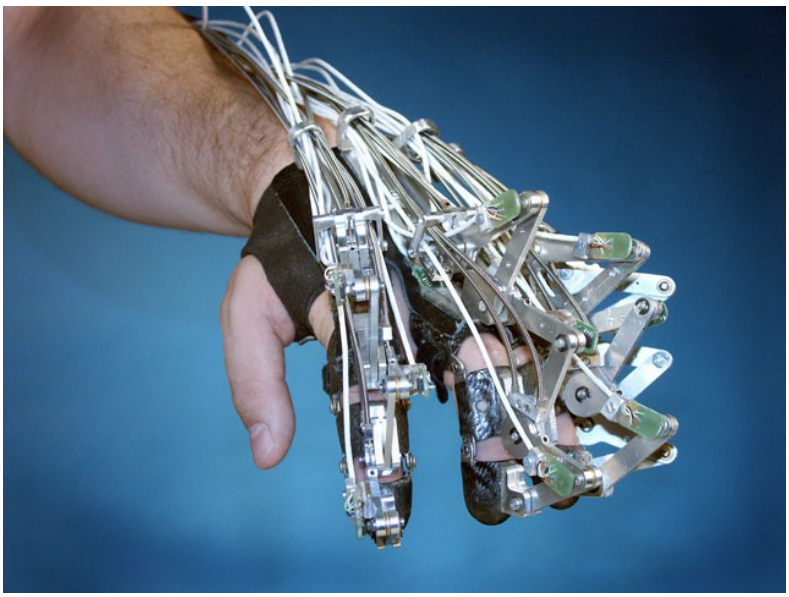

Figure 2-17 The Poared Hand Exoskeleton for Hand Rehabilitation [20]

2.2.5. Computer Animation

Two techniques are mostly used in computer animation. One is the key-frame technique which is similar to the conventional hand animation. The animation is produced by generating the frames between keys positions and postures and usually looks very unnatural. The other one Programmed animation yields motion that is occasionally life-like, but often too regular to be a product of life itself. To inject life into computer animation, and as a way to overcome the trade-off between animation time and motion quality, production companies have turned to body motion capture for computer animation of characters. Putting a performer in direct interactive control of a character, as in puppetry, or capturing body motion for later processing, translates the nuances of natural motion to computer characters, making them seem very much alive. [21] One interesting application that edits captured hand motion data by using the data glove is illustrated as follows: The animator first wears a glove and mimics the human body motion using his hand. Then, a mapping function that converts the

motion of the hand to that of the whole body will be generated (Figure 2-18). Finally, by moving the hand in a slightly different way, a new motion with different taste will be generated [22].

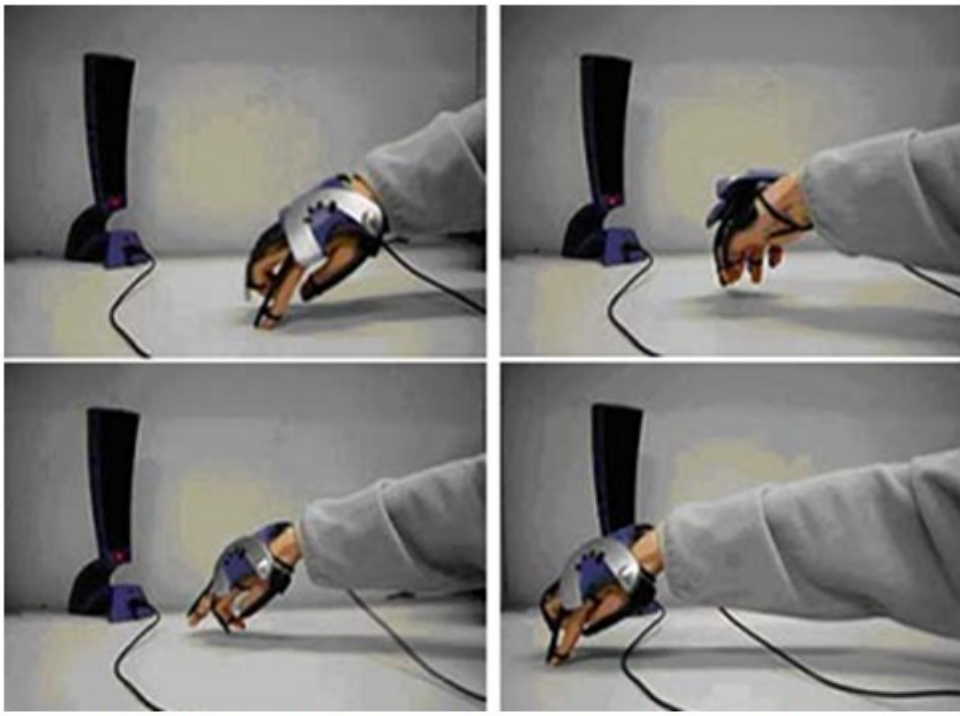

The hand gesture to generate the zigzag walking motion

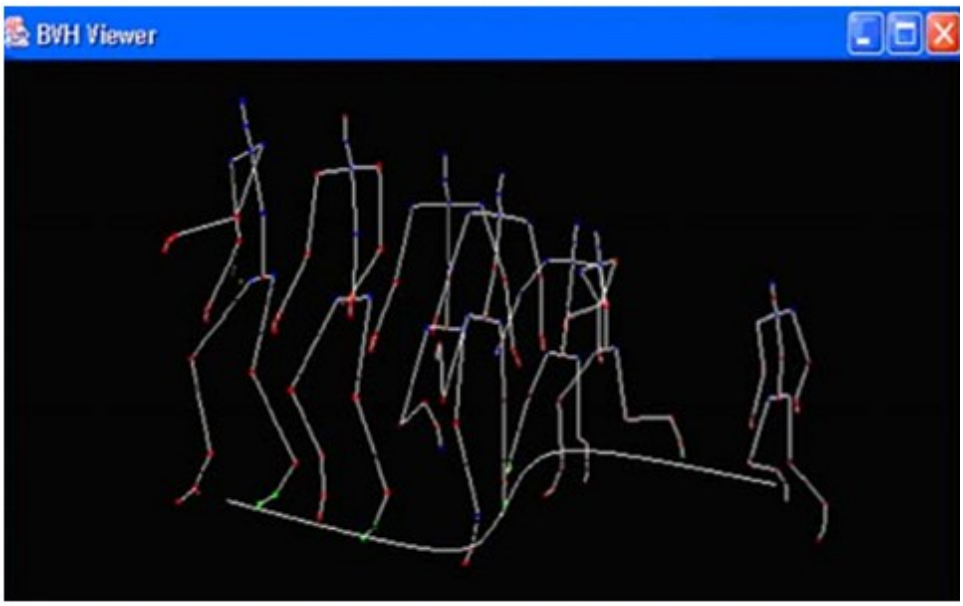

The zigzag walking motion generated by the system

Figure 2-18 Motion Editing with P5 Glove [22]

2.3. Discussion

From the literature review of various glove-based hand motion capture devices with different sensing technologies, it is obvious that the existing glove systems do have shortcomings. First, most glove systems are very expensive. From the survey of the commercialized products it can be found that the prices of such devices all cost over $1,000, which enormously limits the usage and its application. Second, custom sizing of different users is required to reduce tracking errors because measurement errors are decreased when gloves fit snugly according to [23]. Additionally, actions such as wrist movement in full fabric gloves may cause the glove to move over the skin. The friction between the glove and the skin may prevent the material from returning to the original position exactly, leaving the sensors located at different positions over the joints and causing measurement drift. Third, the environment proposed for the glove system to use is also very restrictive. Due to the disadvantage of the sensor, some glove systems cannot produce accurate result under certain circumstances. For example, electromagnetic interference can affect the Hall-Effect sensor; results from strain gauge sensing vary with the change of temperature. Lastly, in most glove systems, sensing units and wires are integrated in the glove and that they are always delicate. Consequently, it is difficult or even impossible to replace the sensor for maintenance.

CHAPTER 3. BIOMECHANICS OF HUMAN HAND

Before starting to capture hand motion, it is necessary to understand the biomechanics of the hand. In this chapter, the modeling of human hand's skeleton, constraints, and kinematics will be discussed.

3.1. Skeleton Model

Human hand is the most articulated part in the human body. As shown in the Figure 3-1, the hand consists of a palm (metacarpus), four fingers and one thumb. It is attached to the forearm by the wrist (carpus).

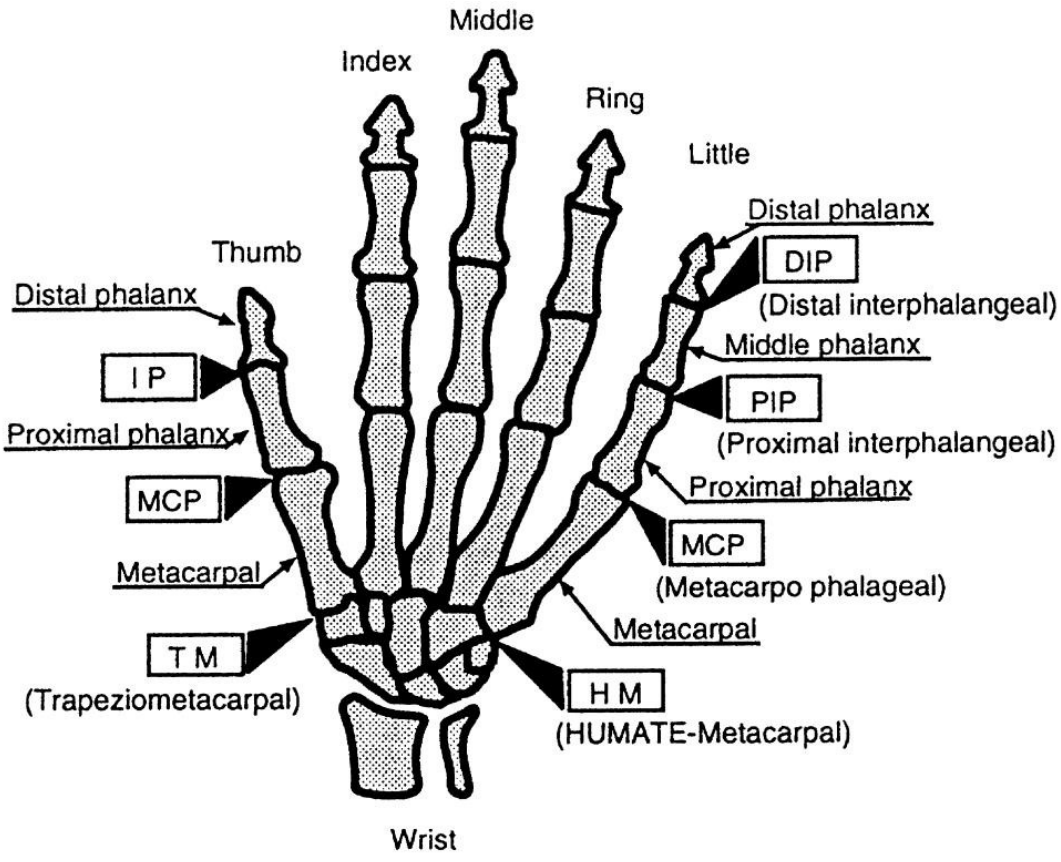

Figure 3-1 Diagram for the Human Hand Skeleton [24]

There are a total of 27 bones in a hand: the carpus (or wrist) includes eight bones which are arranged in two rows; the metacarpus (or palm) contains five bones; the remaining

14 are phalanx bones with three in each of the four fingers (index finger, middle finger, ring finger, and little finger) which are the distal phalanx, the intermediate (or middle) phalanx, and the proximal phalanx, and two in the thumb (no middle phalanx). [24]

Totally 23 internal degrees of freedoms (DOF) are located in the above hand skeleton model based on anatomical and medical analysis of the hand by previous studies and researches. [25][26]

Each of the four fingers has four DOFs. The Distal Interphalangeal (DIP) joint and the Proximal Interphalangeal (PIP) joint both have one DOF and the remaining two DOFs are located at the Metacarpophalangeal (MCP) joint as shown in Figure 3-1.

Different from the four fingers, the thumb has five DOFs. There are two DOFs at the Trapeziometacarpal (TM) joint (also referred as Carpometacarpal (CMC) joint), and two DOFs at the Metacarpophalangeal (MP) joint. The remaining one DOF of the thumb is located at the Interphalangeal (IP) joint as shown in Figure 3-1.

The basic flexion/extension and abduction/adduction motions of the thumb and fingers are performed by the articulation of the above mentioned 21 DOFs. The flexion and extension motions are used to describe rotations toward and away from the palm which occurred at every joint within the hand. The abduction motion is the movement of separation (e.g., spreading fingers apart) and the adduction motion is the movement of approximation (e.g., folding fingers together). The abduction/adduction motions only occur at each finger's MCP joint as well as thumb's MCP and TM joints.

Another two internal DOFs are located at the base of the 4^{th} and 5^{th} (ring and little finger's) metacarpals (as HM joint in Figure 3-1) which performs the curve or fold actions of the palm.

In addition to the 23 internal DOFs in the hand, the wrist also has another three DOFs which determine the overall orientation and rotation in space of the entire hand. [27]

3.2. Constraints of Human Hand Motion

As mentioned above, the human hand is highly articulated with up to 23 internal DOFs. Meanwhile, it is also a highly constrained body part with couplings among fingers and joints. By applying those constraints, the number of DOFs in the hand can be reduced from 23 to 17, making the human hand motion capture more cost-efficient. Besides, the application of the hand motion constraints is able to synthesize natural hand motion in order to produce realistic hand animation.

Although applying human hand motion constraints could greatly reduce the number of DOFs in a human hand, too many or too complicated constraints would also add to computational complexity. Hence, it becomes an important issue of determining the appropriate constraints to be implemented in the hand kinematics. In this project, three common constraints are applied: the constraints of joints within the same finger (Type I constraints), constraints of joints between different fingers (Type II constraints), and the maximum range of the joint motions (Type III constraints). The major reason to adopt these three types of constraints is that all these have been studied and used in many previous works [28,29]. Mathematically these constraints can be presented as either equalities or inequalities of joint angles.

1) Type I constraints [28]

This type of constraints refers to the couplings of joints within the same finger, also called interfinger constraints. A commonly used one based on the hand anatomy states that for the index, middle, ring and little fingers, in order to bend the DIP joints, the corresponding PIP joints must also be bent (as shown in Figure 3-2).

The relations can be approximately presented as follows:

$$\theta_{DIP} = \frac{2}{3}\theta_{PIP} \tag{3-1}$$

Where θ_{DIP} refers to the flexion angle of the DIP joint and θ_{PIP} refers to the flexion angle of the PIP joint (Figure 3-2).

By using this relationship, four DOFs are reduced in a human hand.

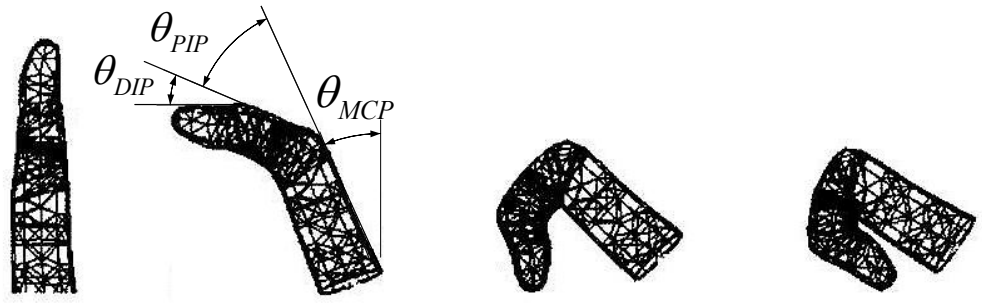

Figure 3-2 Finger Flexion after Constraint Application [28]

2) Type II constraints [28]

This type of constraints refers to the couplings of joints between different fingers, also called intrafinger constraints. For instance, when an index finger's MCP joint is bent, the middle finger's MCP joint is forced to bend as well. Lee and Kunii [28] have performed measurements on several different subjects and obtained a set of inequalities that approximates the couplings of adjacent finger's MCP joints:

$$\begin{cases} d_{\max}(\theta_{MCP}(I)) = \min(\theta_{MCP}(M)+25, S_{\max}(\theta_{MCP}(I))) \\ d_{\min}(\theta_{MCP}(I)) = \max(\theta_{MCP}(M)-54, S_{\min}(\theta_{MCP}(I))) \\ d_{\max}(\theta_{MCP}(M)) = \min(\theta_{MCP}(I)+54, \theta_{MCP}(R)+20, S_{\max}(\theta_{MCP}(M))) \\ d_{\min}(\theta_{MCP}(M)) = \max(\theta_{MCP}(I)-25, \theta_{MCP}(R)-45, S_{\min}(\theta_{MCP}(M))) \\ d_{\max}(\theta_{MCP}(R)) = \min(\theta_{MCP}(M)+45, \theta_{MCP}(L)+48, S_{\max}(\theta_{MCP}(R))) \\ d_{\min}(\theta_{MCP}(R)) = \max(\theta_{MCP}(M)-20, \theta_{MCP}(L)-44, S_{\min}(\theta_{MCP}(R))) \\ d_{\max}(\theta_{MCP}(L)) = \min(\theta_{MCP}(R)+45, S_{\max}(\theta_{MCP}(L))) \\ d_{\min}(\theta_{MCP}(L)) = \max(\theta_{MCP}(R)-48, S_{\min}(\theta_{MCP}(L))) \end{cases} \quad (3\text{-}2)$$

In the above inequalities, *I, M, R,* and *L* refer to the index finger, middle finger, ring finger, and little finger; $d_{\max}$ and $d_{\min}$ refer to the maximum and minimum dynamic angles of a specific joint's movement; and $S_{\max}$ and $S_{\min}$ refer to the maximum and minimum static angle of a specific joint [29].

3) Type III constraints [29]

This type of constraints refers to the couplings of the range of the joint's motion based on the hand anatomy. Here the only precondition is that the range of motion of each joint that can be achieved without applying external forces. Some common Type III constraints can be presented by the following inequalities:

$$\begin{cases} -15° \le \theta_{MCP\_AA} \le 15° \\ 0° \le \theta_{MCP\_FE} \le 90° \\ 0° \le \theta_{PIP} \le 110° \\ 0° \le \theta_{DIP} \le 90° \end{cases} \tag{3-3}$$

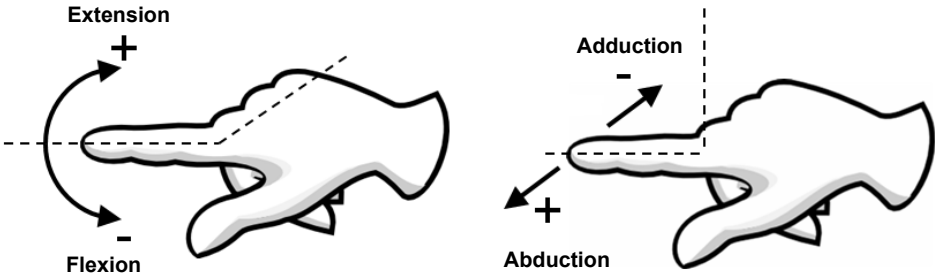

Figure 3-3 Denotation of FE & AA motion

where the subscript FE denotes the flexion/extension motion of the MCP joint and AA denotes abduction/adduction motion of the MCP joint (as illustrated in Figure 3-3). Another commonly adopted constraint states that the middle finger displays little abduction/adduction motion, as presented:

$$\theta_{MCP\_AA} = 0° \tag{3-4}$$

This will reduce one DOF from the 23-DOF model. Similarly, the TM joint also displays limited abduction motion and will be approximated by zero as well:

$$\theta_{TM\_AA} = 0° \tag{3-5}$$

This condition reduces another one DOF.

By applying the above three types of constraints, the 23-DOF model can be approximately reduced to a 17-DOF model. Previous researches have shown that the

natural hand postures can be approximately estimated using these constraints without severe degradation in performance [30]. Also, there are other constraints imposed by the naturalness of hand motions and which are difficult to detect or quantify. This type of constraints will not be considered in this project because it is not possible to be explicitly represented by equations or inequalities.

3.3. Kinematic Model

A kinematic model of the hand is formulated. As described in the skeleton model, four DOFs are used for each finger, and the thumb is modelled by five DOFs. Another two DOFs are for the palm motions. This hand kinematics can be illustrated by forward kinematics using Denavit-Hartenberg transformation (D-H) [31].

3.3.1. Coordinate System Setup

Suppose there are *n* joints in a model, the joints numbered from *1* to *n* starting with the base and ending with the end-effecter. A right-handed orthonormal coordinate system (X_0, Y_0, Z_0) is established at the supporting base with Z_0 axis lying along the axis of motion of the i^{th} joint. Align the Z_i with the axis of motion (rotary or sliding) of the $(i+1)^{th}$ joint. Locate the origin of the i^{th} joint's coordinate at the intersection of the Z_i and Z_{i-1} axes or at the intersection of the common normal between the Z_i and Z_{i-1} axes and the Z_i axis. Establish $X_i = \pm(Z_{i-1} \times Z_i) / \| Z_{i-1} \times Z_i \|$ or along the common normal between the Z_i and Z_{i-1} axes (when the Z_i and Z_{i-1} axes are parallel) and assign $Y_i = \pm(Z_i \times X_i) / \| Z_i \times X_i \|$ to complete the right-handed coordinate system as shown in Figure 3-4.

3.3.2. Link and Joint Parameters

The joint parameters illustrated in Figure 3-4 are defined as follows:

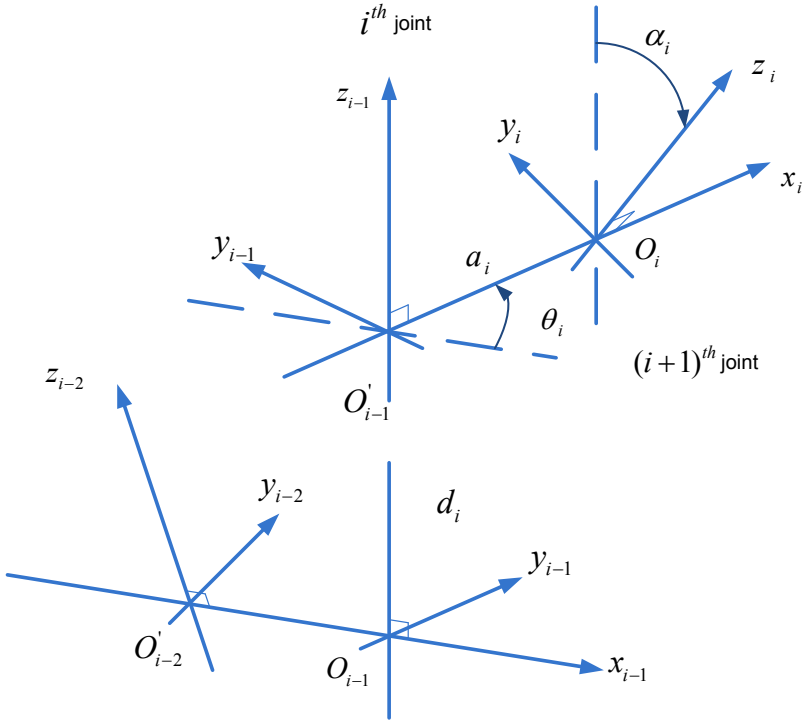

Figure 3-4 Coordinate System and Joint Parameters

- Joint angle θ_i: the angle of rotation from the X_{i-1}-axis to the X_i-axis about the Z_{i-1}-axis. It is the joint variable if the i^{th} joint is rotary.
- Joint distance d_i: the distance from the origin of the *(i-1)*th coordinate system to the intersection of the Z_{i-1}-axis and the X_i-axis along the Z_{i-1}-axis. It is the joint variable of the i^{th} joint is prismatic.
- Link length a_i: the distance from the intersection of the Z_{i-1}-axis to the origin of the i^{th} coordinate system along the X_i-axis.
- Link twist angle α_i: the angle of rotation from the Z_{i-1}-axis to the Z_i-axis about the X_i-axis.

3.3.3. Transformation of the Coordinate Frames

Four successive elementary transformations are required to relate the i^{th} coordinate frame to the *(i-1)*th coordinate frame:

- Rotate about the Z_{i-1} axis an angle of θ_i to align the X_{i-1} axis with the X_i axis.
- Translate along the Z_{i-1} axis a distance of d_i to bring X_{i-1} axis to the X_i axis into coincidence.
- Translate along the X_i axis a distance of a_i to bring the two origins O_{i-1} and O_i as well as the X axis into coincidence.
- Rotate about the X_i axis with the angle of α_i (in the right-handed sense), to bring the two coordinates into coincidence.

The position and orientation of the i^{th} frame coordinate can be expressed in the $(i\text{-}1)^{th}$ frame by the following homogeneous D-H transformation matrix:

$$
\begin{aligned}
A_{i-1}^{i} &= R(z_{i-1},\theta_i)T(z_{i-1},d_i)T(x_i,a_i)R(x_i,\alpha_i) \\
&= \begin{bmatrix} \cos\theta_i & -\sin\theta_i & 0 & 0 \\ \sin\theta_i & \cos\theta_i & 0 & 0 \\ 0 & 0 & 1 & 0 \\ 0 & 0 & 0 & 1 \end{bmatrix}\begin{bmatrix} 1 & 0 & 0 & 0 \\ 0 & 1 & 0 & 0 \\ 0 & 0 & 1 & d_i \\ 0 & 0 & 0 & 1 \end{bmatrix}\begin{bmatrix} 1 & 0 & 0 & a_i \\ 0 & 1 & 0 & 0 \\ 0 & 0 & 1 & 0 \\ 0 & 0 & 0 & 1 \end{bmatrix}\begin{bmatrix} 1 & 0 & 0 & 0 \\ 0 & \cos\alpha_i & -\sin\alpha_i & 0 \\ 0 & \sin\alpha_i & \cos\alpha_i & 0 \\ 0 & 0 & 0 & 1 \end{bmatrix} \\
&= \begin{bmatrix} \cos\theta_i & -\cos\alpha_i\sin\theta_i & \sin\alpha_i\sin\theta_i & a_i\cos\theta_i \\ \sin\theta_i & \cos\alpha_i\cos\theta_i & -\sin\alpha_i\cos\theta_i & a_i\sin\theta_i \\ 0 & \sin\alpha_i & \cos\alpha_i & d_i \\ 0 & 0 & 0 & 1 \end{bmatrix}
\end{aligned}
\tag{3-6}
$$

The location of the i^{th} coordinate frame is specified with reference to the base coordinate system as A_0^i, which is the chain product of successive coordinate transformation matrices of A_{i-1}^i:

$$
\begin{aligned}
A_0^i &= A_0^1 A_1^2 \ldots A_{i-1}^i = \prod_{j=1}^{i} A_{j-1}^j \\
&= \begin{bmatrix} R_0^i & P_0^i \\ 0 & 0 \end{bmatrix} = \begin{bmatrix} n_i & s_i & a_i & P_0^i \\ 0 & 0 & 0 & 1 \end{bmatrix}
\end{aligned}
\tag{3-7}
$$

where $R_0^i = \begin{bmatrix} n_i & s_i & a_i \end{bmatrix}$ is the 3×3 orientation matrix of the i^{th} coordinate frame and P_0^i is the position vector of the i^{th} coordinate frame related to the base coordinate system.

3.3.4. Kinematic Model of the Hand

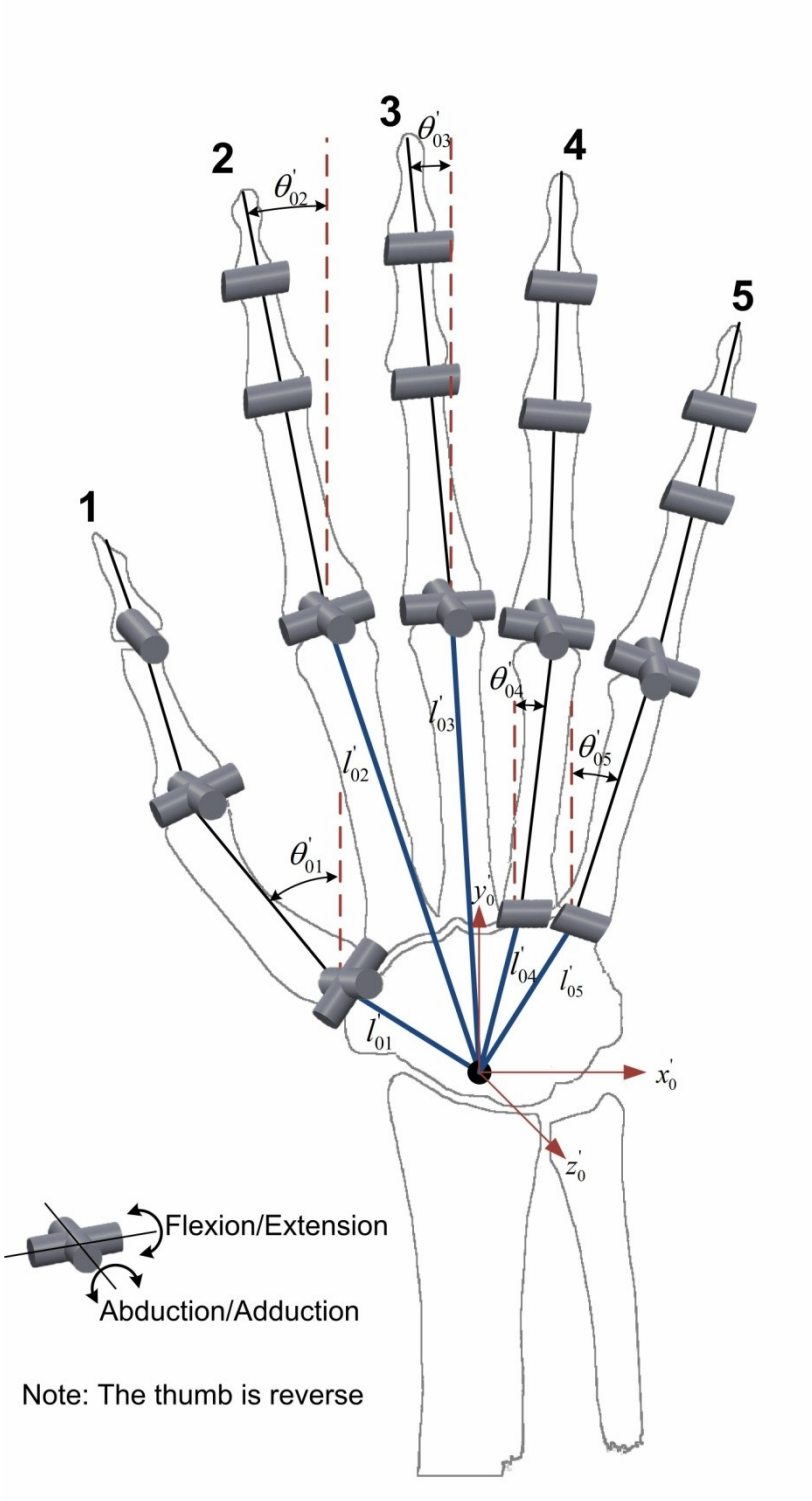

Figure 3-5 Hand's Kinematic Model (Left Hand) [32]

Human hand is modelled with a hierarchical tree structure that consists of rigid links and joints. Each joint consists of one or two degrees of freedom. This hierarchical structure is represented in Figure 3-5 and each joint's position is described using D-H

representation with reference to the heel of the hand (the world coordinate system (x_0^r, y_0^r, z_0^r)). The posture of each finger ray (labelled as 1 to 5 from the thumb to the little finger as shown in Figure 3-5) is represented by a local coordinate system. Using D-H representation, the position of each joint can be transformed from the local coordinates to the world coordinates sequentially.

As shown in Figure 3-5, the five finger rays can be divided into three groups based on the different kinematic structures (thumb ray with five DOFs, index and middle finger rays with four DOFs, ring and little finger rays with five DOFs). The kinematic model for each group is described respectively as follows [32,33].

1) Thumb kinematic model

The model of the thumb is shown in Figure 3-6. There are totally five DOFs within the three joints (one DOF at the IP joint, two DOFs at the MP joint and another two DOFs at the TM joint). The coordination system is set up according to D-H principles. The flexion/extension motion of the joint can be treated as the rotation about z_{1j}-axis (*j=1,3,4*) and the abduction/adduction motion of the joint can be treated as the rotation about z_{1j}-axis (*j=0,2*), where *1* is the notation of the thumb and *j* is the notation of a specific rotation axis as illustrated in Figure 3-6.

Comparing with the other four fingers, the major difference of the thumb is the initial position of the coordinate frame of the TM (MCP in the four fingers) joint with respect to the palm's coordinate system. There is an initial angle (approximately 90°) between the flexion/extension motion plane of the thumb's TM joint and the flexion/extension motion planes of the other four fingers' MCP joints which will cause the difference when linking the local coordinate system to the world coordinate system in the following descriptions.

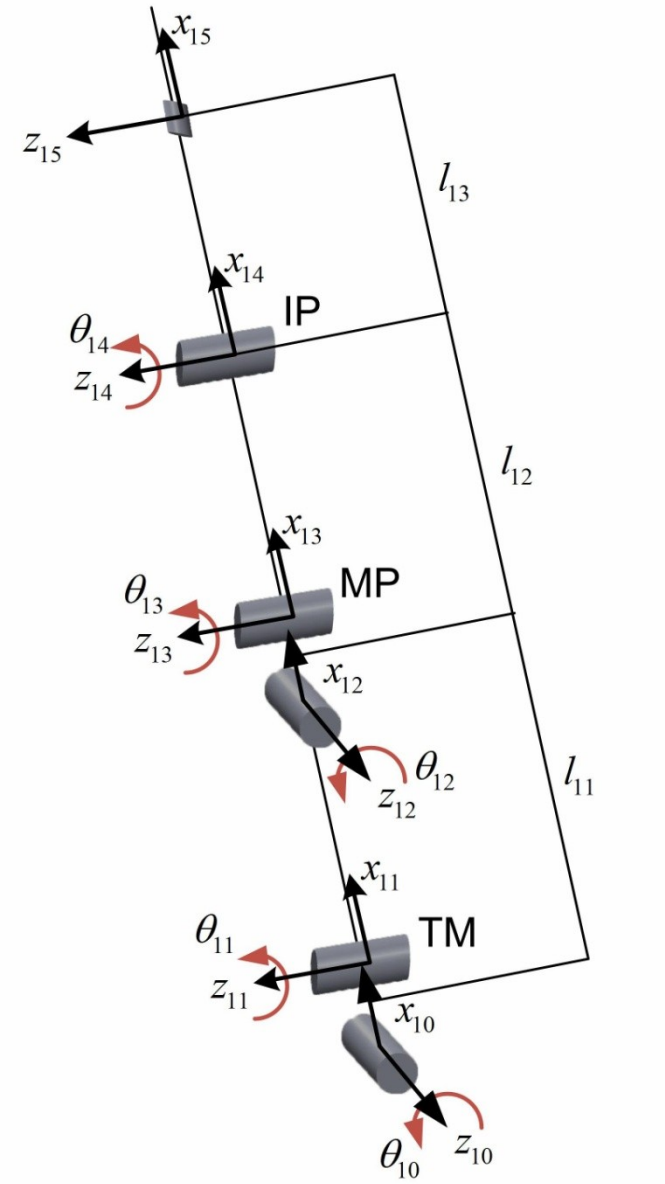

Figure 3-6 Thumb kinematic Model

The D-H parameters of the thumb can be defined in Table 3-1:

Table 3-1 Thumb's D-H Model Parameters

i^{th} *joint*	θ_i	d_i	α_i	a_i	*Joint range*	$\cos\alpha$	$\sin\alpha$
1	θ_{10}	0	-90°	0	0°~ 60°	0	-1
2	θ_{11}	0	90°	l_{11}	-25°~ 35°	0	1
3	θ_{12}	0	-90°	0	0°~ 60°	0	-1
4	θ_{13}	0	0°	l_{12}	0°~ 55°	1	0
5	θ_{14}	0	0°	l_{13}	0°~ 80°	1	0

Two DOFs at the TM joint can be divided into two motions: One is the abduction/adduction motion about the z_{10} -axis represented by θ_{10} . Putting the parameters in Table 3-1 into the D-H transformation matrix, we have

$$A_0^1(1)=\begin{bmatrix}\cos\theta_i & -\cos\alpha_i\sin\theta_i & \sin\alpha_i\sin\theta_i & a_i\cos\theta_i\\ \sin\theta_i & \cos\alpha_i\cos\theta_i & -\sin\alpha_i\cos\theta_i & a_i\sin\theta_i\\ 0 & \sin\alpha_i & \cos\alpha_i & d_i\\ 0 & 0 & 0 & 1\end{bmatrix}=\begin{bmatrix}\cos\theta_{10} & 0 & -\sin\theta_{10} & 0\\ \sin\theta_{10} & 0 & \cos\theta_{10} & 0\\ 0 & -1 & 0 & 0\\ 0 & 0 & 0 & 1\end{bmatrix} \tag{3-8}$$

The other is the flexion/extension motion about the z_{11} -axis represented by θ_{11} . Putting the parameters in Table 3-1 into the D-H transformation matrix, we have

$$A_1^2(1)=\begin{bmatrix}\cos\theta_{11} & 0 & \sin\theta_{11} & l_{11}\cos\theta_{11}\\ \sin\theta_{11} & 0 & -\cos\theta_{11} & l_{11}\sin\theta_{11}\\ 0 & 1 & 0 & 0\\ 0 & 0 & 0 & 1\end{bmatrix} \tag{3-9}$$

Also we can divide the two DOFs at the MP joint into two motions: One is the flexion/extension motion about the z_{12} -axis represented by θ_{12} . Putting the parameters in Table 3-1 into the D-H transformation matrix, we obtain

$$A_2^3(1)=\begin{bmatrix}\cos\theta_{12} & 0 & -\sin\theta_{12} & 0\\ \sin\theta_{12} & 0 & \cos\theta_{12} & 0\\ 0 & -1 & 0 & 0\\ 0 & 0 & 0 & 1\end{bmatrix} \tag{3-10}$$

The other is the abduction/adduction motion about the z_{13}-axis represented by ϕ_{13}. Putting the parameters in Table 3-1 into the D-H transformation matrix, we obtain

$$A_3^4(1)=\begin{bmatrix}\cos\theta_{13} & -\sin\theta_{13} & 0 & l_{12}\cos\theta_{13}\\ \sin\theta_{13} & \cos\theta_{13} & 0 & l_{12}\sin\theta_{13}\\ 0 & 0 & 1 & 0\\ 0 & 0 & 0 & 1\end{bmatrix} \tag{3-11}$$

The IP joint only has one DOF: the flexion/extension motion about the z_{14} -axis represented by θ_{14} . Putting the parameters in Table 3-1 into the D-H transformation matrix, we have

$$A_4^5(1)=\begin{bmatrix}\cos\theta_{14} & -\sin\theta_{14} & 0 & l_{13}\cos\theta_{14}\\ \sin\theta_{14} & \cos\theta_{14} & 0 & l_{13}\sin\theta_{14}\\ 0 & 0 & 1 & 0\\ 0 & 0 & 0 & 1\end{bmatrix} \tag{3-12}$$

Consequently, the D-H transformation matrix of the thumb tip's coordinate frame with reference to the local coordinate system is $A_0^5(1)=\prod_{j=1}^{5}A_{j-1}^{j}(1)$. With respect to the world coordinate system (the heel of hand as shown in Figure 3-5), an additional transformation matrix is needed to represent the position vector which is defined as

$$H_{0'}^{0}(1)=\begin{bmatrix}\cos\theta_{01}^{'} & 0 & -\sin\theta_{01}^{'} & l_{01}^{'}\cos\theta_{01}^{'}\\ \sin\theta_{01}^{'} & 0 & \cos\theta_{01}^{'} & l_{01}^{'}\sin\theta_{01}^{'}\\ 0 & -1 & 0 & 0\\ 0 & 0 & 0 & 1\end{bmatrix} \tag{3-13}$$

where $\theta_{01}^{'}$ is the angle between the thumb and the world $y_0^{'}$-axis and $l_{01}^{'}$ is the length between the root of the thumb's local coordinate system and the world coordinate system, as shown in Figure 3-5.

Therefore, the thumb tip's coordinate frame with respect to the world coordinate system is defined by $A_{0'}^{5}(1)=A_0^5(1)H_{0'}^{0}(1)$

2) Index & Middle finger's kinematic model

There are totally four DOFs within the three joints (one DOF at the DIP joint, one DOF at the PIP joint and another two DOFs at the MCP joint). The coordination system is set up according to D-H principles similar to the thumb's model. The flexion/extension motion of the joint can be treated as the rotation about z_{ik}-axis (*i=2,3* and *k=1,2,3*) and the abduction/adduction motion of the joint can be treated as the rotation about z_{i0}-axis (*i=2,3*), where *i* is the notation of index finger (*i=2*) and middle finger (*i=3*) and *k* is the notation of a specific rotation axis. Take the index finger as an example as illustrated in Figure 3-7.

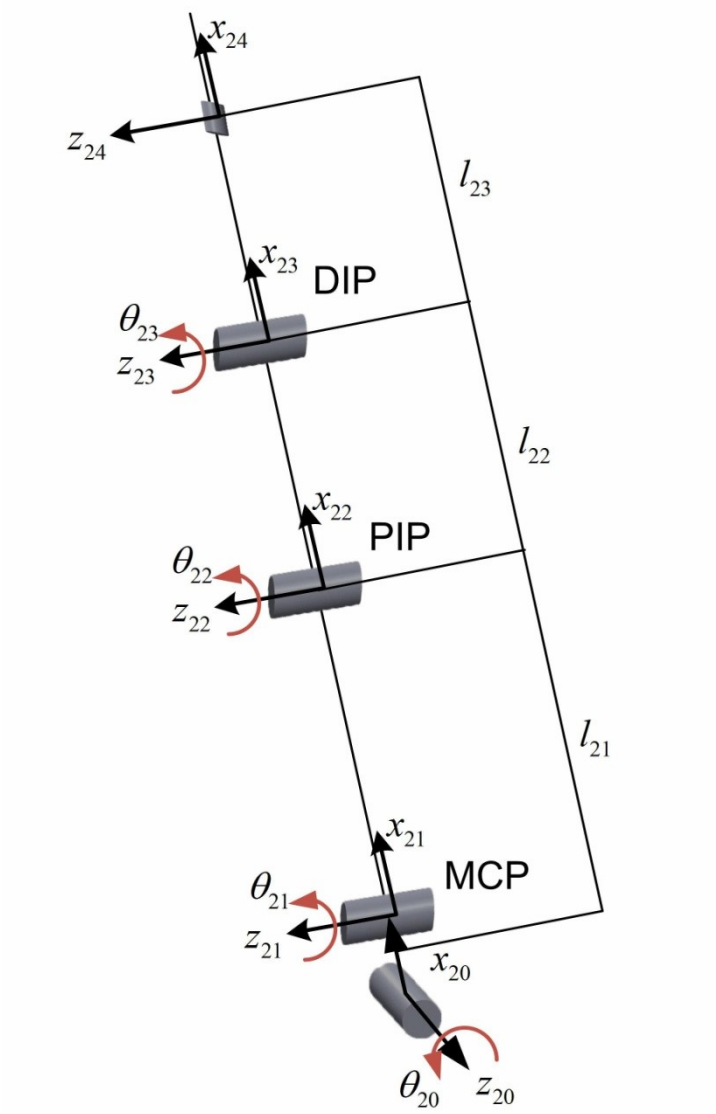

Figure 3-7 Index & Middle finger's Kinematic Model

The D-H parameters of the thumb are shown in Table 3-2:

Table 3-2 Index & Middle Finger's D-H Model Parameters

i^{th} *joint*	θ_i	d_i	α_i	a_i	*Joint range*	$\cos\alpha$	$\sin\alpha$
1	θ_{20}	0	-90°	0	-15°~ 45° (-10°~ 45° for the middle finger)	0	-1
2	θ_{21}	0	0°	l_{21}	0°~ 80°	1	0
3	θ_{22}	0	0°	l_{22}	0°~ 100°	1	0
4	θ_{23}	0	0°	l_{23}	0°~ 90°	1	0

With these parameters in Table 3-2 and the method used in analysing the thumb, the D-H transformation matrix of the index finger can be obtained:

$$A_0^1(2)=\begin{bmatrix}\cos\theta_{20} & 0 & -\sin\theta_{20} & 0\\ \sin\theta_{20} & 0 & \cos\theta_{20} & 0\\ 0 & -1 & 0 & 0\\ 0 & 0 & 0 & 1\end{bmatrix} \tag{3-14}$$

$$A_1^2(2)=\begin{bmatrix}\cos\theta_{21} & -\sin\theta_{21} & 0 & l_{21}\cos\theta_{21}\\ \sin\theta_{21} & \cos\theta_{21} & 0 & l_{21}\sin\theta_{21}\\ 0 & 0 & 1 & 0\\ 0 & 0 & 0 & 1\end{bmatrix} \tag{3-15}$$

$$A_2^3(2)=\begin{bmatrix}\cos\theta_{22} & -\sin\theta_{22} & 0 & l_{22}\cos\theta_{22}\\ \sin\theta_{22} & \cos\theta_{22} & 0 & l_{22}\sin\theta_{22}\\ 0 & 0 & 1 & 0\\ 0 & 0 & 0 & 1\end{bmatrix} \tag{3-16}$$

$$A_3^4(2)=\begin{bmatrix}\cos\theta_{23} & -\sin\theta_{23} & 0 & l_{23}\cos\theta_{23}\\ \sin\theta_{23} & \cos\theta_{23} & 0 & l_{23}\sin\theta_{23}\\ 0 & 0 & 1 & 0\\ 0 & 0 & 0 & 1\end{bmatrix} \tag{3-17}$$

Consequently, the D-H transformation matrix of the index finger's coordinate frame with reference to the local coordinate system is $A_0^4(2)=\prod_{j=1}^{4}A_{j-1}^{j}(2)$. With respect to the world coordinate system (the heel of hand as shown in Figure 3-5), an additional transformation matrix is needed to represent the position vector which is defined as

$$H_{0'}^0(2)=\begin{bmatrix}\cos\theta_{02}^{'} & -\sin\theta_{02}^{'} & 0 & l_{02}^{'}\cos\theta_{02}^{'}\\ \sin\theta_{02}^{'} & \cos\theta_{02}^{'} & 0 & l_{02}^{'}\sin\theta_{02}^{'}\\ 0 & 0 & 1 & 0\\ 0 & 0 & 0 & 1\end{bmatrix} \tag{3-18}$$

where $\theta_{02}^{'}$ is the angle between the index finger and the world $y_0^{'}$-axis and $l_{02}^{'}$ is the length between the root of the index finger's local coordinate system and the world coordinate system, as shown in Figure 3-5.

Therefore, the index finger tip's coordinate frame with respect to the world coordinate system is defined by $A_{0'}^4(2)=A_0^4(2)H_{0'}^0(2)$

3) Ring & little finger's kinematic model

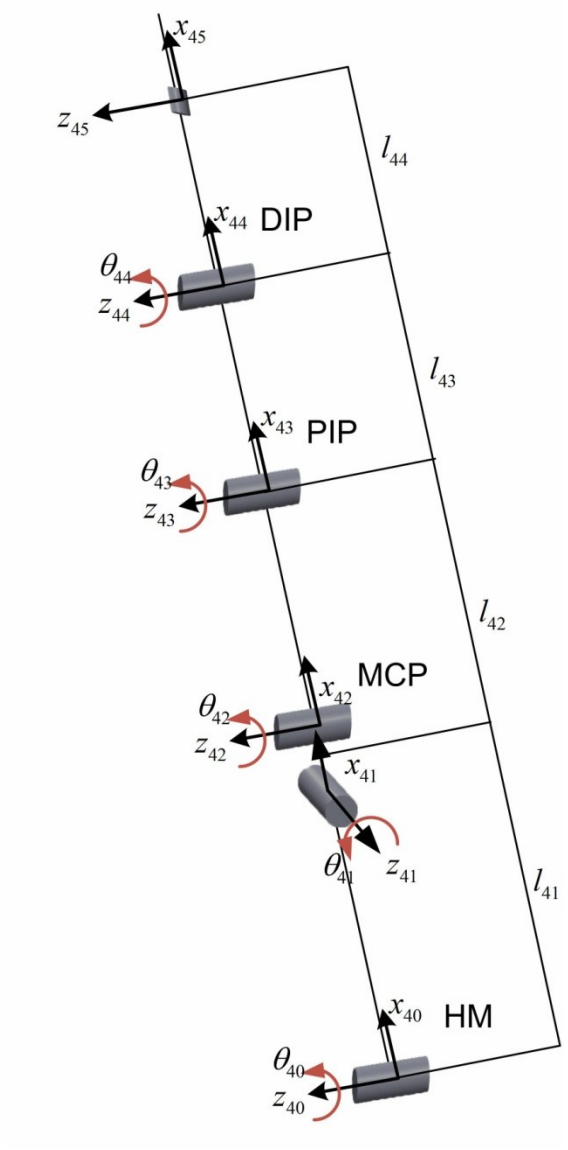

Figure 3-8 Ring & Little finger's Kinematic Model

Different from the index and middle finger, there are totally four DOFs within the four joints (one DOF at the DIP joint, one DOF at the PIP joint, two DOFs at the MCP joint, and another one DOF at the HM joint). The coordination system is set up according to D-H principles similar to the previous two models. The flexion/extension motion of the joint can be treated as the rotation about z_{in} -axis ($i=4,5$ and $n=0,2,3,4$) and the abduction/adduction motion of the joint can be treated as the rotation about z_{i1} -axis ($i=4,5$), where i is the notation of ring finger ($i=4$) and little finger ($i=5$) and n is the notation of a specific rotation axis. Take the ring finger as an example as illustrated in Figure 3-8.

The D-H parameters of the thumb are shown in Table 3-3:

Table 3-3 Index & Middle Finger's D-H Model Parameters

i^{th} joint	θ_i	d_i	α_i	a_i	*Joint range*	$\cos\alpha$	$\sin\alpha$
1	θ_{40}	0	90°	l_{41}	0°~ 10° (0°~ 20° for the little finger)	0	1
2	θ_{41}	0	-90°	0	-15°~ 20° (-20°~ 35° For the little finger)	0	-1
3	θ_{42}	0	0°	l_{42}	0°~ 80°	1	0
4	θ_{43}	0	0°	l_{43}	0°~ 100°	1	0
5	θ_{44}	0	0°	l_{44}	0°~ 90°	1	0

With these parameters in Table 3-3 and the same method, the D-H transformation matrix of the ring finger can be obtained:

$$A_0^1(4)=\begin{bmatrix}\cos\theta_{40} & 0 & \sin\theta_{40} & 0\\ \sin\theta_{40} & 0 & -\cos\theta_{40} & 0\\ 0 & 1 & 0 & 0\\ 0 & 0 & 0 & 1\end{bmatrix} \tag{3-19}$$

$$A_1^2(4)=\begin{bmatrix}\cos\theta_{41} & 0 & -\sin\theta_{41} & l_{41}\cos\theta_{41}\\ \sin\theta_{41} & 0 & \cos\theta_{41} & l_{41}\sin\theta_{41}\\ 0 & -1 & 0 & 0\\ 0 & 0 & 0 & 1\end{bmatrix} \tag{3-20}$$

$$A_2^3(4)=\begin{bmatrix}\cos\theta_{42} & -\sin\theta_{42} & 0 & l_{42}\cos\theta_{42}\\ \sin\theta_{42} & \cos\theta_{42} & 0 & l_{42}\sin\theta_{42}\\ 0 & 0 & 1 & 0\\ 0 & 0 & 0 & 1\end{bmatrix} \tag{3-21}$$

$$A_3^4(4)=\begin{bmatrix}\cos\theta_{43} & -\sin\theta_{43} & 0 & l_{43}\cos\theta_{43}\\ \sin\theta_{43} & \cos\theta_{43} & 0 & l_{43}\sin\theta_{43}\\ 0 & 0 & 1 & 0\\ 0 & 0 & 0 & 1\end{bmatrix} \tag{3-22}$$

$$A_4^5(4)=\begin{bmatrix}\cos\theta_{44} & -\sin\theta_{44} & 0 & l_{44}\cos\theta_{44}\\ \sin\theta_{44} & \cos\theta_{44} & 0 & l_{44}\sin\theta_{44}\\ 0 & 0 & 1 & 0\\ 0 & 0 & 0 & 1\end{bmatrix} \tag{3-23}$$

Consequently, the D-H transformation matrix of the ring finger's coordinate frame with reference to the local coordinate system is $A_0^5(4) = \prod_{j=1}^{5} A_{j-1}^{j}(4)$. With respect to the world coordinate system (the heel of hand as shown in Figure 3-5), an additional transformation matrix is needed to represent the position vector which is defined as

$$H_{0'}^{0}(4) = \begin{bmatrix} \cos\theta_{04}^{'} & 0 & -\sin\theta_{04}^{'} & l_{04}^{'}\cos\theta_{04}^{'} \\ \sin\theta_{04}^{'} & 0 & \cos\theta_{04}^{'} & l_{04}^{'}\sin\theta_{04}^{'} \\ 0 & 0 & 1 & 0 \\ 0 & 0 & 0 & 1 \end{bmatrix} \tag{3-24}$$

where $\theta_{04}^{'}$ is the angle between the ring finger and the world $y_0^{'}$-axis and $l_{04}^{'}$ is the length between the root of the ring finger's local coordinate system and the world coordinate system, as shown in Figure 3-5.

Therefore, the ring finger tip's coordinate frame with respect to the world coordinate system is defined by $A_{0'}^{5}(4) = A_0^5(4)H_{0'}^{0}(4)$

4) Palm motion

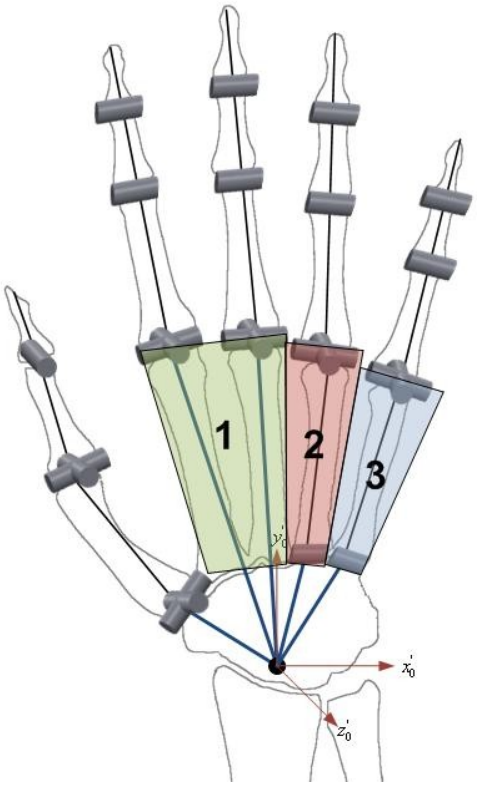

Figure 3-9 Palm motion (Left Hand)

As described above, the palm can be divided into three parts as shown in Figure 3-9. The first part (part 1 in Figure 3-9) is fixed which includes the metacarpal bones of the index and middle finger. The rest two parts (part 2 and part 3 in Figure 3-9) are movable due to the rotation of the two HM joints located at the end of the ring and little finger rays. The transverse deformation of the palm arch is formed by the relative movements of these three parts. The D-H transformation matrixes of the HM joints are described in Equation 3-19 and 3-24.

5) Simplified hand model

At the first stage of this project, the main focus is on the simple finger motion capture (basically the FE motion of the joint). Thus, a simplified kinematic model, which does not include the palm arch motion and the MCP joint's AA motion, is proposed based on the full kinematic model (Figure 3-10). The rest part of this thesis project is based on this simplified model.

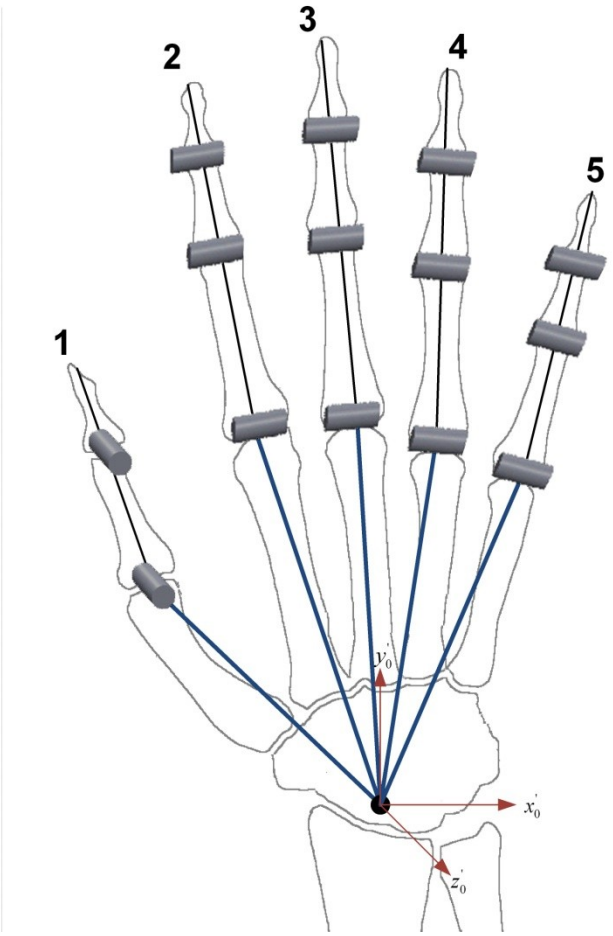

Figure 3-10 Simplified Hand's Kinematic Model (Left Hand)

3.4. Discussion

In this chapter, the biomechanics of human hand are studied, including the skeleton model, constraints of joint motions and the kinematic model. Twenty three major DOFs are derived from the skeleton model, including five DOFs in the thumb, four DOFs in each of the four fingers and another two DOFs in the palm. A full hand kinematic model based on these twenty three DOFs is defined using D-H representation to illustrate the realistic motions of the hand. The proposed kinematic model is able to represent the transverse deformation of the palm arch, which brings a significant improvement of hand posture and motion representation with comparison to the normal kinematic models [32,33] without palm arch. Based on the different structure, three different kinematic models are setup respectively for the thumb, the index & middle finger, and the ring & little finger, in which the joints and links are defined by D-H notation.

In the constraints part, three kinds of hand constraints are introduced. By applying these constraints, it can to reduce seven DOFs from the full 23-DOF model, which directly results in using fewer sensors to capture the whole hand movement. Meanwhile, the motion range of each joint is also defined by the constraints.

A simplified model with the joint's flexion/extension motion only is proposed to fulfil the requirements for the motion capture of the basic and simple finger motions.

CHAPTER 4. SENSING PRINCIPLE

This chapter describes the multi-point sensing principle for SmartGlove which is based on the inverted OLE sensing modules. In the SmartSuit project we have carried out, a new OLE module (as shown in Figure 4-1) is developed by using the optical sensor to convert the joint's linear displacement to the joint's angle [34]. However, this OLE is too large to be used in hand motion capture. Thus, an inverted OLE sensing principle is formulated to reduce the size. Based on this, a multi-point sensing principle which uses multiple OLEs to detect multiple joints' movement along the same strip is presented.

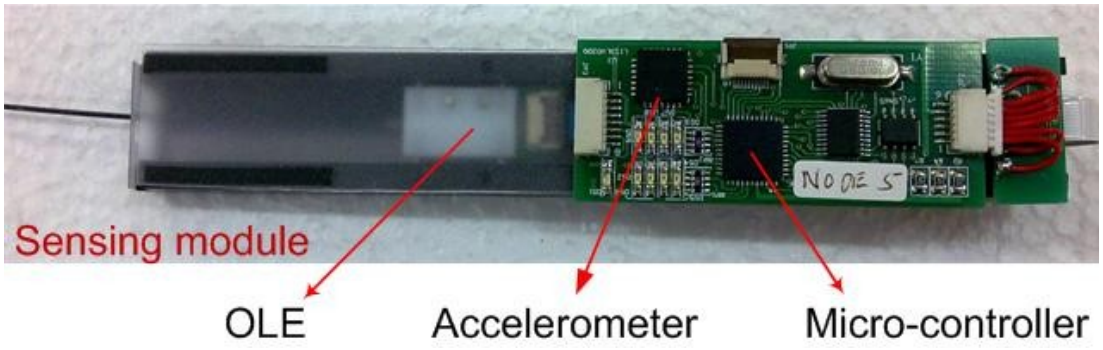

Figure 4-1 OLE for SmartSuit

4.1. Inverted OLE Sensing Principle

In the SmartSuit project, joint angle of a human body joint (such as elbow) is obtained through a new linear encoder sensor. The linear encoder is attached to a wire that is fixed on one forearm while the linear encoder assembly is fixed on upper arm and the wire will be displaced along the circumference of the joint (as shown in Figure 4-2(a)). The linear encoder is free to slide along its longitudinal axis. When the elbow bends, the bending causes the skin to stretch. This stretch is translated into a linear displacement and can be captured by the linear encoder assembly.

However, the OLE developed for the SmartSuit project is aimed for limb motion capture. The size of the sensor assembly is too large for the finger joint motion capture. Thus, an inverted sensing principle for OLE is formulated for the SmartGlove project. As shown in Figure 4-2(b), in the inverted OLE, the encoder is fixed on the finger segment to capture the displacement of the moving strip. Without the moving

mechanism, the size of the OLE for SmartGlove can be reduced significantly to fulfil the dimensional requirement.

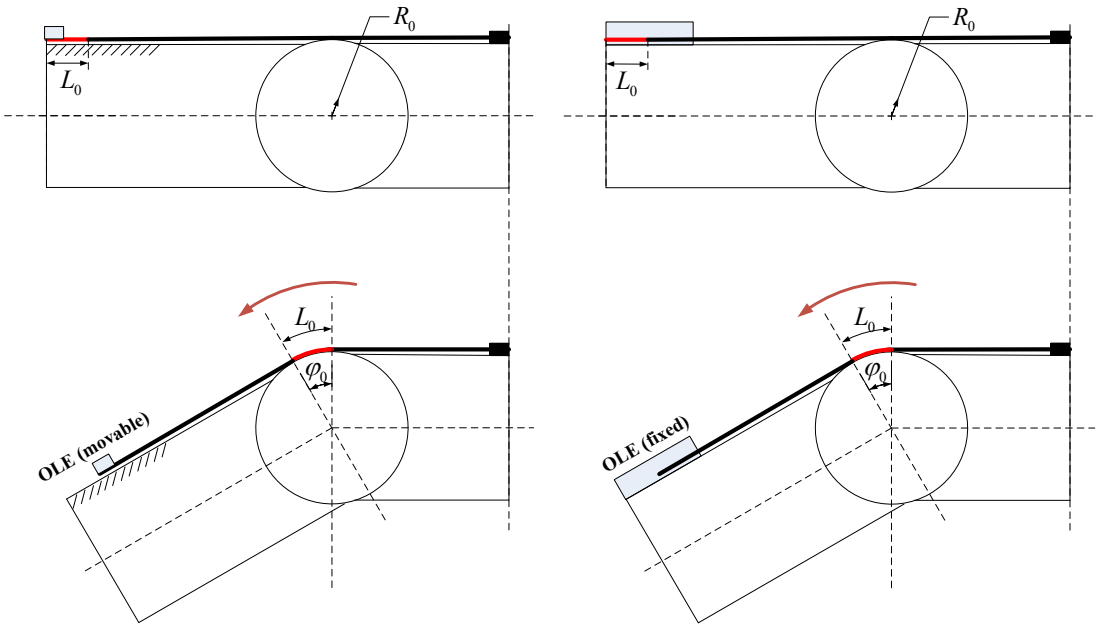

(a) OLE Sensing Principle **(b) Inverted OLE Sensing Principle**

Figure 4-2 OLE and Inverted OLE's Sensing Principles

From the studies of human hand anatomy it is obvious that the joint axis is not fixed as the finger bends. However, the displacement of the change of the finger joint centre is very small compared to the dimension of the fingers. Hence, in this study we assume that the finger joint centre is a fixed point instead of a moving point. Based on this assumption, it is possible to use a circular disk to model the finger joint rotation. The strip is placed on the surface of the finger with one end fixed (Figure 4-2(a)). As the finger joint bends, it causes the skin the stretch. This stretch is translated into a linear displacement and is captured by the OLE. As shown in Figure 4-2(b), when the joint bends, the movement of the two segments can be approximated by the rotation of a circular disk when the centre of the joint becomes the centre of the disk. The radius of the circle is based on the biometric data on the subject under consideration and can be approximately obtained via physical measurement. Assume the radius of the joint is R_0 and the bend angle of the joint is φ_0, by measuring the displacement of the strip (L_0) with the linear encoder, φ_0 can be estimated by

$$\varphi_0 = \frac{L_0}{2\pi R_0} \times 360° \tag{4-1}$$

In principle, the calculation of the joint angle (Equation (4-1)) is identical to the OLE sensor [34]. However, in next section, we will describe using the same principle to detect multiple joints' movement along the same strip.

4.2. Multi-point Sensing Principle

The above discussed inverted sensing principle is valid for single joint condition. As there are more than three joints in one finger, multiple OLEs are required to get all the three finger joints' angle information. Therefore, an improved version is improvised for this situation and is termed multi-point sensing. The basic working principle of multi-point sensing is to place multiple OLEs in series on different finger segments to capture the displacements of different detecting points using the same strip. As shown in Figure 4-3, three disks (from left to right) represent three in-line joints with radius of R_1, R_2 and R_3 respectively. Denote their bend angles as φ_1, φ_2 and φ_3 respectively. Three OLEs are to be placed and fixed at positions (A), (B) and (C) as shown in Figure 4-3. Assume the displacement readings obtained by these three OLEs are D_1, D_2 and D_3. Because of the accumulated displacement at the distal joints, we have

$$D_1 = L_1 = \frac{2\pi R_1 \varphi_1}{360} \tag{4-2}$$

$$D_2 = L_1 + L_2 = \frac{2\pi R_1 \varphi_1}{360} + \frac{2\pi R_2 \varphi_2}{360} \tag{4-3}$$

$$D_3 = L_1 + L_2 + L_3 = \frac{2\pi R_1 \varphi_1}{360} + \frac{2\pi R_2 \varphi_2}{360} + \frac{2\pi R_3 \varphi_3}{360} \tag{4-4}$$

From Equations (4-2), (4-3) and (4-4), we can obtain

$$\varphi_1 = \frac{360 D_1}{2\pi R_1} \tag{4-5}$$

$$\varphi_2 = \frac{360(D_2 - D_1)}{2\pi R_2} \tag{4-6}$$

$$\varphi_3 = \frac{360(D_3 - D_2 - D_1)}{2\pi R_3} \tag{4-7}$$

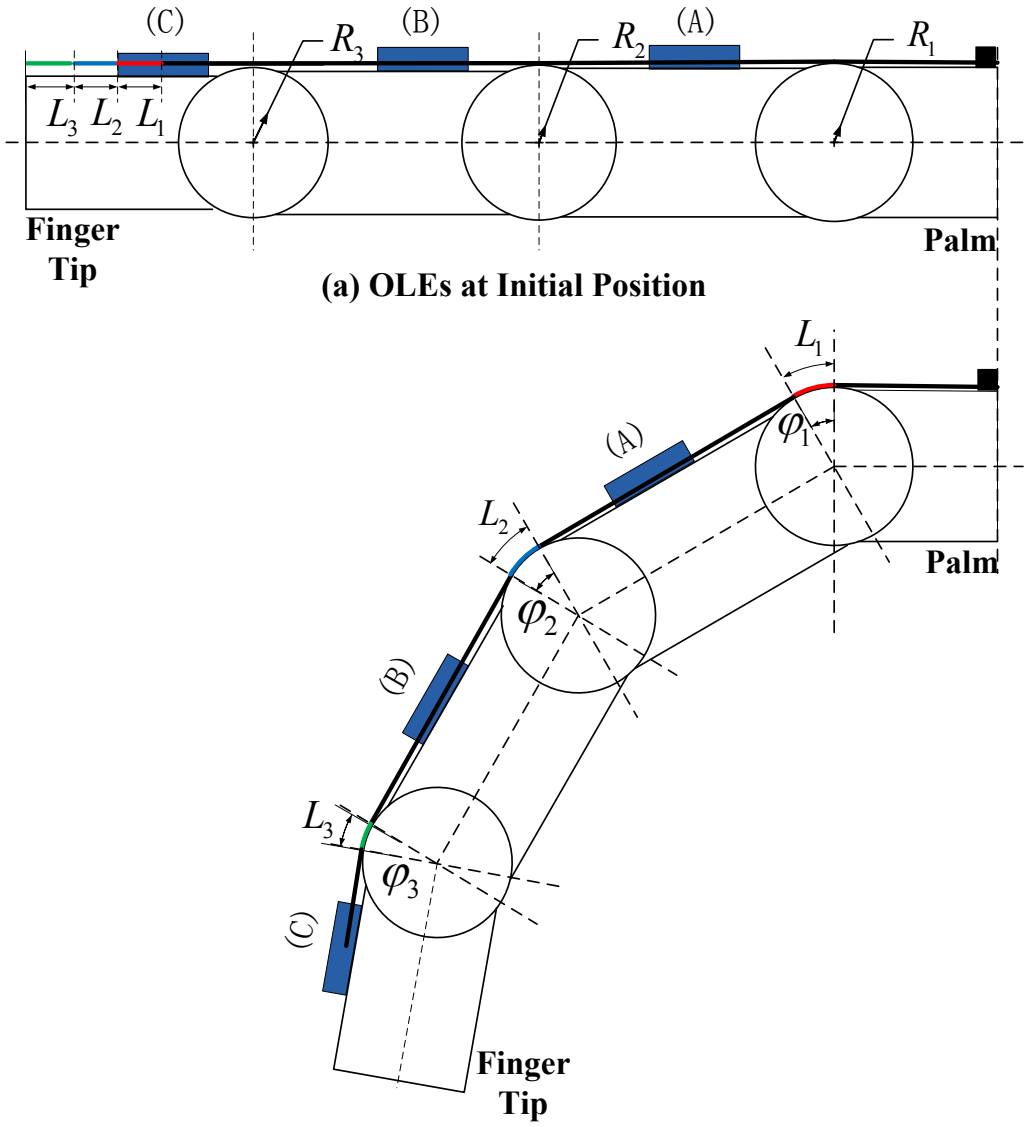

Figure 4-3 Multi-point Sensing Principle

Due to the natural arches of human hand, the multi-point sensing can be adopted in finger motion capture. As shown in Figure 4-4, the hand has five longitudinal arches, one for each of the five digital rays. Each arch is composed of a metacarpal and its phalanges, linked by the MCP, PIP, and DIP joints. (The longitudinal arch for thumb is linked by the MCP and IP joints) [35] As introduced in the hand kinematics, there are at least 14 joints' FE motions need to be captured in order to perform basic multi-finger sensing, and all these 14 joints are all within the five longitudinal arches. Hence, by introducing one strip for each longitudinal finger arch, it is able to use the multi-point sensing method to capture the finger's movement. In other words, multi-point sensing

only a single encoding strip is needed for sensing the multiple DOF movement of an articulated object.

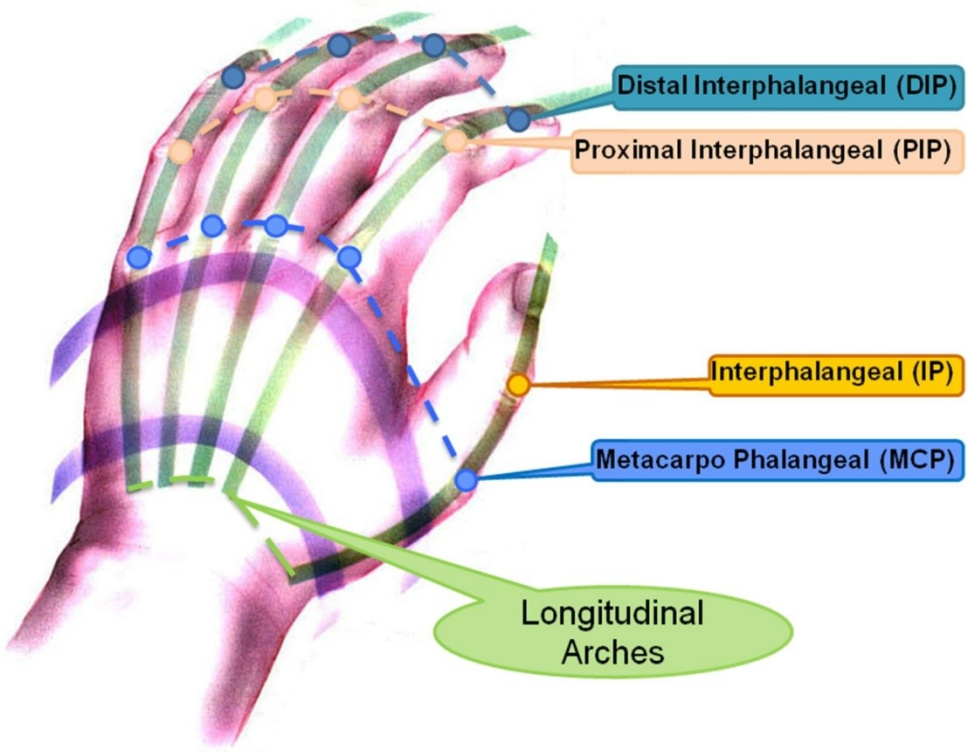

Figure 4-4 Arches of the Hand [35]

Based on the difference in the structures of the thumb and fingers, the detailed multi-point sensing method and encoder placement for the thumb and fingers are introduced separately as follows.

4.2.1. Finger Model

As introduced in the last chapter, there are three joints in one finger, and at least two OLEs are required to obtain the three angle information. (The constraint of $\theta_{DIP} = \frac{2}{3}\theta_{PIP}$ is applied to reduce one sensor.) In order to obtain the joint angles of a finger joint, the OLEs is fixed on the dorsal side of the hand. A strip goes through the OLE's plastic casing with one end attached to the back of the hand. The strip and the two OLEs form a multiple encoder chain on the finger's longitudinal arch. When the

finger starts to bend, the strip will move along the circumference of the joint angle, as shown in Figure 4-5.

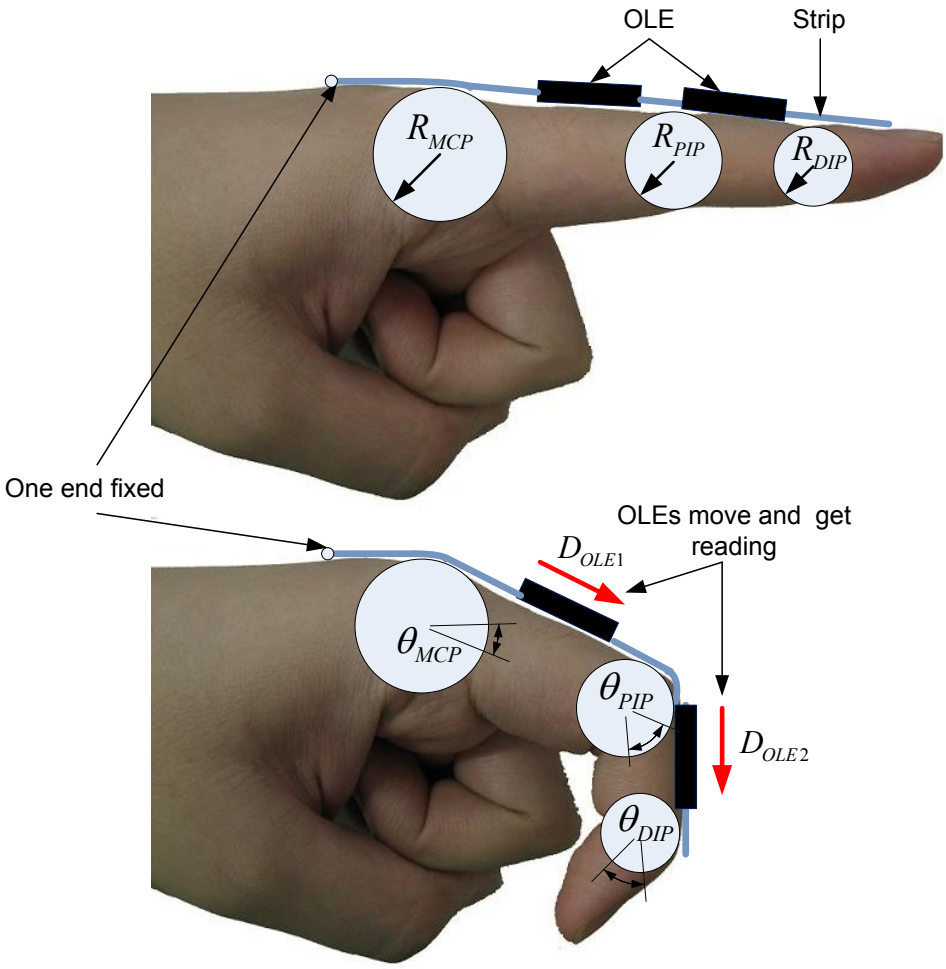

Figure 4-5 Finger Model

In Figure 4-3, three disks (from left to right) are used to represent MCP, PIP and DIP joints in a finger with radius of R_{MCP}, R_{PIP} and R_{DIP}. Assume that the bend angles of MCP, PIP and DIP are θ_{MCP}, θ_{PIP} and θ_{DIP} respectively and the two OLEs' readings are D_{F1} and D_{F2}. The bend angles of MCP and PIP joints can be calculated using Equations (4-5) and (4-6).

$$\theta_{MCP} = \frac{360 D_{F1}}{2\pi R_{MCP}} \tag{4-8}$$

$$\theta_{PIP} = \frac{360(D_{F2} - D_{F1})}{2\pi R_{PIP}} \tag{4-9}$$

The bend angle of the DIP joint can be obtained using the following constraint equation:

$$\theta_{CIP} = \frac{2}{3}\theta_{PIP} = \frac{240(D_{F2} - D_{F1})}{2\pi R_{DIP}} \tag{4-10}$$

Using Equations (4-8), (4-9) and (4-10) the posture of the finger's first three joints can be calculated by converting linear encoder's displacement reading to joint's angle information.

4.2.2. Thumb Model

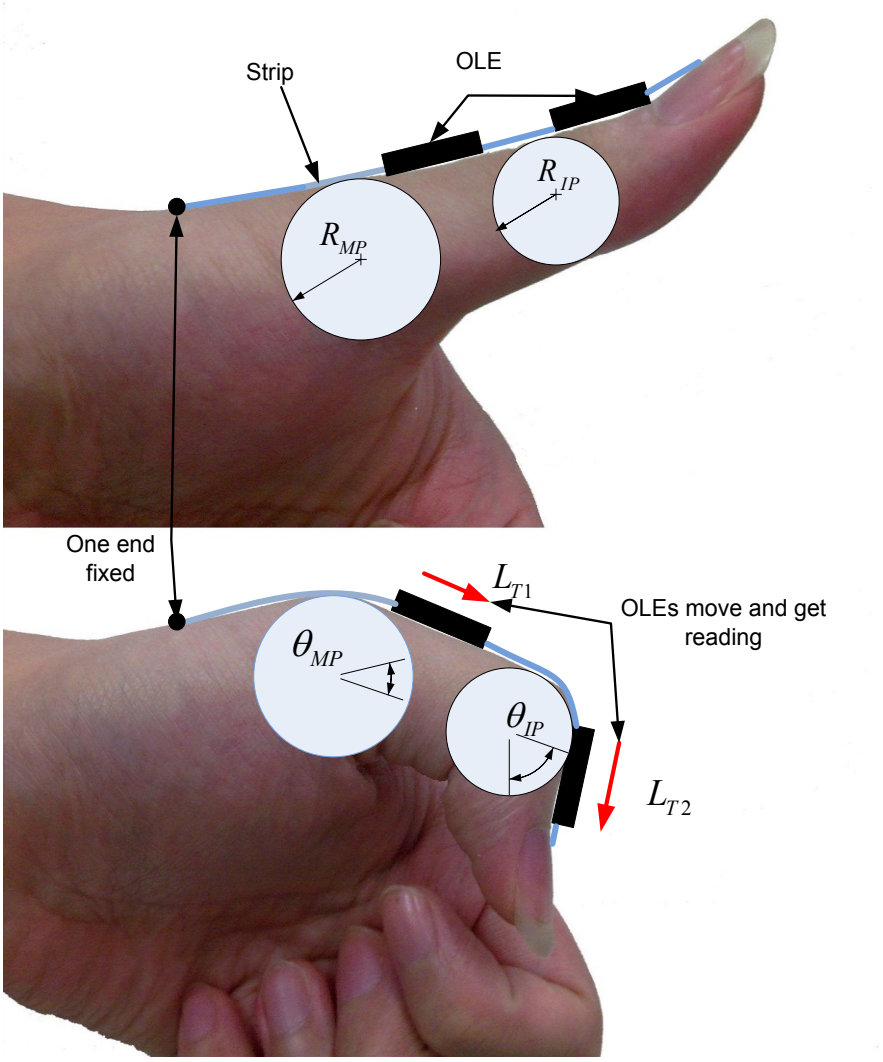

Figure 4-6 Thumb model

The kinematic modelling of fingers and thumb in Chapter 3 show that the structure of thumb is similar to that of the other four fingers. Thus, the same multi-point sensing method can be applied to capture the thumb's motion. The only difference is that only

two joints in the thumb need to be measured compared to three joints in other fingers. The setup of the OLEs on the thumb is as shown in Figure 4-6. Two OLEs are fixed on the back of the thumb's first and second segments to capture the rotation angles of the MP and IP joint.

The way to obtain the rotation of finger's MCP and PIP joints can also be implemented in obtaining the rotation angle of thumb's MP and IP joints:

$$\theta_{MP} = \frac{180 \times L_{T1}}{\pi R_{MP}} \tag{4-11}$$

$$\theta_{IP} = \frac{180 \times (L_{T2} - L_{T1})}{\pi R_{IP}} \tag{4-12}$$

4.3. Discussion

In this chapter, a new sensing principle of using multiple OLEs to measure the joint angle of a finger is illustrated. It is an improved OLE sensing method using multiple OLEs to capture the displacement of different points along one strip. The advantage of the multi-point sensing method is in its application for sensing multiple DOF movement in an articulated object such as fingers or even the spine with unlimited number of joints and unlimited number of sensors. The multiple DOF may be in the form of joint angles, or curvature of the spine.

However, at this moment, the multi-point sensing method can only capture the planar flexion/extension motions of the fingers (14 joints), but not the out-of-plane motion due to the construction of the OLE. Although the flexion/extension motion is sufficient for most finger actions, the abduction/adduction of the TM and MCP joints are also important for the hand motion. Thus, further improvements on the multi-point sensing method to include the detection of out-of-plane finger movement are needed in order to capture the full hand motion in high fidelity.

CHAPTER 5. SMARTGLOVE DEVELOPMENT

This chapter focuses on the development of the multi-finger sensing system – SmartGlove based on the sensors and method described in Chapter 4. As shown in the system block diagram (Figure 5-1), the SmartGlove system includes three main parts: 1) hardware (OLE sensors, microcontroller and glove); 2) firmware in the microcontroller for sensor data handling; 3) application software in the computer for data management.

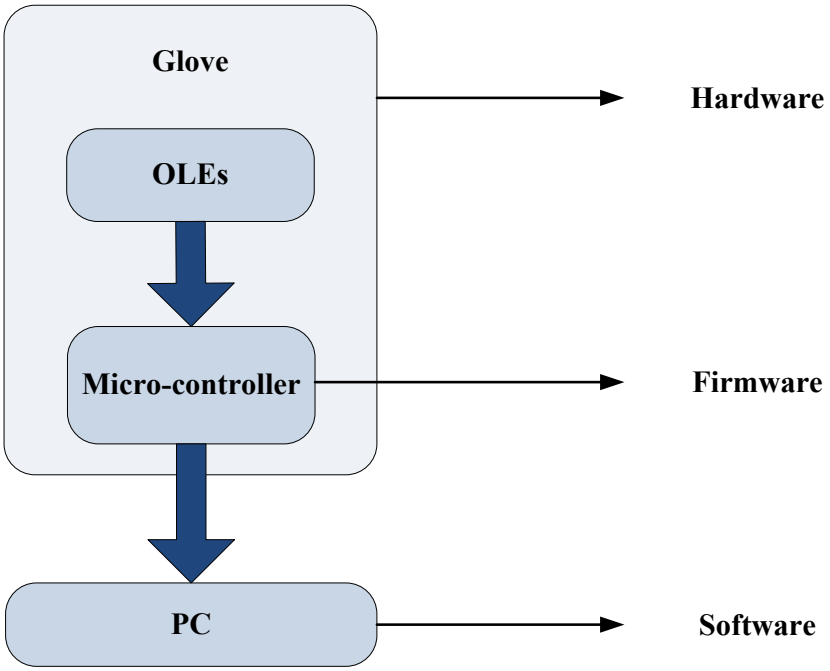

Figure 5-1 System Block Diagram

In order to capture the finger's motion effectively, the proposed system will fit the following requirements:

- High accuracy (±1°)
- High resolution (0.2°)
- Low cost (<S$1000 per glove)
- Comfortable to wear, easy to use
- Replaceable sensor
- Highly usable (un-obtrusive to user, wireless)
- Wearable over long periods
- Wireless

5.1. Hardware Design

Based on different specific tasks, the hardware of SmartGlove can be divided into three modules: the OLE module, the microcontroller module, and the glove module. The designs for each module are introduced respectively as follows.

5.1.1. OLE Module Design

The OLE module is the sensing module in the system which includes three basic units: the sensing unit (sensor and lens), the interface unit (the customized PCB board), and the housing unit (the customized base plate & strip), as shown in Figure 5-2. The sensing unit is fixed in the housing unit to obtain the displacement of strip and to communicate with the microcontroller through the interface unit.

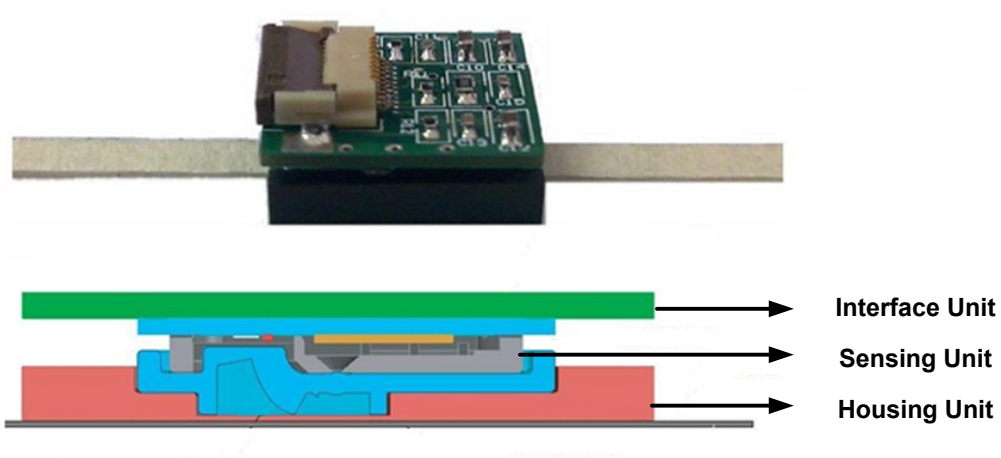

Figure 5-2 OLE & Its Cross Sectional View

1) Sensing Unit (Sensor and lens)

The core sensor used in OLE is Avago's optical mouse sensor product ADNS-3530 [36] as shown in Figure 5-3, which is based on Optical Navigation Technology that measures changes in position by optically acquiring sequential surface images (frames) and mathematically determining the direction and magnitude of movement.

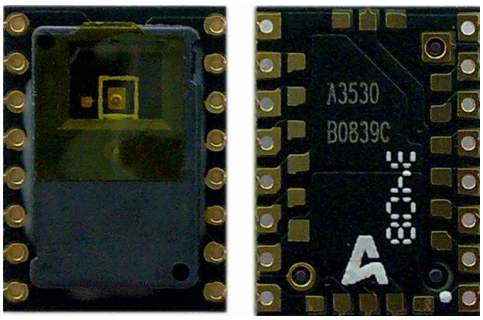

Figure 5-3 Avago ADNS-3530 [36]

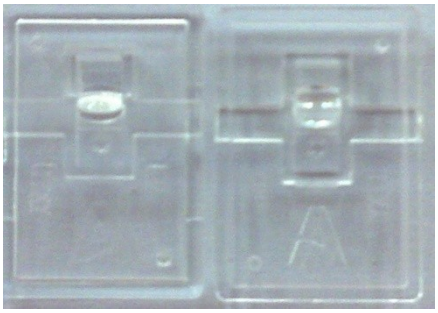

Figure 5-4 Avago lens ADNS-3150-001 [36]

The ANDS-3530 is a compact optical navigation sensor with low-power architecture and automatic power management modes. It is capable of high-speed motion detection – up to 20 inch per second (ips) in velocity and 80m/s^2 in acceleration. All these features make it ideal for the SmartGlove. In addition, it consists of an on-chip oscillator and integrated LED in order to minimize external components. The ADNS-3530, along with the ADNS-3150-001 lens (Figure 5-4) [36], forms a complete and compact linear tracking system. There is no moving part which means high reliability and less maintenance.

The ANDS-3530 contains an Image Acquisition System (IAS), a Digital Signal Processor (DSP), and a four-wire serial port (SPI communication). The working principle of the ANDS-3530 is: the IAS acquires microscopic surface images via the illumination system (Figure 5-5). The acquired images are processed by the internal DSP to determine the direction and distance of motion. The DSP calculates the relative displacements and send them out to the external microcontroller via the sensor serial port. The microcontroller then translates the date into USB or Bluetooth before sending them to the host PC.

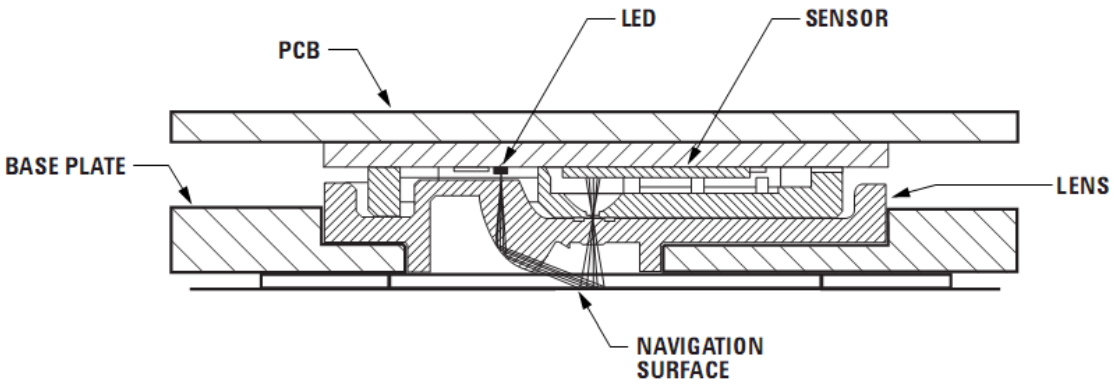

Figure 5-5 Lens and Illumination System [36]

2) Interface Part (PCB)

In order to make the size of the OLE compact, the ADNS-3530 sensor is designed for surface mounting on a PCB board. Based on the recommendation of the official data sheet, the PCB board is designed as shown in Figure 5-6. The latest version has a compact size which is about the same size as ADNS-3530.

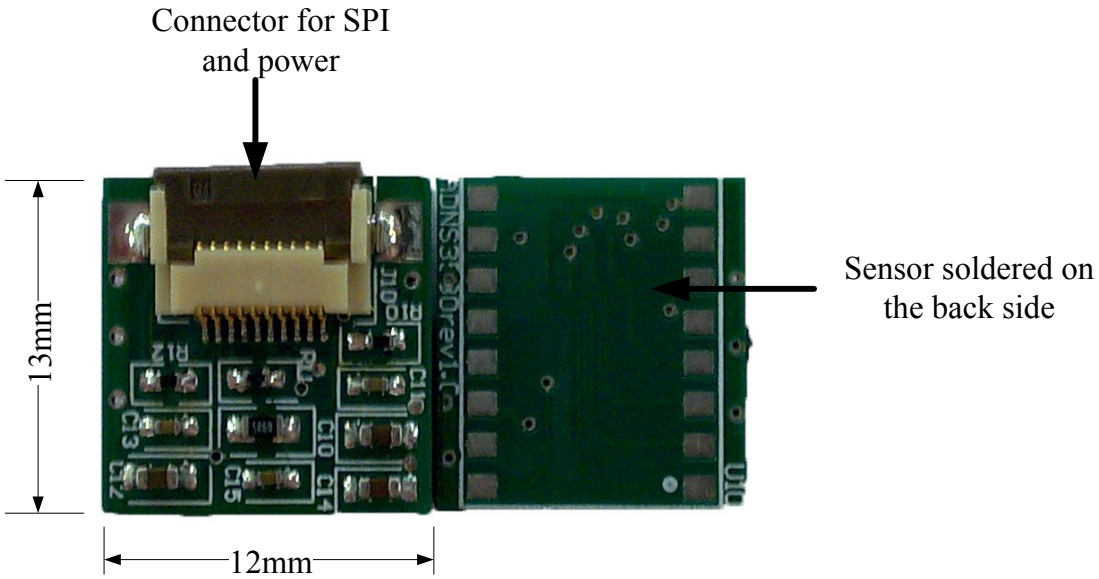

Figure 5-6 OLE Circuit

There are seven output pins in the connector: two pins for 3.3V power supplier and the other five pins for the Serial Peripheral Interface Bus (SPI) which is used for communicating with the microcontroller. The Schematics and PCB layout, and several considerations of PCB and sensor assembly are listed in Appendix A.

3) Housing Unit (Base plate and strip)

The housing unit is the holder for the optical navigation sensor and the moving strip. According to [36], the distance between the lens and the moving strip (z-height) determines the resolution of the result. As shown in Figure 5-7, in order to get high resolution of the sensor, the distance should be within the range of 0.77mm to 0.97mm. Furthermore, the surface material of the strip also affects the sensor's resolution. To make sure the strip sliding smoothly in the housing, there must be a gap between the strip and the base plate. Consequently, for the stable readout, white Formica is the

ideal choice for surface material of the strip because the mean resolution is very stable within the pre-defined range (0.77mm to 0.97mm).

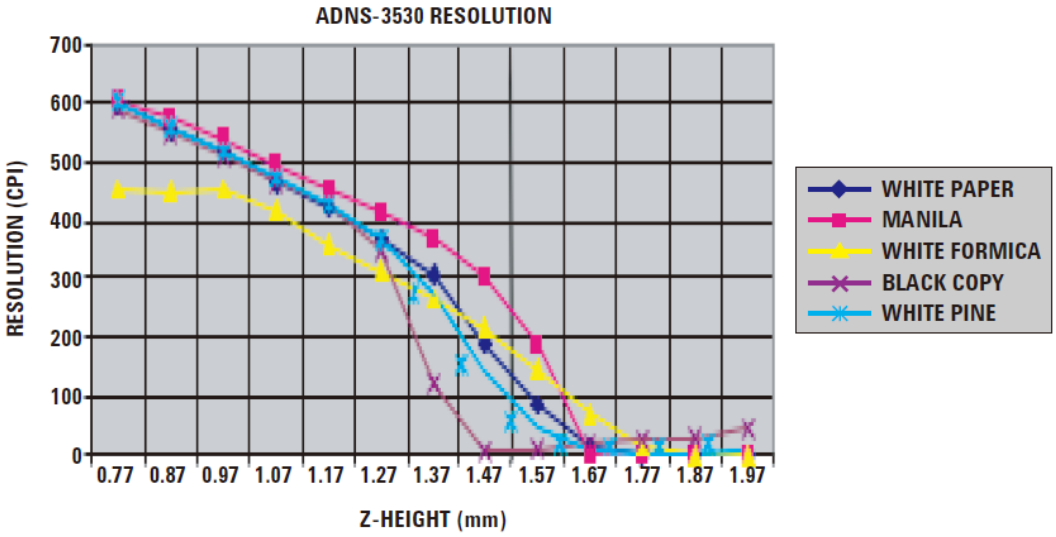

Figure 5-7 Mean Resolution vs. z-height [36]

Taking all the above into design consideration, the strip and the housing are designed as shown in Figure 5-8 (The dimensions of the housing refer to Appendix B.). The bottom slot of the housing is for the sliding strip with a depth of 0.9mm. The material of the housing is Delrin – a high quality engineering plastic used for reel parts and even side plates.

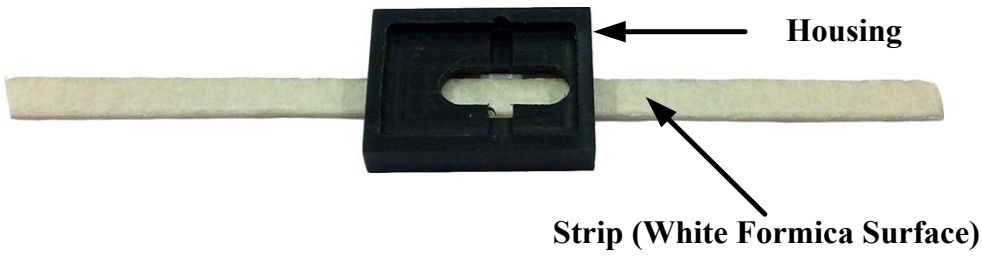

Figure 5-8 Housing and Strip

The detailed assembly drawing with several important dimensions is shown in Appendix C.

5.1.2. Microcontroller

This project uses the Arduino Diecimila [37] (Figure 5-9) as the microcontroller to communicate with the encoder. Arduino is an open-source physical computing platform based on a simple I/O board. The programming language for the Arduino microcontroller is an implementation of Wiring/Processing language.

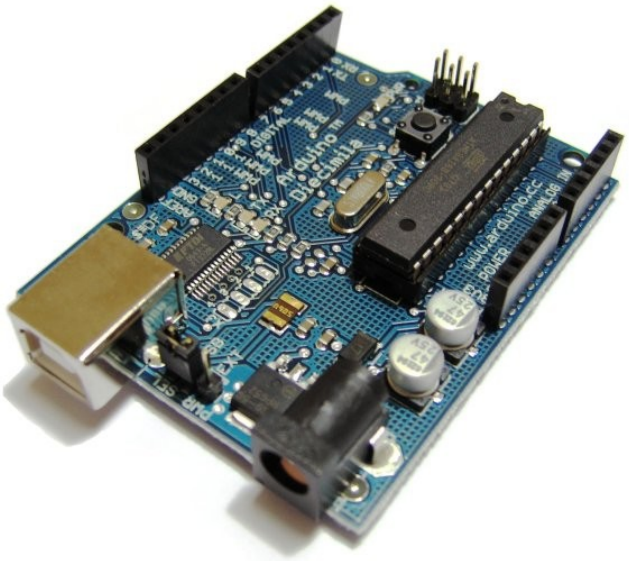

Figure 5-9 Arduino Diecimila [37]

Arduino Diecimila is a microcontroller board based on the ATmega168. The on-board ATmega168 microcontroller has 16K bytes of program memory pre-loaded with boot loader which allows user to download program without additional hardware. The ATmega168 supports SPI communication which can be used to communicate with the mouse sensors.

The Arduino Diecimila has several ways to communicate with a computer. The ATmega168 provides five-volt Universal Asynchronous Receiver/Transmitter (UART) Transistor-Transistor Logic (TTL) serial communication, which is available on the digital receive pin 0 (RX), and transmit pin 1 (TX). An FTDI^{TM} FT232RL chip on the board channels this serial communication over USB and the FTDI drivers provide a virtual COM port for the software on the computer to communicate.

The Arduino Diecimila can be powered either by the USB or by an external power supply of 6 to 20 volts. The on-board USB chip can generate a 3.3 volt supply with a maximum current of 50mA.

In order to connect ten OLEs in an easy way, an interface board (Figure 5-10) is designed to work with the Arduino Diecimila. Because the on-board USB chip can only generate a maximum current of 50mA, a voltage regulator is designed in the interface board to draw 500mA current directly from the USB port to make sure that the microcontroller is able to power up the ten OLEs. For safe operation, open-collector buffers are added to the MOTION pin [36] which is used to get motion signal from the encoder, and voltage translators are added to the four SPI pins (SCLK, MOSI, MISO, and NCS) to avoid the violation of the different voltage level between the microcontroller and the encoder. The detailed schematic drawing and PCB layout of the interface board are in Appendix D.

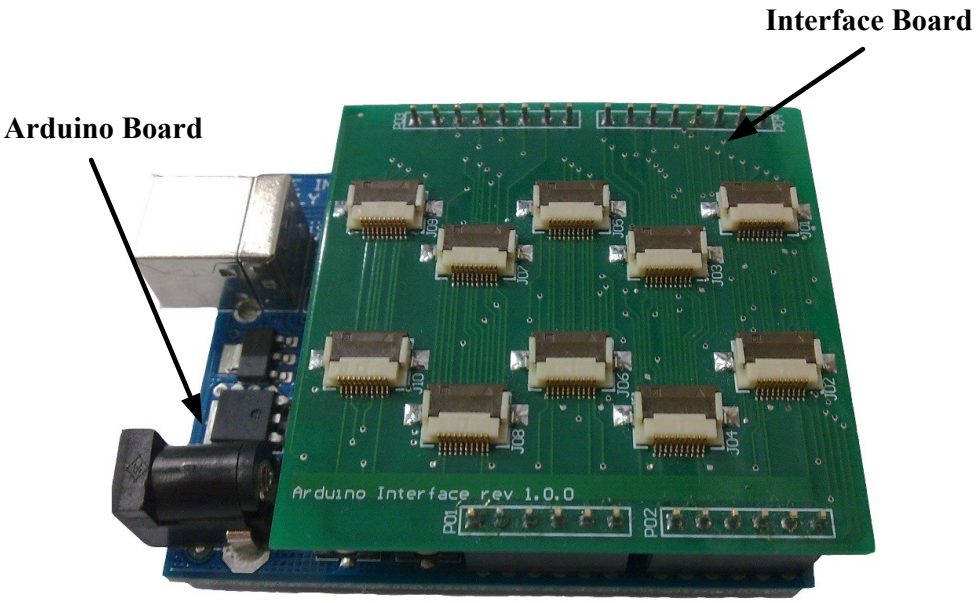

Figure 5-10 Arduino with Interface Board

5.1.3. Glove Design

The layout of OLEs, strips, and the microcontroller is as shown in Figure 5-11. On the back of each finger, there is one strip placed along the finger's midline. One end of the strip is fixed to the dorsoulnar side of the glove (the five dots in Figure 5-11) as mentioned in the multi-point sensing principle. Two encoders are chained by the strip to measure the joint motion on each finger. The microcontroller is placed on the back of the hand.

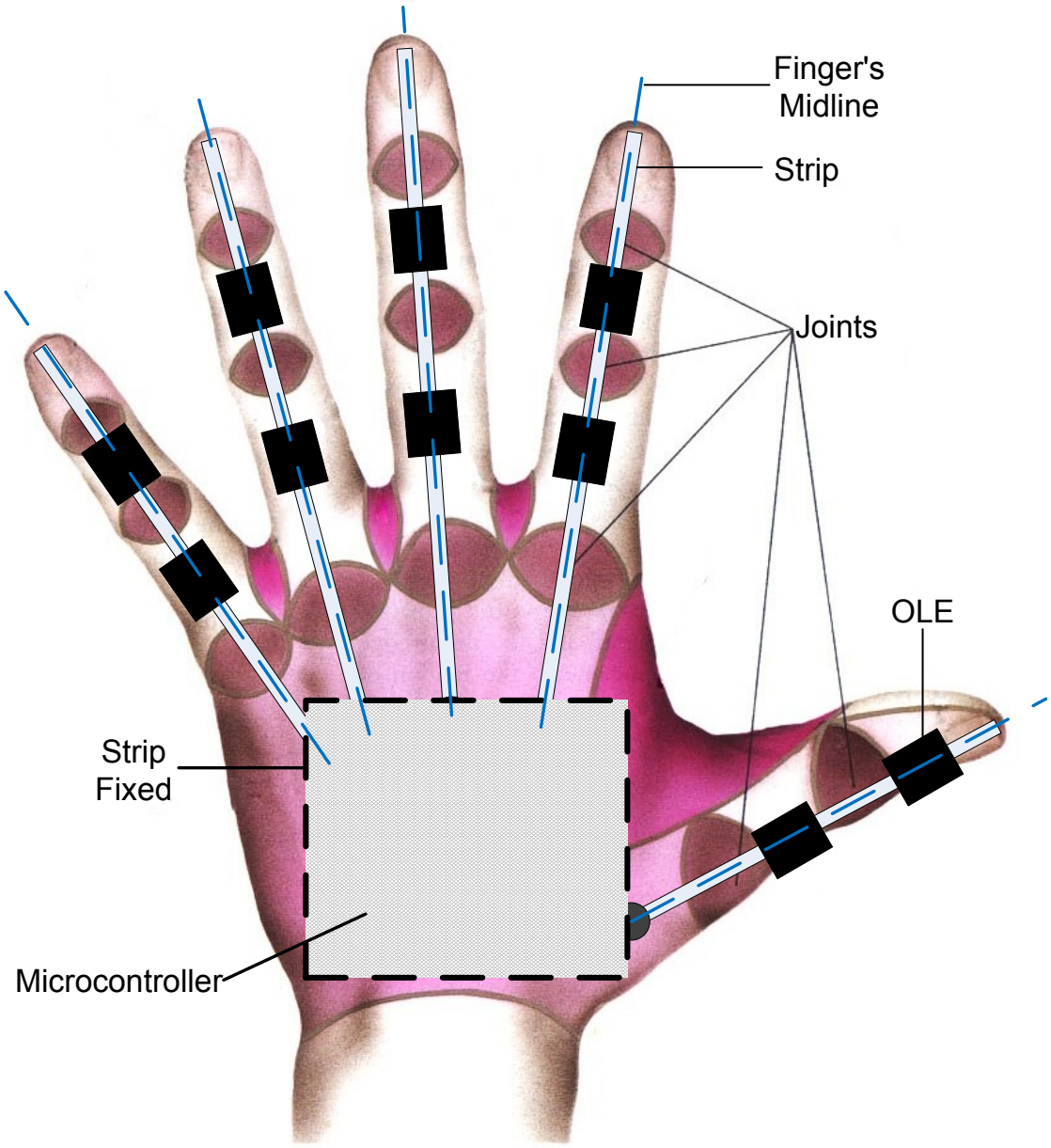

Figure 5-11 Glove Layout

In order to make the glove type OLEs sensitive, the glove should fit nicely on the human hand. At the same time, the glove should not hinder free motions of the hand. Therefore, soft and stretchable fabric is used for the SmartGlove. In this project, two different fabrics are used: the semi-stretching fabric, which can be stretched only in a single direction, and the stretching fabric, which stretches in all directions. The glove uses stretching fabric for backside of the MCP joints and semi-stretching fabric for the palm side to avoid stretching along the finger direction. Thus, the glove has good elasticity to fit the hand of users.

For ease of the replacement or maintenance of the sensors, the OLEs are mounted onto the glove using Velcro and the microcontroller connects OLEs by ribbon wires. Thus, the glove can be separated from the OLEs and the hardware for cleaning. This feature is a significant step towards using data gloves in common daily living.

The photo type of the multi finger sensing device is shown in Figure 5-12.

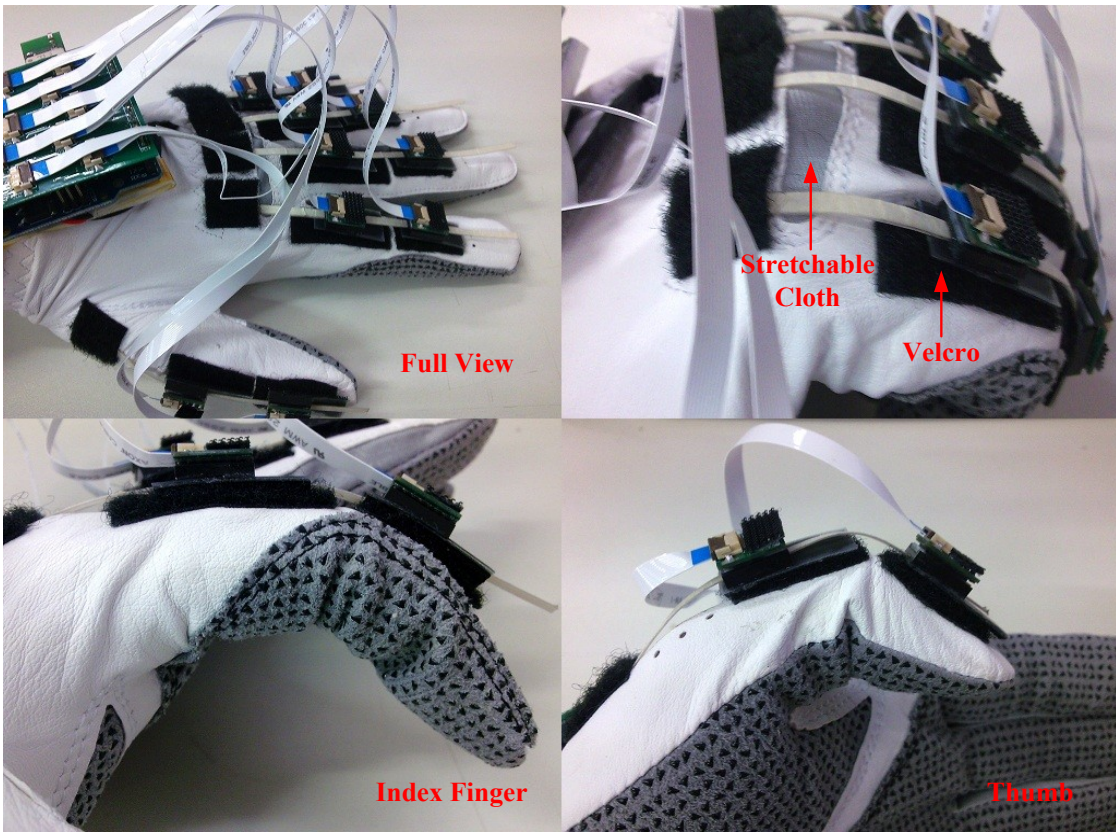

Figure 5-12 Glove Prototype

5.2. Firmware Design

Firmware is a computer program that is embedded in the microcontroller (ATmega168). It is somewhere between hardware and software. Similar to software, it is a computer program which is executed by a microcontroller. It is also tightly linked to a piece of hardware, and has little meaning outside of it. The function of the firmware here is to

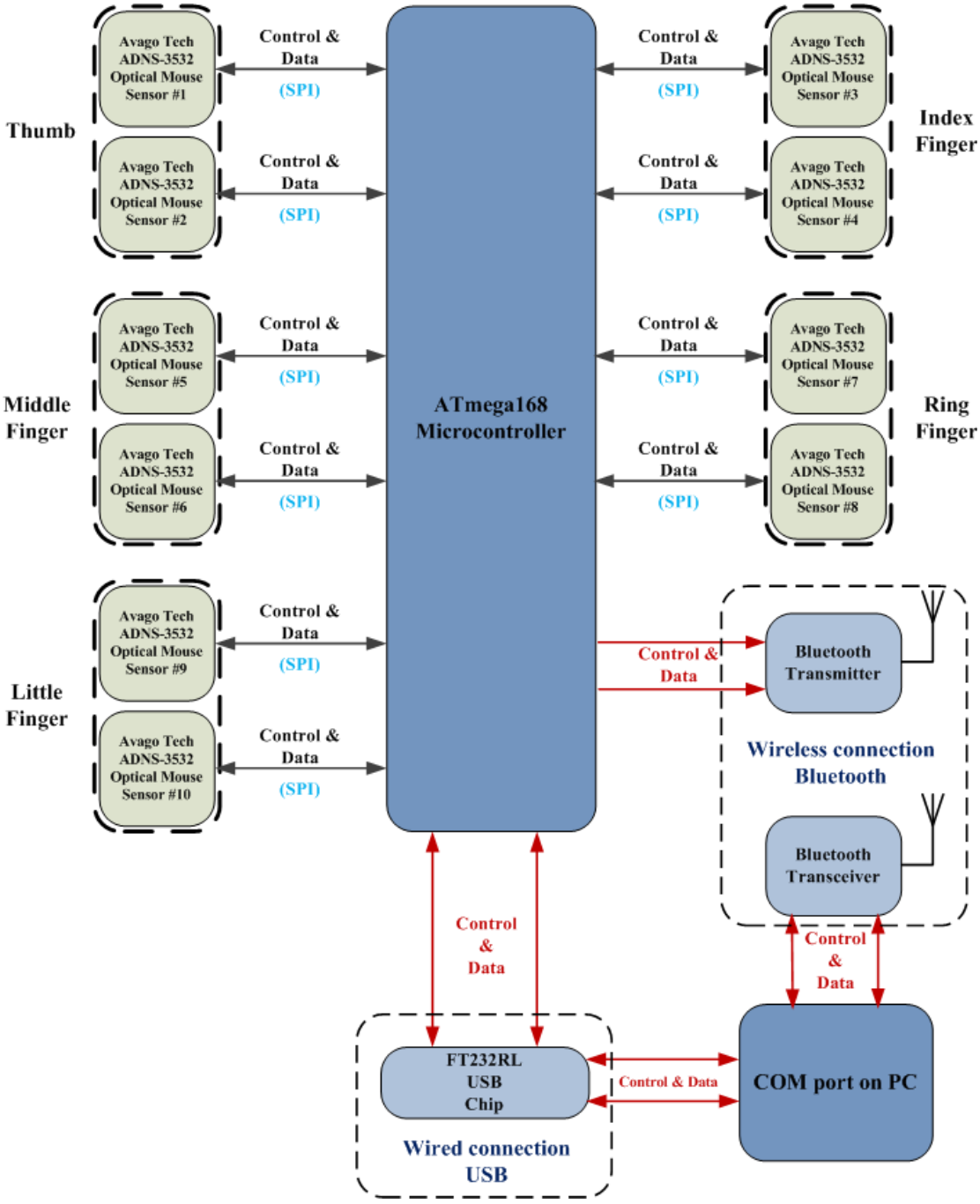

Figure 5-13 Firmware Architecture

communicate with the optical mouse sensor through SPI, including setting up communication, sending enquiry data, receiving displacement data, and sending out received data to PC's COM port. The architecture of the firmware is illustrated in Figure 5-13.

5.2.1. Serial Communication

A serial port is a computer interface that transmits data one bit at a time. In the computer, applications access most serial ports as COM ports. Some USB devices function as virtual COM ports so that application can interface with computer in the same way as physical serial ports. Microcontrollers in embedded systems can use serial ports to communicate with other embedded systems and PCs.

There are several advantages about the serial communication:

- Serial ports can exchange almost any type of information, suitable for applications like reading sensors or other inputs.
- The hardware is inexpensive and readily available. Almost every PC and microcontroller family includes built-in serial ports.
- Other than the Start, Stop, and optional parity bits added to each transmitted byte, serial interfaces assume nothing about the content of the data being transmitted.
- For devices that connect to PC, Windows and other operation systems provide drivers for accessing COM ports.
- Wireless technologies (like Bluetooth) enable transmitting serial data without cables.

Based on these advantages, serial communication is chosen to transmit data from encoders to PC, in wired way (USB) or wireless way (Bluetooth).

5.2.2. Communication Protocol

A communication protocol defines how the bits travel. Based on the specification of the optical mouse sensor, the Serial Peripheral Interface (SPI) is chosen to be the

communication protocol. The SPI bus contains four logical signals: SCLK (Serial Clock, output from master), MOSI (Master Output, Slave Input), MISO (Master Input, Slave Output), NCS (Chip Select, active low, output from master) [38]. Another MOTION pin of the optical sensor is a level-sensitive output that signals the microcontroller when motion has occurred. The SPI bus can operate with a single master device (microcontroller) and multiple slave devices (OLE). An independent NCS signal is required from the microcontroller to identify and select each sensor. As the example of one master and three slaves shown in Figure 5-14, three slaves share the same SCLK, MOSI, MISO and MOTION pin. NCS is identical in order to select the specific slave device when the voltage level is active low. In this case, only one slave can be selected at one time. Thus, the slave devices can only be operated by the master device one by one in sequence. Additionally, the control (SCLK, MOSI, and NCS) and data (MISO, MOTION) signal in each pin can only be transferred in one-way direction (the arrows in Figure 5-14 show the direction of data transfer).

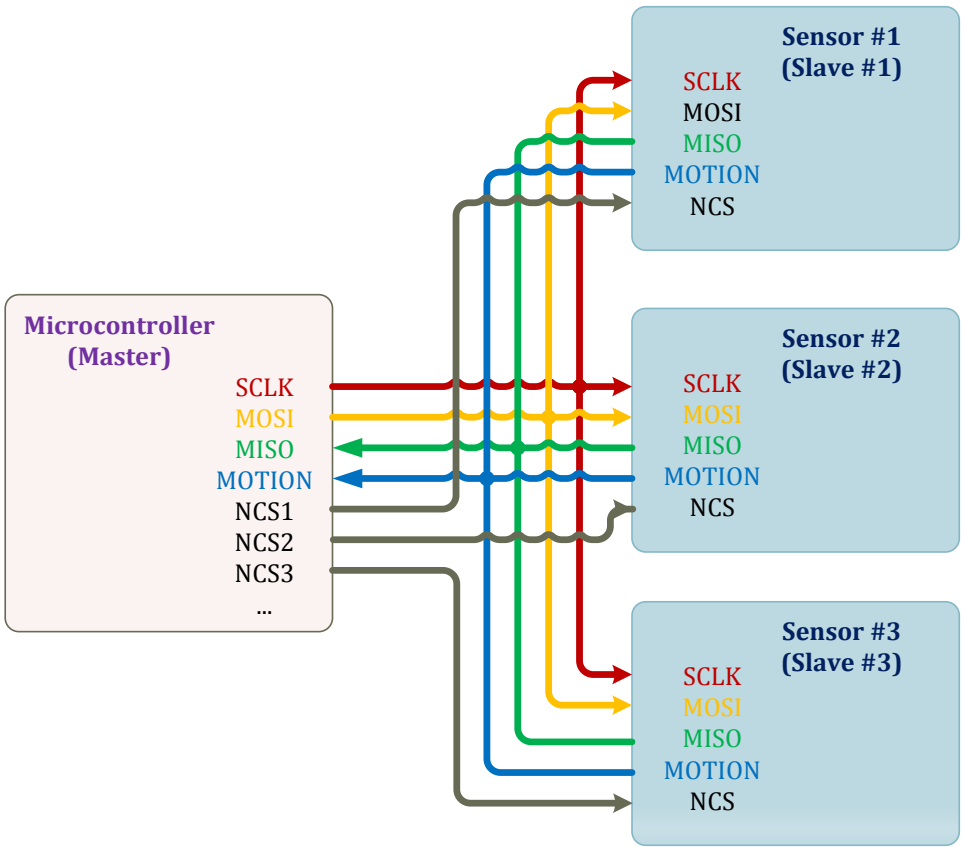

Figure 5-14 SPI Bus: One Master with Three Slaves

5.2.3. Flow Chart

According to the specification of ADNS-3530, the baud rate of the serial communication is 9600bps for USB and 15200bps for Bluetooth, which is defined at the beginning of the firmware.

In the system, the microcontroller needs an acknowledgement after an inquiry is sent from PC, and the PC also needs an acknowledgement after the required data is received. When sending to a PC that has no input buffer or a very small buffer, the PC uses a full handshake to ensure that it is ready to receive a block of data (e.g. sending "I" as an enquiry to the microcontroller). The microcontroller begins by sending a block of data in a certain format (start with a capital letter and a three-digit number) as a reply. The PC receives and sorts the data block based on the first capital letter – "A" refers to the data from the first OLE; "B" refers to the data from the second OLE, etc. (Table 5-1)

Table 5-1 Data Block Structure

Data Form	*A---*	*B---*	*C---*	*D---*	*E---*	*F---*	*G---*	*H---*	*I---*	*J---*
Referred Joint	MCP (thumb)	IP (thumb)	MCP (index)	PIP (index)	MCP (middle)	PIP (middle)	MCP (ring)	PIP (ring)	MCP (little)	PIP (little)
D-H Angle	θ_{13}	θ_{14}	θ_{21}	θ_{22}	θ_{31}	θ_{32}	θ_{42}	θ_{43}	θ_{52}	θ_{53}

The microcontroller will scan ten OLEs as a loop, and the communication with each OLE is identical. Based on the above information, the firmware flow chart for the microcontroller to communicate with one encoder is indicated in Figure 5-15.

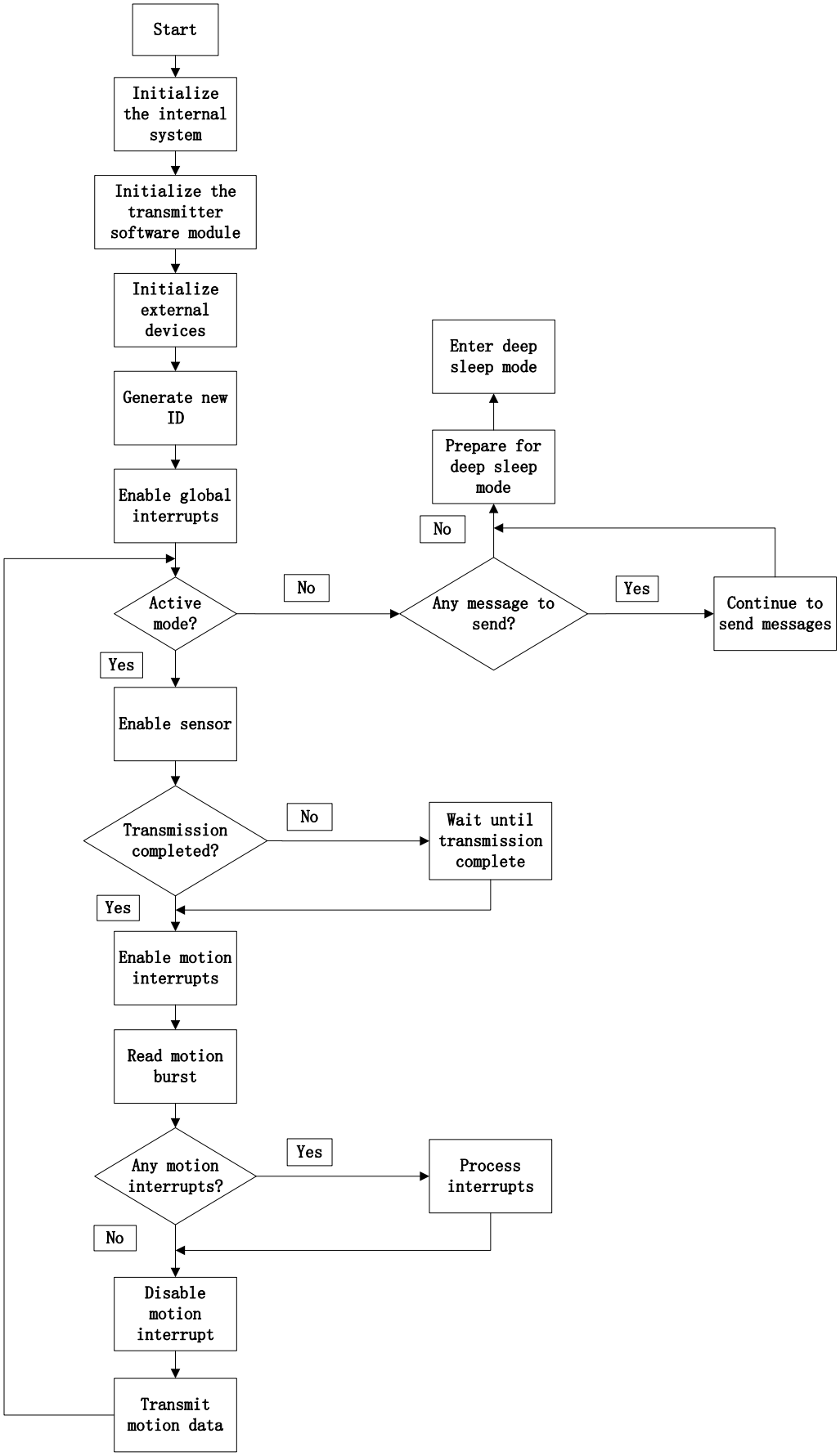

Figure 5-15 Firmware Flow Chart

5.3. Application software Design

In order to be intuitive, real time response is one of the critical issues in the system design. As a consequence, a software application is designed in the OpenGL environment where a 3D virtual hand is displayed and controlled by the SmartGlove directly.

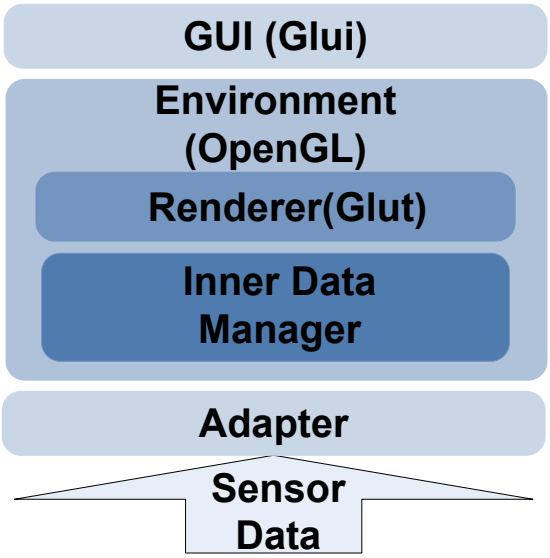

Figure 5-16 Application Software Structure

As shown in Figure 5-16, the application software consists of three components: the Adapter, the 3D Environment and the Graphical User Interface (GUI). The OpenGL environment is the primary part which contains the hand avatar with a defined structure and specific movement constraints [39]. The hand avatar is a 3D object in the OpenGL environment with three spatial coordinates for the position and three angles for the orientation, the setup of the hand avatar is based on the simplified kinematic model (including the FE motion of 14 finger joints as shown in Figure 3-10). There are two subcomponents of the OpenGL environment: the Inner Data Manager and the Renderer.

As mentioned in the firmware design section, the microcontroller gathers data from ten OLEs and converts them into a packet form as in Table 5-1. The Adapter pushes the data packages into the Inner Data Manager. The Inner Data Manager converts the data package and maps the individual OLE's data to the specific joint angle. Meanwhile, the Renderer, which is based on the OpenGL Utility Toolkit (GLUT) library, automatically redraws the 3D scene and generates the hand avatar (Figure 5-17).

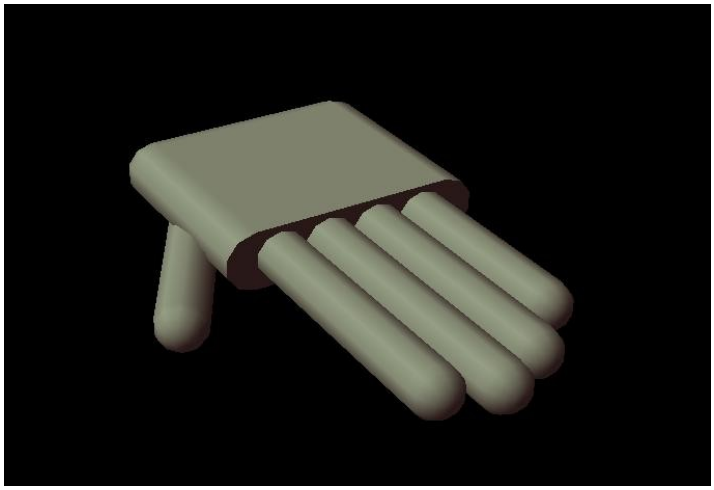

Figure 5-17 Hand Avatar

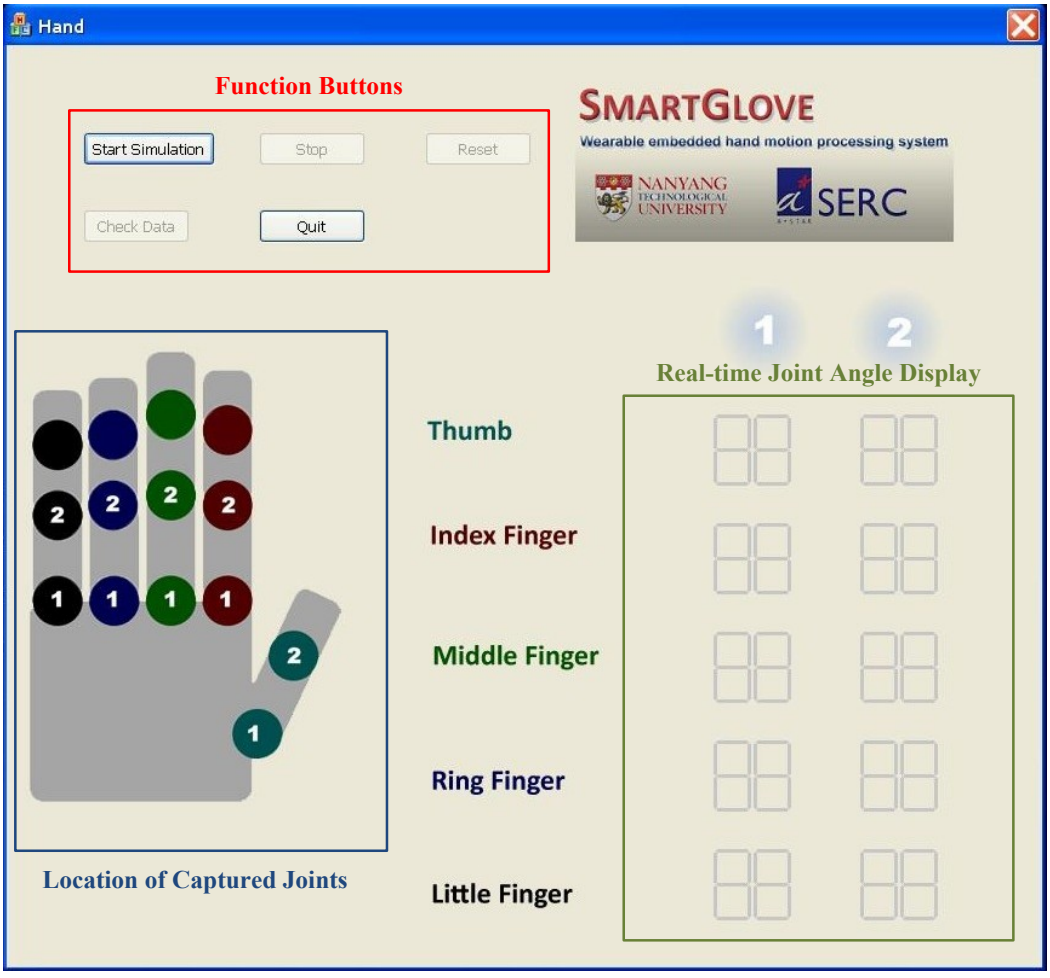

Figure 5-18 Graphical User Interface

Due to the needs for debugging the application software and testing the individual OLE, a control GUI (Figure 5-18) is developed with the GLUT-based C++ User Interface (GLUI) open source library. This GUI has three main function areas which are 1)

Function Buttons; 2) Location of Captured Joints; 3) Real-time Joint Angle Display. There are several control buttons in the function button area, such as starting or stopping the hand avatar simulation, resetting system, checking data and quitting software. After pressing the Start Simulation button, the software will acquire data from ten OLEs. Each OLE's data will display in the Real-time Joint Angle Display area and the 3D hand avatar will move accordingly (Figure 5-19). The notation of each OLE is illustrated in the Location of Captured Joints area with different colors and numbers. The system can be reset by pressing the Reset button in the Function Buttons area. This will clear all the displayed number in the Real-time Joint Angle Display area and initialize the hand gesture (Figure 5-20).

The software also has several additional functions for certain applications. For example, there is a red dot beside the displayed data of every joint which will be turned on if the joint angle of a certain joint exceeds the preset limitation (as shown in Figure 5-19). This function will be useful in training or rehabilitation to monitor the object's motion and give intuitive visual feedback of the abnormal motion. Besides, during one process, the real-time data from each OLE is saved into a text file based on the structure as shown in Table 5-1 and can be opened and checked by pressing the Data Check button (Figure 5-21). The saved data can be used afterwards in hand motion analysis or motion playback.

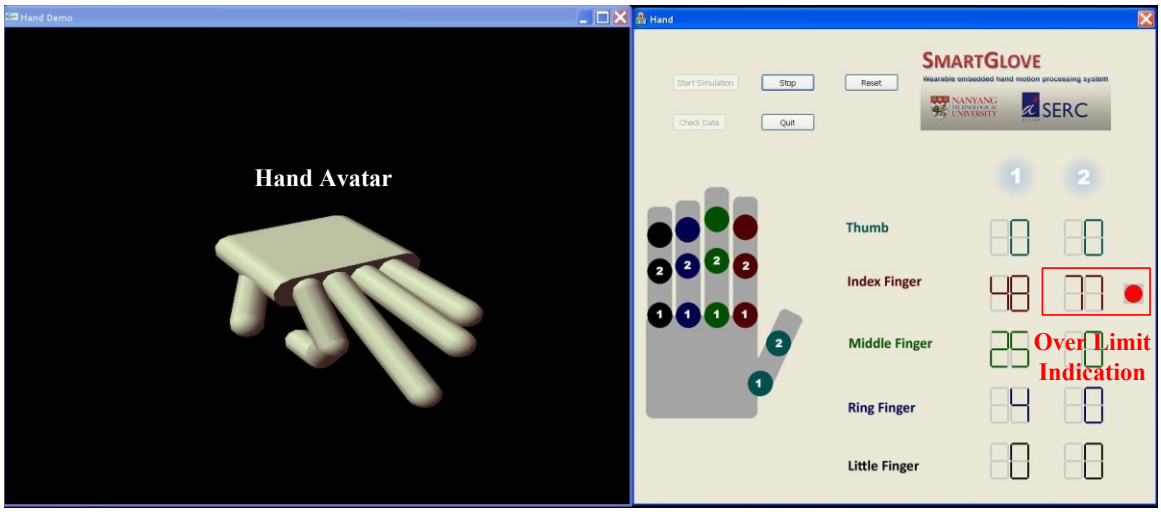

Figure 5-19 Real-time Data Display and Hand Simulation

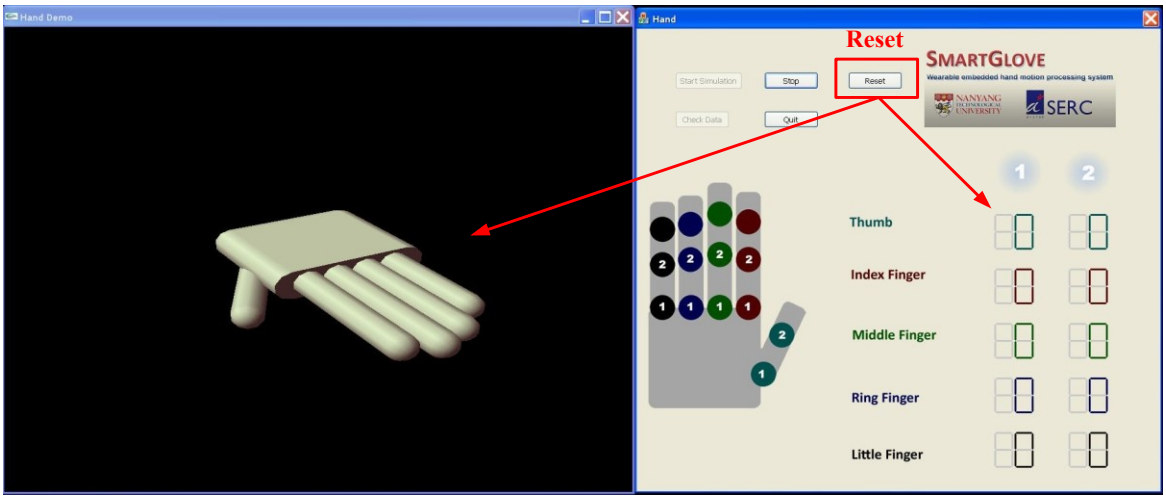

Figure 5-20 System Reset

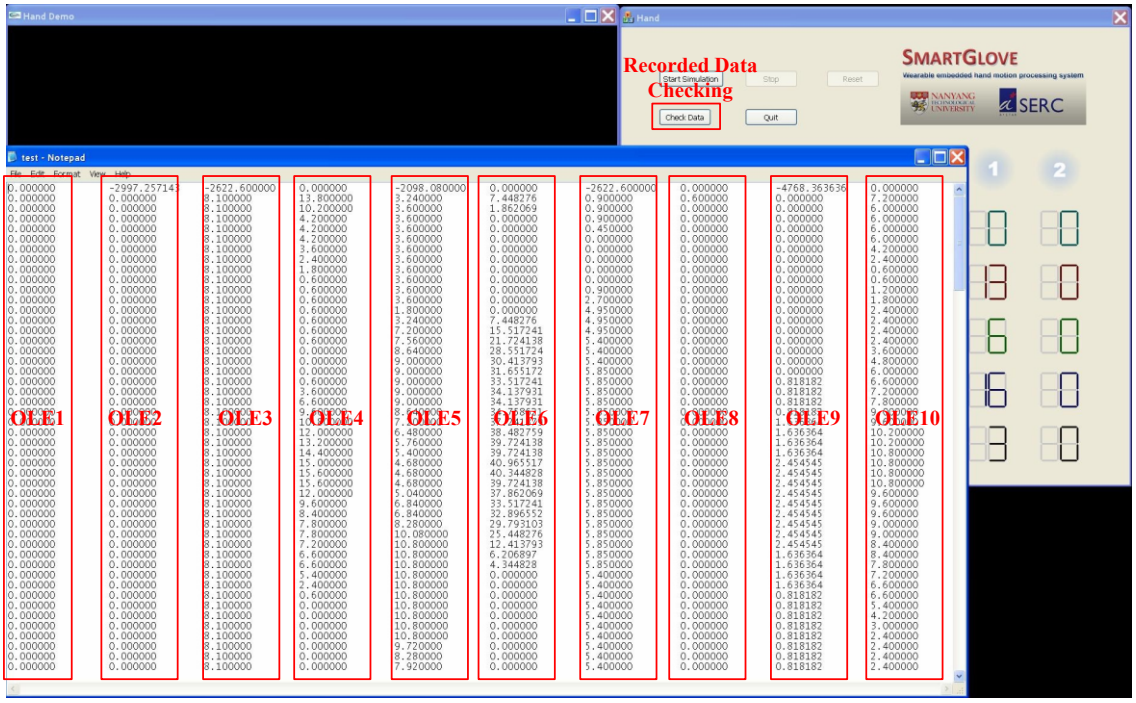

Figure 5-21 Recorded Data Checking

5.4. Discussion

In this chapter, the SmartGlove is described, including hardware design, firmware design, and the application software design.

The hardware design consists of three main parts: OLE module design, microcontroller design, and glove design. In the OLE module design, Avago's optical mouse sensor

product ADNS-3530 is chosen to be the main sensing unit of OLE. This is because of its advantages such as low power, high resolution, fast speed and tiny size. Based on the specifications of the sensor, a customized PCB, a housing unit, and a sliding strip are designed to match the sensor. The final specifications of the OLE module are listed in Table 5-2. From the specifications, it is obvious that the OLE is capable of capturing the normal motion of the finger. As for the microcontroller, Arduino Diecimila, an open-source electronics prototyping platform, is selected to obtain motion data from the OLEs. In order to make it able to communicate with ten OLEs at the same time, an additional interface board with voltage regulator and data buffer units are designed. Lastly, the glove is designed based on the layout of the OLEs and strips. However, the first prototype can only capture the FE motion of finger joints. An improved design is needed for the capture of the MCP joint's AA motion.

Table 5-2 Technical Specifications of OLE

Size	*Weight*	*Data Rate*	*Resolution*	*Linear Speed of the Strip*	*Linear Acceleration of the Strip*	*Power Consumption*
13mm(L) 12mm(W) 4mm(H)	10 g	>100Hz	0.06mm/s	<0.51 m/s	<80 m/s^2	3.6mA

The firmware is programmed based on the SPI protocol and ADNS-3530's preloaded operation commands. The SPI protocol is used in the communication between the microcontroller and the OLEs. The data structure of the final data string which contains displacement information from ten OLEs is also defined.

A presentation software with a 3D hand avatar and GUI is programmed in the OpenGL environment which could provide real-time animation of hand movement and display of joint angle data. There are also several basic functions integrated into the software, such as over-limit indication and data store. However, it is only an early form of the software which needs further improvement based on application requirements. For example, the hand avatar is based on the 14-joint simplified kinematic model that can only show the FE motion of the finger joints. In order to animate the full hand motion, a complete hand avatar based on the 23-joint kinematic model is required. Additionally, other useful functions are not integrated: calibration and playback of the recorded motion, for instance.

CHAPTER 6. CALIBRATION OF SMARTGLOVE

Calibration is a process to find a relationship between raw sensor data captured by the data glove and the actual joint angles of the finger joint, which is necessary for the linear encoder to obtain accurate measurement on different hand sizes. A standard way of doing the calibration is to use external sensors (e.g. vision systems or hand masters) to provide the ground-truth of the measurements. Fischer et al. [40] used a stereo vision system to measure the real 3D positions of the fingertips, while also storing the joint sensor readings of the data glove. The drawback of this approach is that any extra hardware required for calibration will prevent the method from achieving wide-spread usage. Chou et al. [41] also developed a method for CyberGlove calibration, which used linear regression to establish the mappings between joint angle values and raw sensor readings of the CyberGlove. The advantage of this method is the elimination of external devices. However, lacking of enough calibration data for the linear regression, the calibration results are not satisfactorily accurate. Based on the calibration method proposed by Chou et al., a flexible and easy calibration process which can work without complex external sensory devices is designed based on the sensing principle of the linear encoder.

6.1. Notations

The skeleton model has been introduced in Chapter 3. But for now, based on the sensing principle of the multi-point sensing, only FE motion of 14 joints can be measured in one hand. A simplified hand skeleton based on these 14 joints is shown in Figure 6-1.

A notation for the representation of the joint angles in the simplified skeleton model and the sensor data from the OLEs is developed as follows. The FE rotational position of each joint of a finger is represented by θ_{mi}, where m represents the fingers ($m=1$: thumb; $m=2$: index finger; $m=3$: middle finger; $m=4$: ring finger; $m=5$: little finger.) and i represents the number of the joint on the finger m as shown in Figure 6-1 ($i=1$: MCP joint; $i=2$: PIP joint; $i=3$: DIP joint). For example, θ_{11} refers to a rotation around the x-axis of the thumb's MP joint.

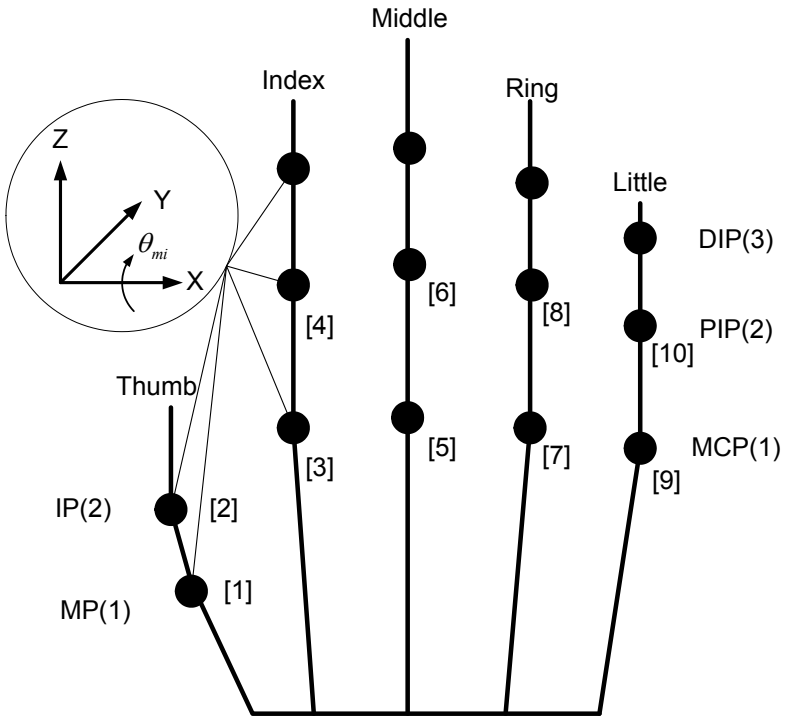

Figure 6-1 Simplified Hand Skeleton Notational Diagram (Left Hand)

Next, notation χ_j (where $1 \le j \le 10$, to denote the 10 OLEs as shown in Figure 6-1) is used to describe the data from a specific linear encoder. For example, χ_6 refers to the reading from OLE 6.

6.2. Data Mapping

As mentioned in Chapter 3, one joint angle may depend on the values of two OLEs (e.g. the FE motion of each finger's MCP joint depends on the values of both two OLEs on that finger.) [41]. These relationships are summarized in Table 6-1 as followed.

Table 6-1 Joint/Encoder Relationships

Joint	*Relation*	*Joint*	*Relation*	*Joint*	*Relation*
θ_{11}	χ_1	θ_{12}	$\chi_1\ \chi_2$	θ_{13}	$2/3\ \theta_{12}$
θ_{21}	χ_3	θ_{22}	$\chi_3\ \chi_4$	θ_{23}	$2/3\ \theta_{22}$
θ_{31}	χ_5	θ_{32}	$\chi_5\ \chi_6$	θ_{33}	$2/3\ \theta_{32}$
θ_{41}	χ_7	θ_{42}	$\chi_7\ \chi_8$	θ_{43}	$2/3\ \theta_{42}$
θ_{51}	χ_9	θ_{52}	$\chi_9\ \chi_{10}$		

6.3. Calibration Model

Based on the two different relationships as described in Table 6-1, calibration of the human finger is divided into two related models, one-to-one mapping and one-to-two mapping. As described in Chapter4, there is a linear relationship between the joint angle and the corresponding OLE's reading. Thus, the linear regression model is adopted to obtain this functional linear relationship as the calibration model.

6.3.1. One-to-One Mapping

In one-to-one mapping, the joint angles of PIP joints and IP joints (as $\theta_{11}, \theta_{21}, \theta_{31}, \theta_{41}$ and θ_{51} mentioned in the data mapping section) which have a one-to-one relationship with an OLE is considered. A simple linear regression model with least squares analysis is used. The general simple linear regression equation can be written as:

$$\theta_A = G_A(\alpha_A + \beta_A \chi_A) \tag{6-1}$$

where $\theta_A \in (\theta_{11}, \theta_{21}, \theta_{31}, \theta_{41}, \theta_{51})$ is the joint angle in radians, $\chi_A \in (\chi_1, \chi_3, \chi_5, \chi_7, \chi_9)$ is the value from the related OLE, α_A and β_A are the regression coefficients, and the G_A is the conversion factor [42].

In the calculation of the two regression coefficients, we define $\chi_A = \chi_A - \overline{\chi_A}$ and $\theta_A = \theta_A - \overline{\theta_A}$ (where $\overline{\chi_A}$ and $\overline{\theta_A}$ as the average value of χ_A and θ_A). Then the equations for G_A, α_A and β_A can be obtained as:

$$\beta_A = \frac{\sum \chi_A \theta_A}{\sum \chi_A^{\,2}} \tag{6-2}$$

$$\alpha_A = \overline{\theta_A} - \beta_A \overline{\chi_A} \tag{6-3}$$

$$G_A = \frac{\overline{\theta_A}}{\alpha_A + \beta_A \overline{\chi_A}} \tag{6-4}$$

.

6.3.2. One-to-Two Mapping

In one-to-two mapping, the FE joint angles of MCP joints (as θ_{12}, θ_{22}, θ_{32}, θ_{42} and θ_{52} mentioned in the data mapping section) which have a one-to-two relationship with the OLEs are considered (as shown in Table 6-1). A multiple linear regression analysis method with least squares analysis is used. The general multiple linear regression equation is defined as:

$$\theta_B = G_B(\alpha_B + \beta_B \chi_A + \gamma_B \chi_B) \tag{6-5}$$

where $\theta_B \in (\theta_{12}, \theta_{22}, \theta_{32}, \theta_{42}, \theta_{52})$ is the joint angle in radians, $(\chi_A, \chi_B) \in ((\chi_1, \chi_2), (\chi_3, \chi_4), (\chi_5, \chi_6), (\chi_7, \chi_8), (\chi_9, \chi_{10}))$ are the values from two related OLEs, α_B, β_B and γ_B are the regression coefficients, and G_B is the conversion factor [42].

In the calculation of the two regression coefficients, we define $\chi_A = \chi_A - \overline{\chi_A}$. $\theta_B = \theta_B - \overline{\theta_B}$ and $\chi_B = \chi_B - \overline{\chi_B}$ (where $\overline{\chi_A}$, $\overline{\theta_B}$ and $\overline{\chi_B}$ as the average value of χ_A, θ_B and χ_B). Then the equations for G_B, α_B, β_B and γ_B can be obtained as follows.

$$\beta_B = \frac{\sum \chi_B^2 \sum \chi_A \theta_B - \sum \chi_A \chi_B \sum \chi_B \theta_B}{\sum \chi_A^2 \sum \chi_B^2 - (\sum \chi_B \chi_A)^2} \tag{6-6}$$

$$\gamma_B = \frac{\sum \chi_A^2 \sum \chi_B \theta_B - \sum \chi_A \chi_B \sum \chi_A \theta_B}{\sum \chi_A^2 \sum \chi_B^2 - (\sum \chi_B \chi_A)^2} \tag{6-7}$$

$$\alpha_B = \overline{\theta_B} - \beta_B \overline{\chi_A} - \gamma_B \overline{\chi_B} \tag{6-8}$$

$$G_B = \frac{\overline{\theta_B}}{\alpha_B + \beta_B \overline{\chi_A} + \gamma_B \overline{\chi_B}} \tag{6-9}$$

6.4. Calibration Methods

As mentioned in the calibration model, in order to calculate the coefficients in Equations (6-1) and (6-5), at least two different angles are needed for each linear encoder. Four simple calibration postures which are easy to perform (Figure 6-2) are

proposed by Rachid Kadouche in order to get two approximately standard angles for each of the 10 linear encoders [43].

- Posture 1 corresponds to an angle of 0°for all the ten measured joints, also the homing position for the ten linear encoders.
- Posture 2 defines the angles for the thumb's MP and IP joints. (θ_{11}=45°; θ_{12}=90°)
- Posture 3 defines a 90° angle for all the fingers' MCP joints. (θ_{21}, θ_{31}, θ_{41} and θ_{51} =90°)
- Posture 4 defines a 90° angle for all the fingers' PIP joints. (θ_{22}, θ_{32}, θ_{42} and θ_{52}=90°)

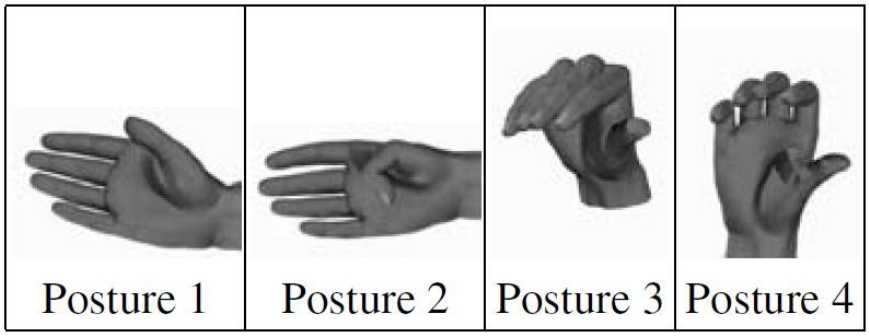

Figure 6-2 Calibration Postures [43]

These four calibration postures are simple and easy to perform, however, the accuracy is not good because there are only two angles (0° and 90°) for each joint to calibrate and also the joints can only approximately reach the desired degree without external tools. Thus, a single-joint calibration, which calibrates each OLE with a specially design calibration tool, is proposed in this project for more precise calibration.

In order to obtain more than two different angles for a single joint, a calibration block with five known angles (0°, 30°, 45°, 60°and 90°) is designed as shown in Figure 6-3. Mechanical drawing is in Appendix E.

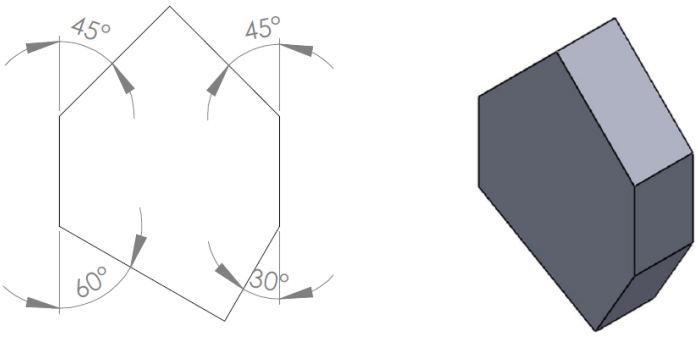

Figure 6-3 Calibration Block

By attaching the finger joint on different edges of the calibration block (Figure 6-4), four standard angles can be obtained. Based on these, a precise calibration for one single joint can be done by resolve Equations (6-2) and (6-6).

Figure 6-4 Calibration Block User Guide

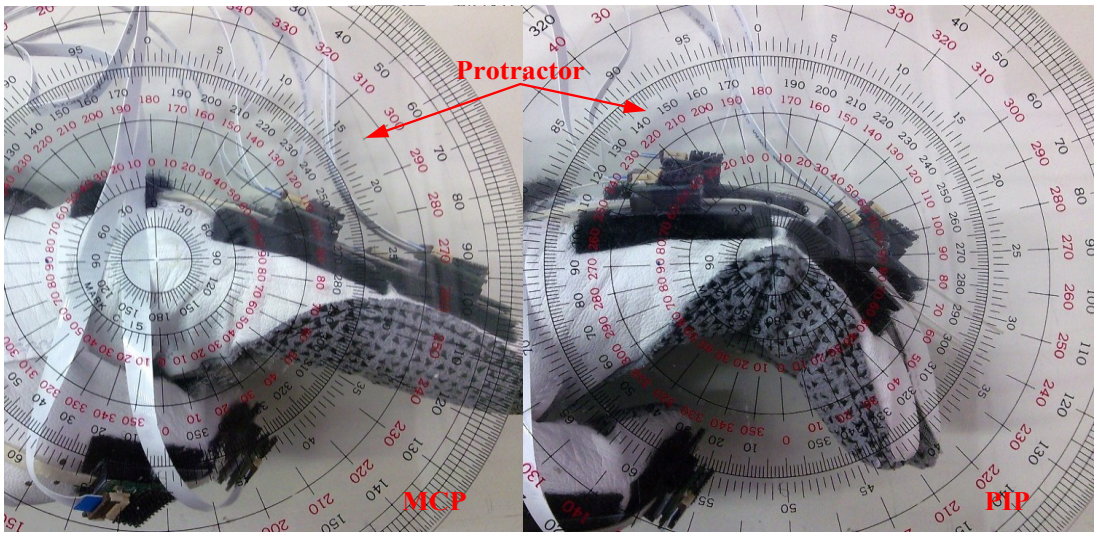

Figure 6-5 Measure Joint Angle by Protractor

6.5. Validation of Calibration Model

The purpose of the calibration validation is to compare the result without any

calibration and the results after the above mentioned two calibration methods. Without loss of generality, only the MCP and PIP joint on the index finger are calibrated. The procedures for calibration verification could be described as follows.

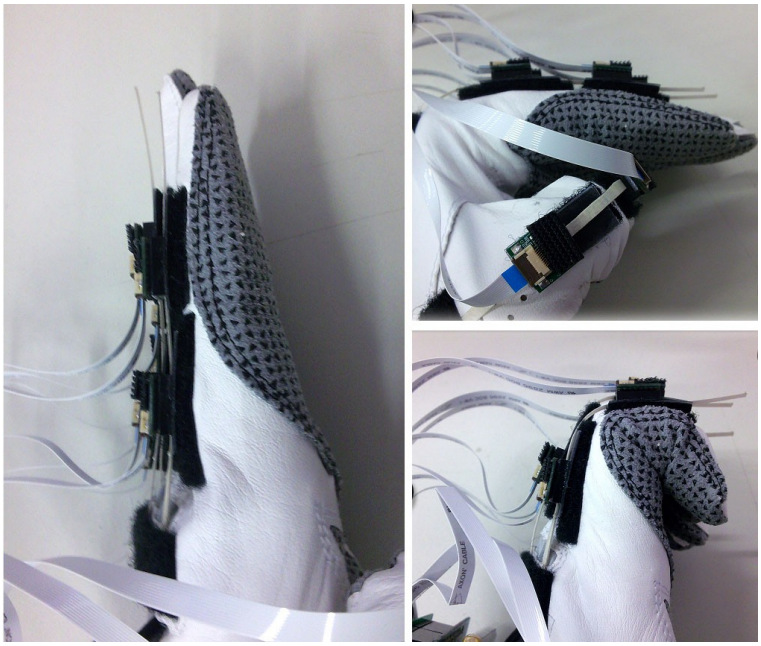

Figure 6-6 Posture1, Posture3 and Posture4

Table 6-2 Calibration Verification Data

		MCP							*PIP*						
Ref.	(°)	0	15	30	45	60	75	90	0	15	30	45	60	75	90
A	Radius (mm)	26.7							23.8						
B	Reading (mm)	0						22.8	0						40.6
C		0	3.7	7.7	11.1	15.3	18.6	22.7	0	6.8	13.8	20	27.3	33.5	40.7

A. Use a vernier caliber to measure the radius of the MCP and PIP joint (Table 6-2). Wear the SmartGlove and use the protractor to obtain seven readings from each joint at 0°, 15°, 30°, 45°, 60°, 75° and 90° respectively (Figure 6-5). The radius and readings are then substituted in Equation (4-5) and (4-6) to generate two sets of angles without calibration (labeled as SetA1 for the MCP joint and SetA2 for the PIP joint) as shown in Table 6-3.

B. As shown in Figure 6-6, perform Posture 1, Posture 3 and Posture 4 to obtain two readings from each joint at 0° and 90° respectively (Table 6-2). Substitute the two readings from the MCP joint (χ_A) in Equation (6-1) to obtain the one-to-one

mapping linear regression equation for the MCP joint.

$$\theta_A = 3.95\chi_A \tag{6-10}$$

Similarly, substitute four readings from both the PIP (χ_B) and MCP (χ_A) joint in Equation (6-5) to obtain the one-to-two mapping multiple linear regression equation for the PIP joint.

$$\theta_B = 5.06(\chi_B - \chi_A) \tag{6-11}$$

Finally, use the protractor to obtain seven readings from each joint at 0°, 15°, 30°, 45°, 60°, 75° and 90° respectively and substitute these readings in Equations (6-10) and (6-11) to generate two sets of angles (labeled as SetB1 for the MCP joint and SetB2 for the PIP joint) as shown in Table 6-3.

C. As shown in Figure 6-4, use the calibration block to obtain five readings from each joint at 0°, 30°, 45°, 60° and 90° respectively (Table 6-2). Substitute the five readings from the MCP joint (χ_A) in Equation (6-1) to obtain the one-to-one mapping linear regression equation for the MCP joint.

$$\theta_A = 3.98(\chi_A + 0.01) \tag{6-12}$$

Similarly, substitute ten readings from both the PIP (χ_B) and MCP (χ_A) joint in Equation (6-5) to obtain the one-to-two mapping multiple linear regression equation for the PIP joint.

$$\theta_B = 5.03(0.05 - \chi_A + \chi_B) \tag{6-13}$$

Finally, use the protractor to obtain seven readings from each joint at 0°, 15°, 30°, 45°, 60°, 75° and 90° respectively and substitute these readings in Equations (6-12) and (6-13) to generate two sets of angles (labeled as SetC1 for the MCP joint and SetC2 for the PIP joint) as shown in Table 6-3.

Table 6-3 Calibration Methods Comparison

		MCP							*PIP*						
Ref.	(°)	0	15	30	45	60	75	90	0	15	30	45	60	75	90
A		0	14.1	28.4	42.5	56.6	70.1	83.9	0	15.5	31.2	46.6	62.3	77.7	93.4
B		0	15.7	31.6	46.8	62.1	76.3	91.2	0	14.7	29.3	44	58.8	73.7	89.1
C		0	14.7	30.8	44.3	61.1	74.5	90.8	0	15.2	30.5	44.7	60.1	74.2	89.8

The deviations of the three sets of angles for the MCP joint (SetA1, SetB1 and SetC1) from the reference angles are plotted as shown in Figure 6-7. Similarly, the deviations of the three sets of angles for the PIP joint (SetA2, SetB2 and SetC2) from the reference angle are plotted as shown in Figure 6-8. It is obvious that both calibration methods (SetB and SetC) can improve the measurement results. Between the two calibration methods, the second one (SetC) by using the calibration block can provide better result.

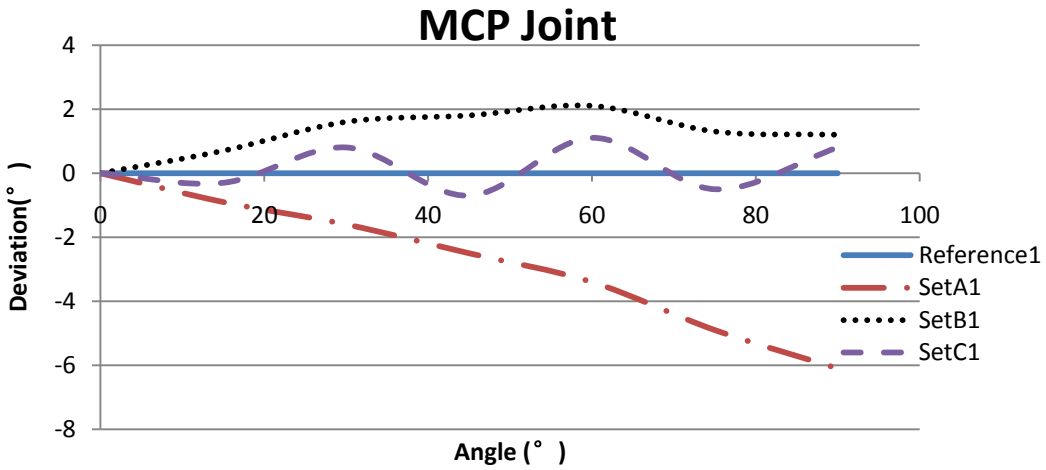

Figure 6-7 Calibration Test Result (MCP Joint)

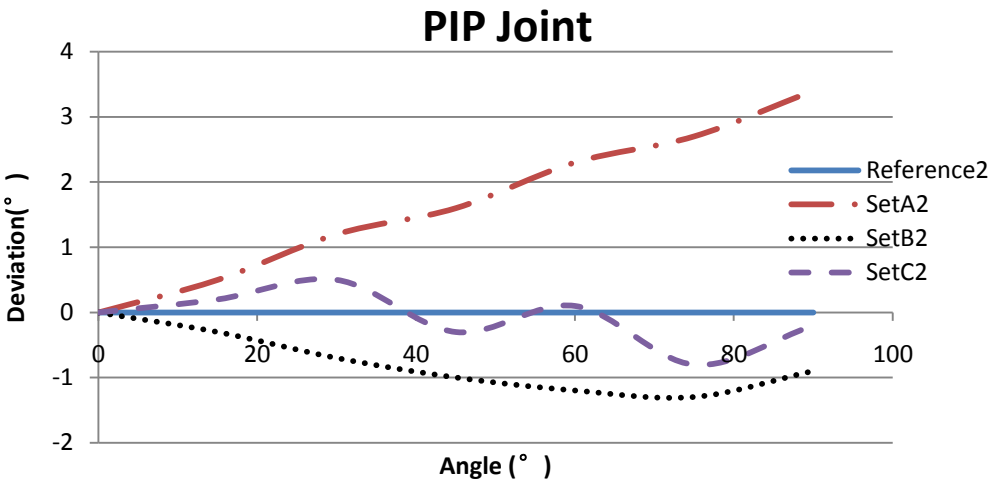

Figure 6-8 Calibration Test Result (PIP Joint)

6.6. Discussion

The general demand for calibration of SmartGlove is that the methods are simple and easy to carry out and can possibly work without complex external sensory hardware.

Two calibration methods are proposed based on this demand. For fast calibration, a protocol with four standard hand postures is able to calibrate all of the ten OLEs roughly. For precise calibration, a special calibration block is designed to calibrate each OLE one by one. The linear regression method is adopted to model the OLE's readings to joint angles. The results of the calibration experiment showed that both methods can improve the accuracy, especially the second tool-based method.

However, both two calibration methods are for the calibration of the joint's FE motion. When the joint's AA motion is able to be captured by the SmartGlove, similar calibration methods for the joint's AA motion will also be our research consideration in the future work.

CHAPTER 7. EXPERIMENTAL VERIFICATION

Based on the completed hardware, firmware and software, it is necessary to conduct a series of experiments to elaborate the performance of the OLE, and verify the design of the SmartGlove. Two kinds of experiments are carried out: OLE characterization tests, and the glove performance test.

7.1. OLE Characterization Test

In order to verify that our innovative OLE is suitable to be used in sensing human finger motion, a series of tests are carried out to characterize the OLE as follows.

7.1.1. Linearity Test

The test on linearity of the OLE signal is carried out first. The purpose of this test is to verify the linearity of the OLE data. The setup of the experiment is shown in Figure 7-1. When the jaw is moving along the scale of the vernier caliper, the reading from the OLE and the displacement of the strip can be recorded. By comparing the two sets of data, the linearity of the OLE reading can be determined.

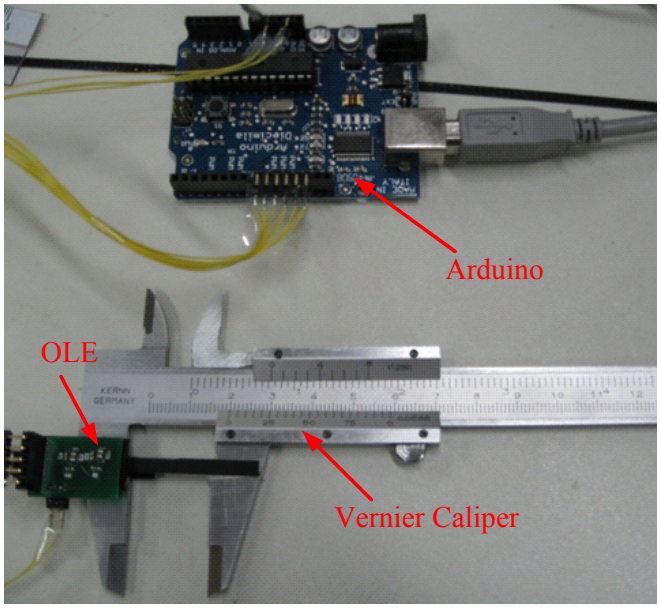

Figure 7-1 Linearity Test

Experimental procedure of the linearity test can be described as follows.

1) Stick the OLE to the fixed jaw of a vernier caliper and stick the other end of the strip to the other jaw of the vernier caliper, calibrate both to zero, wire the OLE to Arduino Diecimila, and connect the Arduino Diecimila to computer through USB.
2) Move the strip from 0 to 20*mm* at an interval of 1*mm*. Read data from the OLE at every interval.
3) Move the strip from 20 to 0*mm* at an interval of 1*mm*. Read data from the OLE at every interval.
4) Repeat step 3) and 4) three times to obtain three sets of data and draw in Figure 7-2.
5) Calculate the average reading at each step upwards from 0 to 20*mm*, as well as downwards from 20 to 0*mm*.
6) Plot the average encoder reading data against the displacement of the strip (read from vernier caliber) in graph (Figure 7-3) and analyze the results.

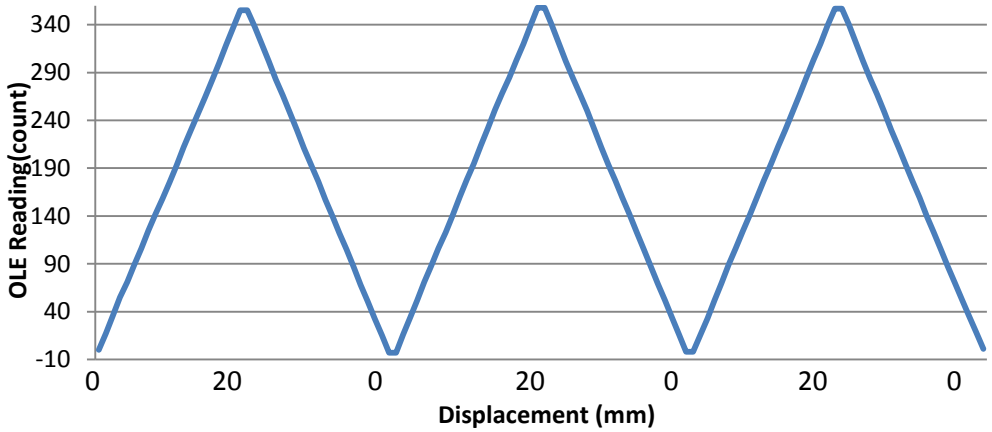

Figure 7-2 Linearity Test Result

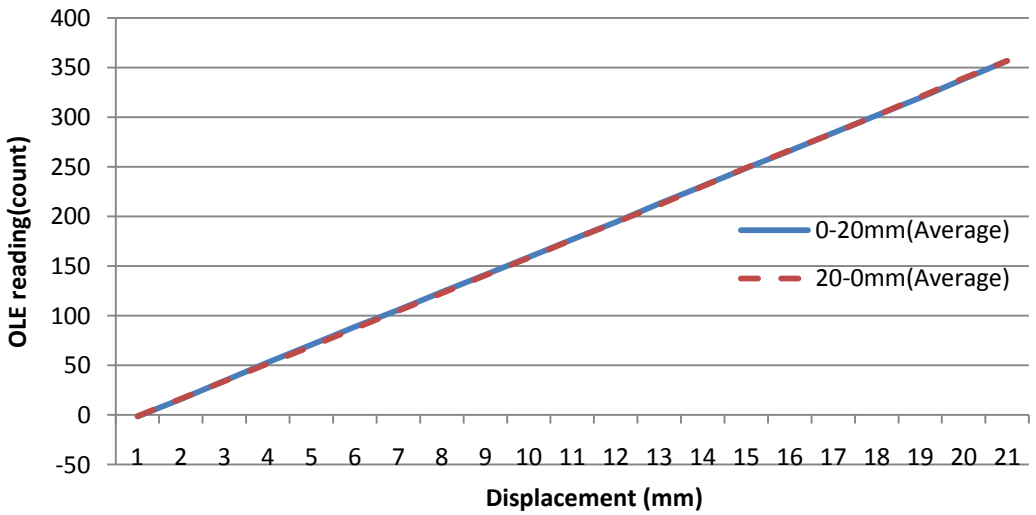

Figure 7-3 Linearity Test Result (Average)

Figure 7-3 indicates that the encoder has good repeatability performance in the linearity test. The above two figures show that both the forward and backward data sets are almost linear in the range of 0 to 20mm, which is the normal range of finger skin deformation when a finger bends.

The slope (*slope1*) of the encoder's average linear test results in Figure 7-3 approximately equals to 18, so the theoretical line can be drawn. Based on this result, the *linearity* of the OLE reading can be obtained as follows:

$$linearity = 1 - \frac{average\ difference}{range} \times 100\% \approx 99.44\% \tag{7-1}$$

7.1.2. OLE Bending Test

The purpose of the OLE bending test is to exam the bending performance of the OLE after the linearity of the OLE data is ensured. In order to eliminate the effect of finger skin deformation, a wooden finger is used in the test. The experiment is carried as indicated in Figure 7-4. The OLE is fastened to the wooden finger with the strip wrapped over the knuckle. When the wooden finger bends, the OLE can read the displacement of the strip, and based on the working principle of the OLE (Figure 4-1), the bending angle could be calculated by Equation (4-1). By comparing the angle captured from the OLE with the angle measured directly from the protractor sticked to the wooden finger, the bending performance of the OLE can be examined.

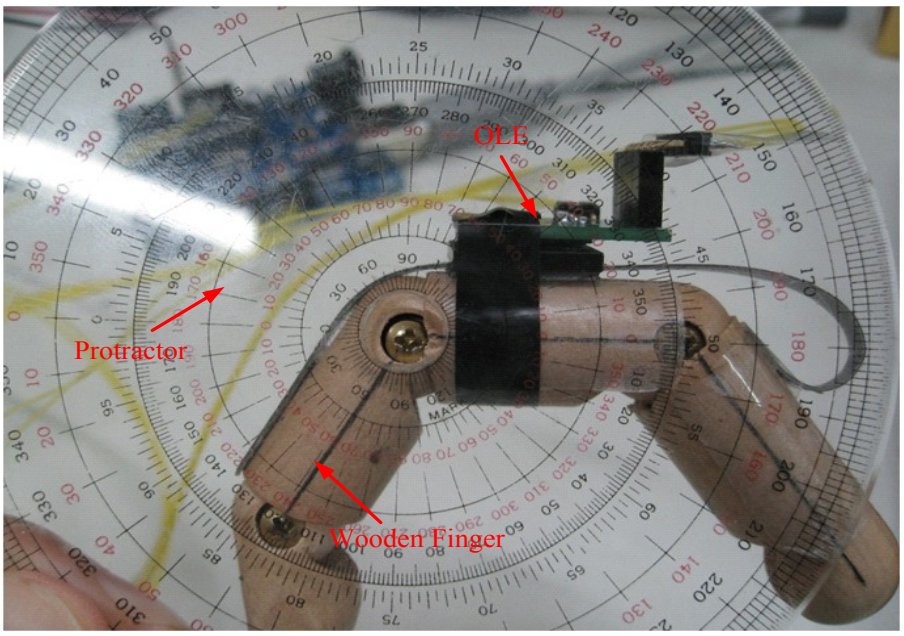

Figure 7-4 OLE Bending Test

The procedure of the OLE bending test is as follows:

1) Fasten the OLE to the back of one rod, wrap the strip over the knuckle and stick the other end of the strip to the neighboring rod.
2) Connect the OLE to Arduino Diecimila.
3) Bend the wooden finger from 0°to 90°at an interval of 5°. Read data from the OLE at each interval.
4) Bend the wooden finger from 90°to 0°at an interval of 5°. Read data from the OLE at each interval.
5) Repeat step 4) and 5) three times to obtain three sets of data and plot.
6) Calculate the average readout at each step from 0°to 90°, as well as from 90°to 0°.
7) Plot the encoder readout data against the angle obtained from the protractor (Figure 7-6).

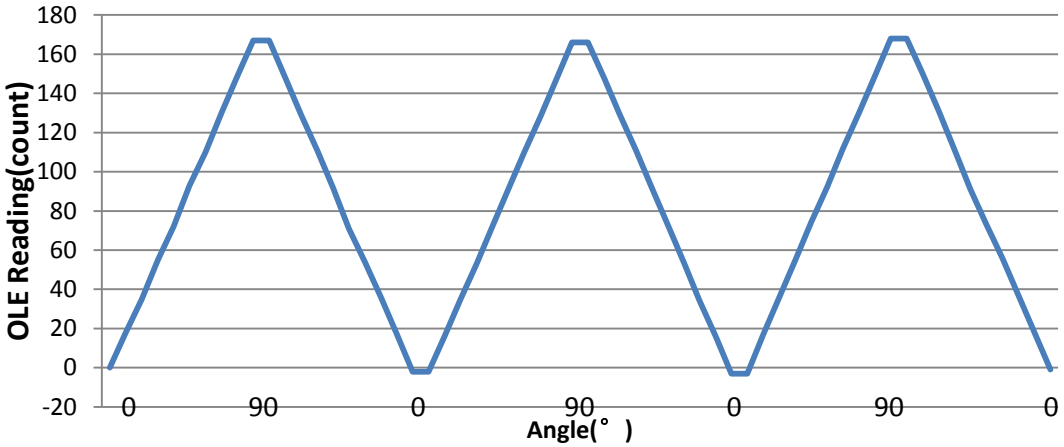

Figure 7-5 OLE Bending Test Result

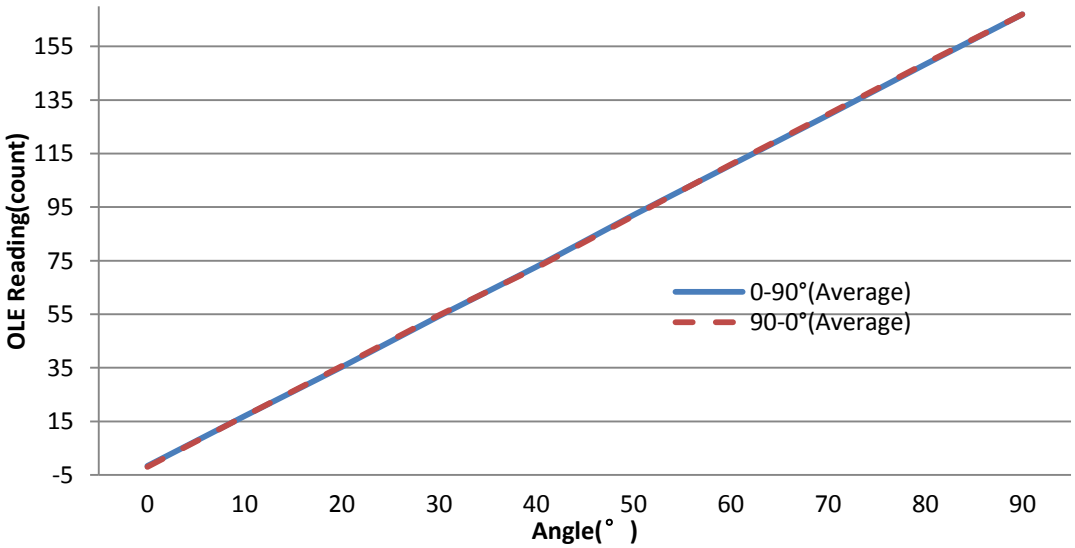

Figure 7-6 Bending Test Result (Average)

Figure 7-6 shows good repeatability, as well as linearity, in the OLE reading in the bending test in between 0° and 90°, which is the normal motion range of finger joints. The slope (*slop2*) of the average bending test result in Figure 7-6 is approximately 1.9. Also, the *linearity* of the OLE reading under bending condition can be calculated as

$$linearity = 1 - \frac{average\ difference}{range} \times 100\% \approx 99.42\% \tag{7-2}$$

The radius of the rotation joint can be obtained from the values of *slope1* and *slope2* by using the equation:

$$R = \frac{360}{2\pi}\frac{\theta}{l} = \frac{360}{2\pi}\frac{slope2}{slope1} = 6.05mm \tag{7-3}$$

(where *slope1* means the value of OLE readout when the strip moves 1mm; *slope2* means the value of OLE readout when the joint bends 1°.). The radius of the rotation joint measured by vernier caliper is *6mm*, which is very close to the value calculated above.

7.1.3. Human Finger Test

The OLE has been demonstrated working in the bending test on a wooden finger. However, the human finger is different from the wooden finger because of the skin deformation which may affect the measure result. Hence, a further test on the real human finger is necessary to test the accuracy of the OLE in deployment status.

The setup of the experiment is as shown in Figure 7-7. The OLE is attached to the first knuckle of the index finger with an accelerometer attached to the second knuckle of the index finger to measure the bending angle of the PIP joint. The palm is placed on a flat metal plate as a stable reference during the test. In the human finger test, the PIP joint of the index finger is bended back and forth three times. In the measurement, data from the OLE and the accelerometer are recorded. By comparing these two sets of data, the linearity of the OLE for actual use can be evaluated.

The model of the accelerometer is LIS3LV02DQ [44], a MEMS inertial sensor from ST microelectronics.

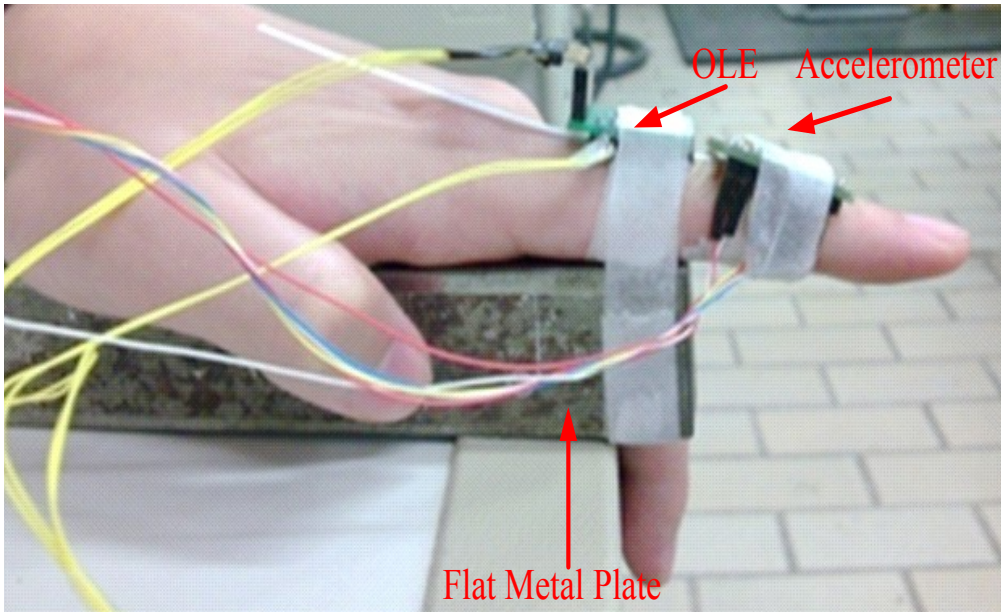

Figure 7-7 Human Finger Test

The procedure for real human finger test is as follows:

1) Attach the OLE to the first knuckle of the index finger; attach the accelerometer to the second knuckle of the index finger.
2) Tape the palm to a metal plate to keep it steady.
3) Connect the encoder and the accelerometer to Arduino Diecimila.
4) Rotate the index finger's PIP joint back and forth three times and obtain two sets of data from both the OLE and the accelerometer (ACC).
5) Convert the obtained two sets of data to angular form and plot them together (as shown in Figure 7-8).

In order to map the output of accelerometer with that of the OLE, both two sensors are connected to the Arduino board. While the finger bends, the microcontroller collects data from the accelerometer and OLE one by one. Thus, the two output plots can be superimposed based on the sensor counts.

Comparing the angular data from the OLE with the angular data from accelerometer (the tilt angle calculated from the three orthogonal acceleration components [45]), it is obvious that the results are very close and the difference between the linear encoder and the accelerometer is within 1°, which indicate that the OLE is suitable for human finger motion capture and can also produce good results.

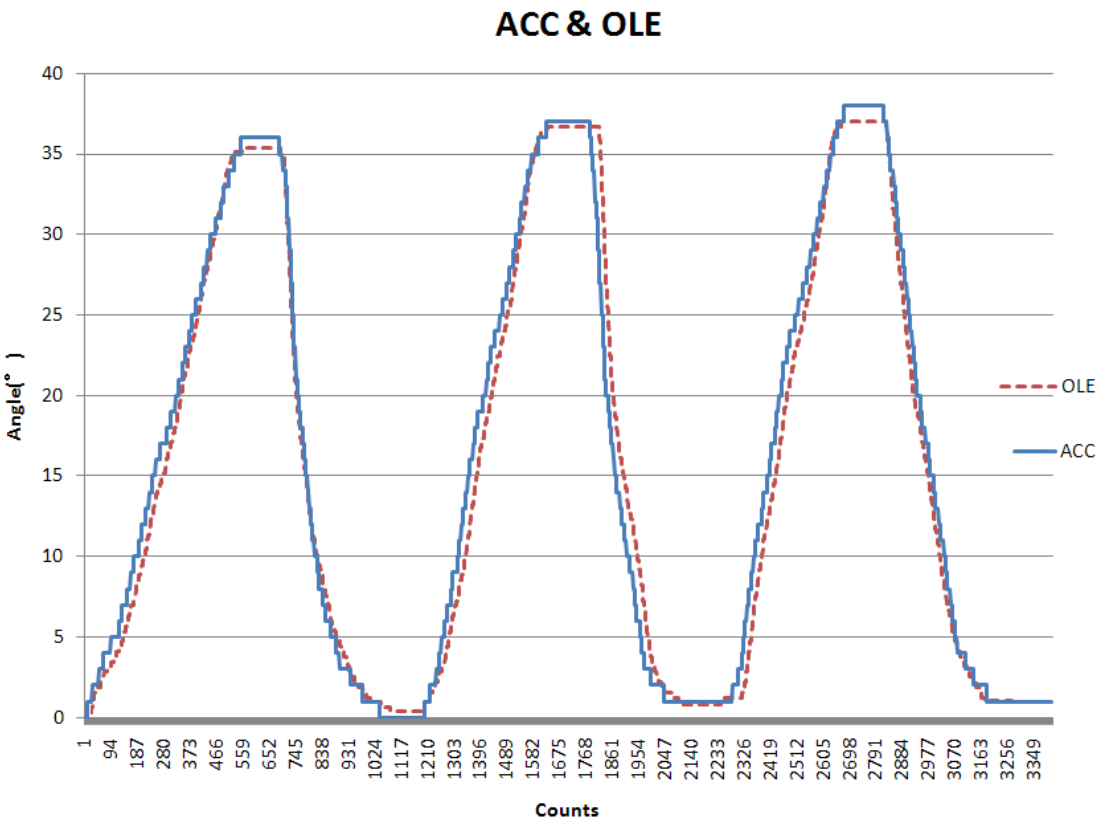

Figure 7-8 Human Finger Test Result

7.2. Glove Testing

The previous three experiments showed that the individual OLE is capable of acting as a sensing unit to capture human finger movements due to good linearity, repeatability and accuracy. The next step is to conduct the glove performance evaluation tests in order to verify the repeatability and reliability of the SmartGlove when ten OLEs work together.

The SmartGlove evaluation procedure adopted in this project is based on the standardized evaluation protocols for sensor glove devices proposed by Wise et al. for the evaluation of Data Glove [46]. Similar tests are also adopted by Williams et al. for SIGMA Glove evaluation [47], by Dipietro et al. for Humanglove evaluation [23], by Lisa et al. for Shadow Monitor evaluation [48], and by Reinhard et al. for a sensor glove evaluation [49].

7.2.1. Material and Subjects

To ensure that every time the finger joints can keep the same posture when gripping an object, a cylindrical metal reference bar is prepared for the grip test so that the relatively same grip characteristics are obtained.

Data is collected from five healthy male students aged 22-27 years with comparable hand size and no hand movement disorders. All subjects are right-handed and the glove is placed on the right hand. Calibration using the calibration block (the second method introduced in Chapter 6) is performed on each subject before the test.

7.2.2. Experiment Protocols and Procedure

The standardized experiment protocols include four tests. However, focusing on repeatability and reliability of multiple measurements over a single data collection session, two tests (Grip Test and Flat Test) are adopted. The Grip Test (uses a gripped hand position) and the Flat Test (uses a flat hand position) are carried out to analyse the repeatability and reliability. Five sets of measurement are performed in each test on each subject and each set of measurement includes ten grip/release actions.

Grip Test

The subject grips the prepared cylindrical reference metal bar (with the radius of 45mm) for six seconds and then releases for six seconds (Figure 7-9). During the release, the subject's hand is placed flat on the table. This grip/release cycle is repeated 10 times. Repeating measurements are taken from each OLE during the grip phase. A single data block is composed of data from ten grip/release actions on one OLE (for instance, Figure 7-12 includes ten data blocks for ten OLEs). The test is repeated five times without removing the glove between successive sets and a total of 50 grip/release cycles are done.

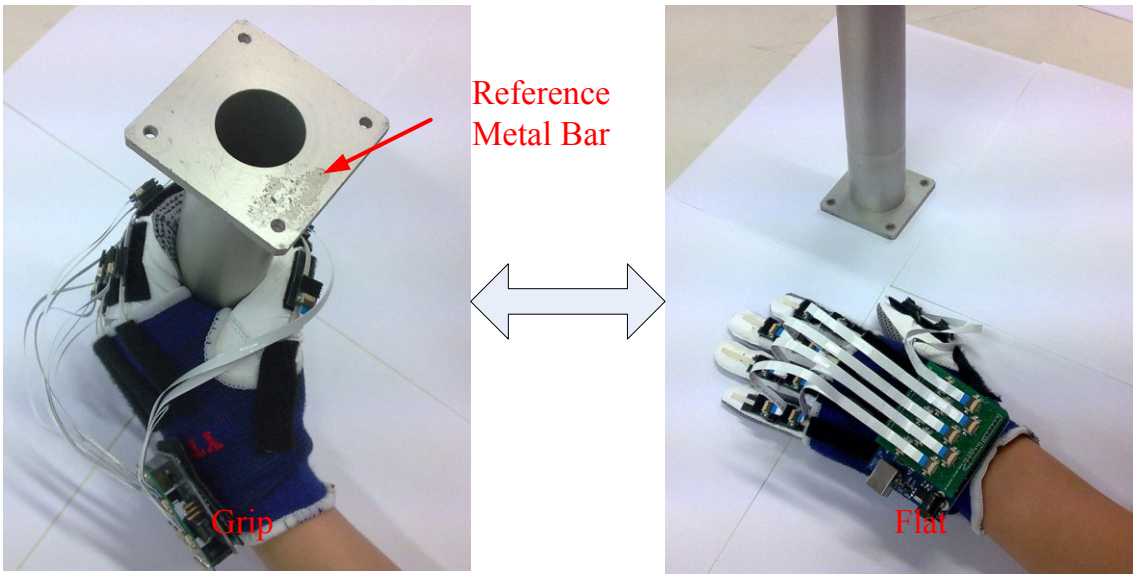

Figure 7-9 Cylindrical Grip Measurement

Flat Test

The subject places the hand on a table and alternately raises the hand and lightly flexed the fingers, and then returns the hand back to the table top (Figure 7-10). Each hand position lasts for six seconds and the flat/flex cycle is repeated for ten times. The repeatability of the flat hand position is explored in this test. In order to keep the hand and fingers in the same position during the flat period, an outline of the subject's hand profile is drawn on a paper and placed on the table. At the flat position, the subject is asked to place the hand and fingers inside this drawn profile as shown in Figure 7-10. The same as the Grip Test, this test is repeated five times without removing the glove between consecutive measurements and a total of 50 flex/flat cycles is done.

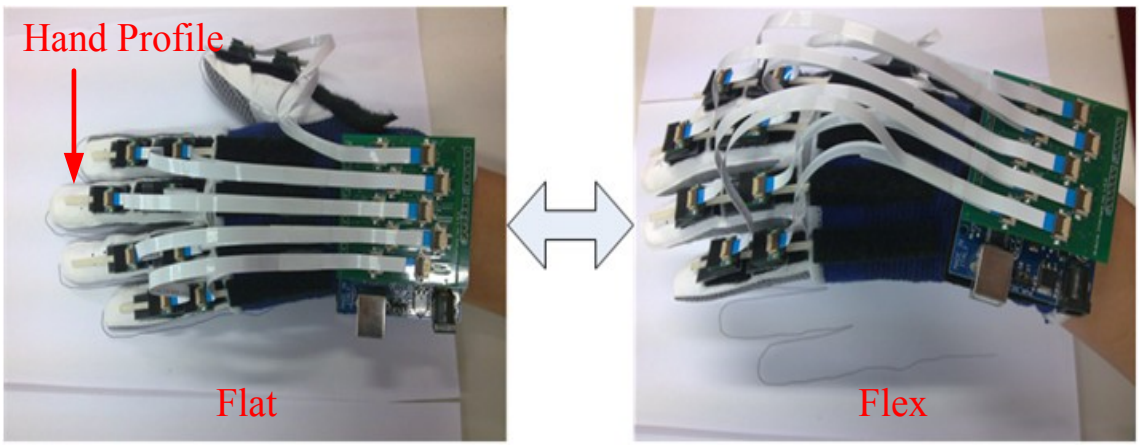

Figure 7-10 Flat Hand Measurement

7.2.3. Statistical Analysis

In each measurement, an array $\{\lambda_{ijk}\}$ is obtained to specify the i^{th} trial in the j^{th} data block which related to the k^{th} encoder, where $i=1,...,10$, $j=1,...,5$, $k=1,...,10$. Two variables are defined:

(1) Average OLE value $\bar{\lambda}_{jk} = \frac{1}{10}\sum_{i=1}^{10}\lambda_{ijk}$;

(2) Range $R_k = (\max_j(\bar{\lambda}_{jk}) - \min_j(\bar{\lambda}_{jk}))$;

(3) Standard deviation (SD) of the $\bar{\lambda}_{jk}$ values;

(4) Average of the SD across the encoders.

For each OLE, the Range and SD are found to be correlated which give an approximate evaluation of repeatability [46].

In order to evaluate the reliability, another statistical procedure is adopted which based on the intraclass correlation coefficient (ICC) [23]. In statistics, the ICC is a descriptive statistic which can be adopted when quantitative measurements are made on objects that are organized into groups. It indicates how strongly objects in the same group resemble each other. A prominent application of ICC is the assessment of consistency or reproducibility of quantitative measurements made by different observers measuring the same quantity. With removing the glove during successive measurements, the data block obtained from each measurement can be treated as different subject samples in the reliability analysis. [50] When the ICC approaches its minimum value of zero, reliability decreases to its minimum value. Contrarily, the reliability increases to its maximum value when the ICC approaches its maximum value of one.

7.2.4. Results

1. Repeatability

A data block is a set of data that includes ten grip/release cycles for each OLE. In the repeatability test, for each subject in each test, ten data blocks are processed to calculate ten averaged angular values for each OLE, as shown in Figure 7-11.

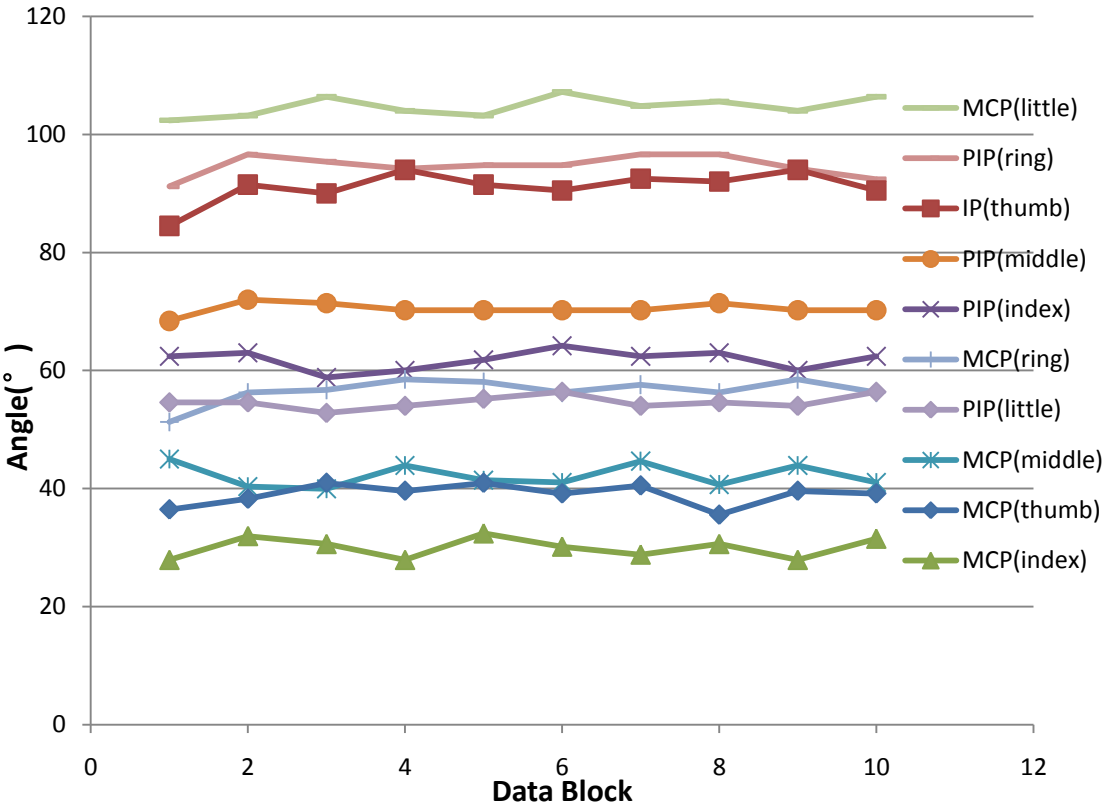

Figure 7-11 Averages of Ten Data Block for a Single Subject for the Grip Test

A sample data block from the Grip Test is shown in Figure 7-12.

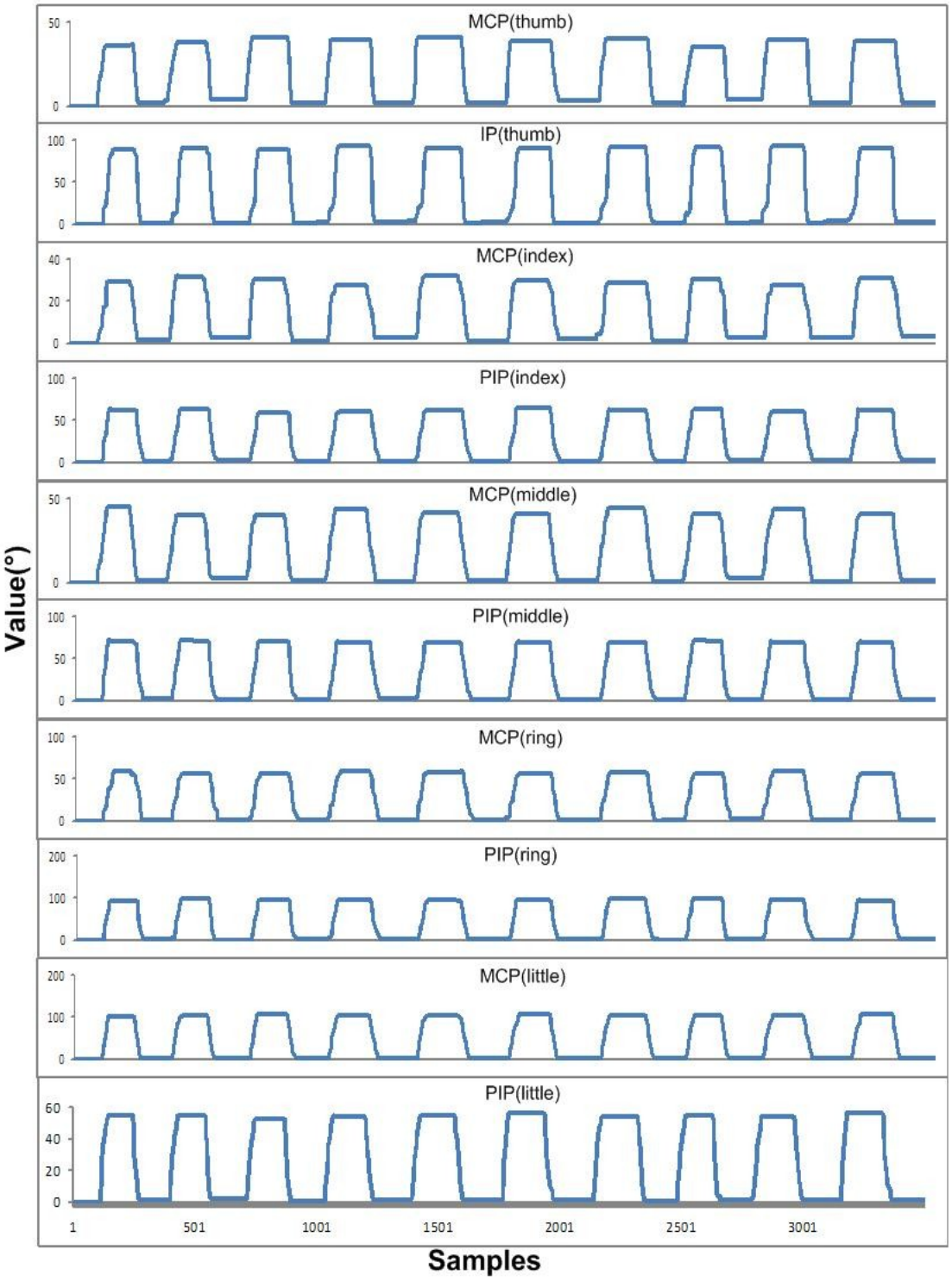

Figure 7-12 Sample Data Block (Grip Test)

Repeatability is generally indicated by the range and standard deviation (SD), consequently, the average range and SD are obtained from each subject in each test as shown in Figure 7-13.

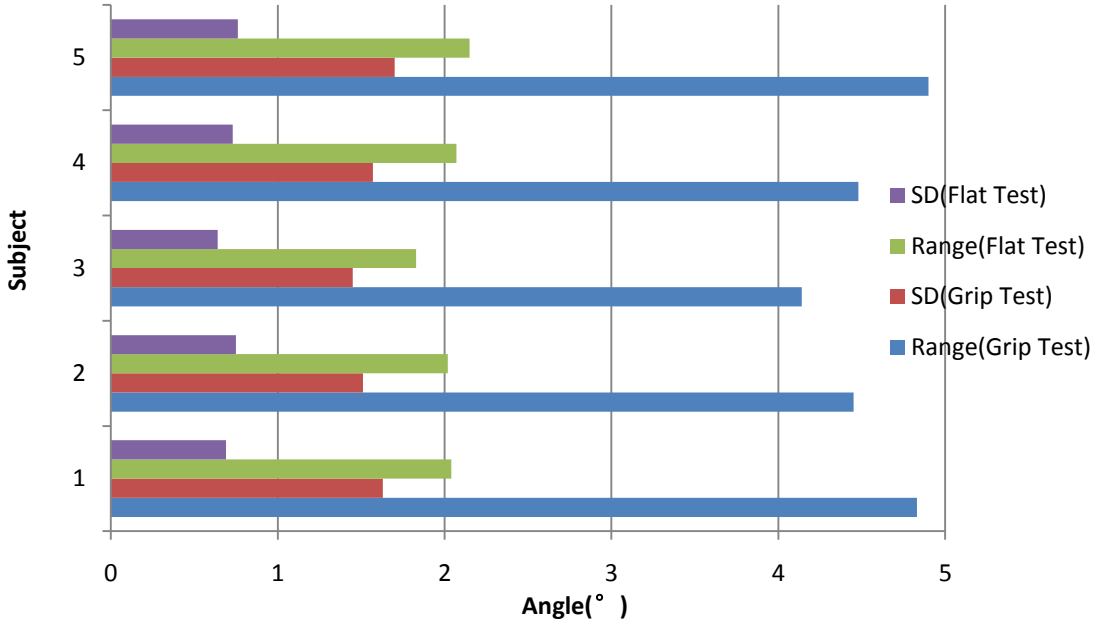

Figure 7-13 Histogram of Averaged Rang and SD for Each Subject and Each Test

Table 7-1 Averaged Range & SD for Each Subject and Each Test

Subject	*Grip Test*		*Flat Test*		*All Tests*	
	Range	**SD**	**Range**	**SD**	**Range**	**SD**
1	4.83	1.63	2.04	0.69	3.44	1.16
2	4.45	1.51	2.02	0.75	3.23	1.13
3	4.14	1.45	1.83	0.64	2.99	1.05
4	4.48	1.57	2.07	0.73	3.27	1.15
5	4.90	1.70	2.15	0.76	3.53	1.23
Average	4.56	1.57	2.02	0.71	3.29	1.14

From Figure 7-13, it is obvious that in all cases, the average flat hand repeatability (from the Flat Test) for all subjects is better than the grip repeatability (from the Grip Test). Average repeatability test for all the five subjects in the Grip Test is $\sigma = 1.57°$ and in the Flat Test is $\sigma = 0.71°$, for an total average of $1.14°$. Similarly, averaged range result for the Grip Test is $4.56°$, and for the Flat Test is $2.02°$, for an total average of $3.29°$.

Looking into each OLE across Subjects 1 to 5 for each test, the histogram of Figure 7-14 summarizes the performance.

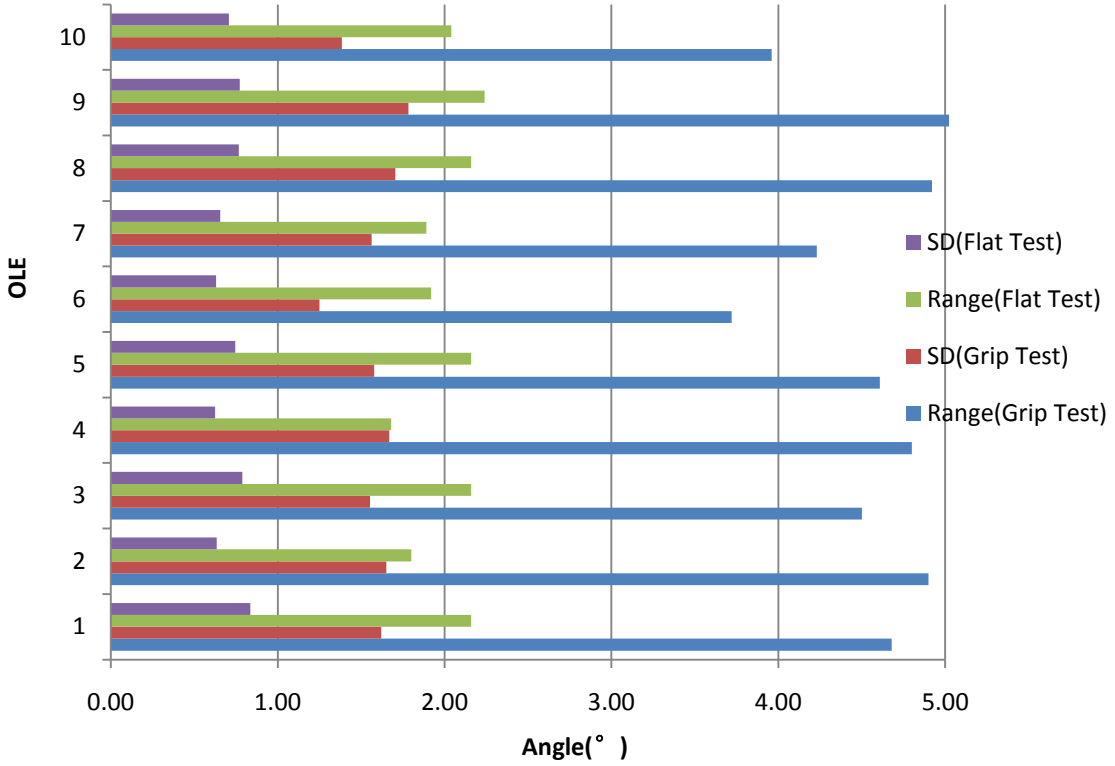

Figure 7-14 Histogram of Averaged Range and SD for Each OLE

The above histogram indicates that the performances of OLEs on different joints are similar, with maximum range= 3.76°, minimum range= 2.82°, overall average range= 3.29° and maximum SD=1.28°, minimum SD= 0.94°, overall average SD= 1.15°. Detailed data is shown in Table 7-2.

Table 7-2 Averaged Range & SD for Each OLE

OLE	*Grip Test*		*Flat Test*		*All Tests*	
	Range	**SD**	**Range**	**SD**	**Range**	**SD**
1.MCP(thumb)	4.68	1.62	2.16	0.83	3.42	1.23
2.IP(thumb)	4.90	1.65	1.80	0.63	3.35	1.14
3.MCP(index)	4.50	1.55	2.16	0.79	3.33	1.17
4.PIP(index)	4.80	1.67	1.68	0.62	3.24	1.15
5.MCP(middle)	4.61	1.58	2.16	0.74	3.38	1.16
6.PIP(middle)	3.72	1.25	1.92	0.63	2.82	0.94
7.MCP(ring)	4.23	1.56	1.89	0.65	3.06	1.11
8.PIP(ring)	4.92	1.71	2.16	0.77	3.54	1.24
9.MCP(little)	5.28	1.78	2.24	0.77	3.76	1.28
10.PIP(little)	3.96	1.38	2.04	0.71	3.00	1.05
Average	4.56	1.58	2.02	0.72	3.29	1.15

2. Reliability

As stated before, reliability is indicated by intraclass correlation coefficient (ICC). ICC analysis is performed for each test and for each OLE individually (ICC is calculated using Excel). As shown in Table 7-3, for the Grip Test, the average ICC for ten OLEs ranged from 0.882 to 0.987 with an overall average of 0.947. For the Flat Test, the average ICC for each OLE ranged from 0.893 to 0.979 with an overall average of 0.953. The combined average of ICC for the Grip Test and the Flat Test is 0.95. The ICC values in Table 7-3 show consistency from one data block to another with no particular OLE showing significant lower reliability than the overall mean.

Table 7-3 Intraclass Correlation Coefficient of Reliability

	Thumb		*Index*		*Middle*		*Ring*		*Little*		*Average*
	MCP	**IP**	**MCP**	**PIP**	**MCP**	**PIP**	**MCP**	**PIP**	**MCP**	**PIP**	
Grip Test	**0.937**	**0.954**	**0.882**	**0.963**	**0.913**	**0.987**	**0.948**	**0.957**	**0.969**	**0.964**	**0.947**
Flat Test	**0.955**	**0.968**	**0.893**	**0.966**	**0.908**	**0.976**	**0.955**	**0.968**	**0.958**	**0.979**	**0.953**
Combined											**0.950**

7.3. Discussion

In this chapter, several tests are carried out to evaluate the characteristics of the OLE as well as its performance when attached on the glove.

The linear relationship between the final digital signal and the real bend angle is a desirable characteristic for the OLE. Unlike strain gauges or fibre optic sensors which need a signal conditioning circuit that proportionally converts the sensor resistance into voltage signals and an A/D converter which digitize the voltage signal, the optical mouse sensor used in this project has an integrated DSP which can directly send out digital signal of the relative displacement value. In this case, the OLE designed for this project can provide better linearity. The results from the linearity test and OLE bending test also show that the OLE's linearity is high under both flat condition (99.44%) and bending condition (99.42%).

Another desirable characteristic is the OLE's accuracy, which is mandatory for the final measurement. It is evaluated in the human finger test. Measuring the same joint's bending angle, the OLE shows satisfactory accuracy against the accelerometer (within 1°). This result also shows that the OLE is able to measure the human hand motion effectively.

While many commercial and non-commercial sensor gloves exist, only a few studies systematically address their repeatability and reliability follow the same standard protocols proposed by Wise et al. As in Table 7-4, compared to the previous four studies, the SmartGlove shows relatively good results in both repeatability and reliability and also lies within the measurement reliability of manual goniometry [46].

Table 7-4 Comparison of Repeatability Results

Glove Tested	*Grip Test*		*Flat Test*		*Total*		*ICC*
	Range(°)	**SD**	**Range(°)**	**SD**	**Range(°)**	**SD**	
Wise et al. (1990) data glove (VPL Research) [46]	6.5	2.6	4.5	1.6	5.5	2.1	0.94
Dipietro et al. (2003) human glove (Humanware) [23]	7.47	2.44	3.84	1.23	5.66	1.84	0.7~1.0
Simone et al. (2007) shadow monitor [48]	5.22	1.61	1.49	0.5	3.36	1.05	0.95
Reinhard et al. (2008) WU Glove [49]	6.09	1.94	2.61	0.86	3.85	1.4	0.93
SmartGlove	**4.56**	**1.57**	**2.02**	**0.71**	**3.29**	**1.14**	**0.95**

CHAPTER 8. CONCLUSION & FUTURE WORK

8.1. Contribution

This thesis documents the development of the SmartGlove based on a novel sensing technology, including the design of OLE which uses the optical mouse sensor as the basic sensing unit to measure joint's flexion, the design of the firmware for microcontroller to communicate with OLEs and gather displacement data, the glove with Velcro that OLEs can be attached to, the calibration methods for both rough and precise calibration, and lastly, the presentation software and GUI for 3D animation and data display. The main contributions of this thesis are summarized as follows:

1. Modeling of the Full Hand Kinematics

Human hand is the most articulated, but also the most constrained part of the body. The high dexterity of the hand also means the large numbers of DOFs need to be captured. Within the hand's relatively small space, there are 23 DOFs with five in the thumb, four in each finger and another two in the palm. In this project, a full hand kinematic model with these 23 DOFs is developed as a basic reference for the full hand motion capture. The modelling of the palm's two DOFs is the major improvement of this kinematic model compared to the normal kinematic model for robotic hand or hand motion capture. For now in the first stage of the project, because of the limitation of the OLE, only a simplified model with 14 joints' FE motion is adopted. In spite of this, the full hand kinematic model is still important to produce realistic hand animation (the DOFs cannot be captured now can be computed by the software). Also, the full hand kinematic model guides the direction for further improvement of the SmartGlove.

2. Novel Sensing Unit for SmartGlove

As introduced in the literature review, several technologies have been adopted to do the hand motion capture for the last three decades. Nowadays, the most popular technologies used are strain gauges and fibre optics, with advantages and disadvantages. Aiming at a low-cost but high performance glove-based hand motion capture device,

this project introduces a novel way which uses the optical mouse sensors to capture human hand joint's flexion. The special designed OLE based on the optical mouse sensor has characteristics such as high resolution (can detect the strip's motion up to *20 inch/s* in linear speed and *80 m/s*^{2} in acceleration), fast speed (at least *150Hz*), low power (*3.6mA*), and low cost (*US$50* per OLE). In the characterizations tests, the OLE also showed good linearity (*99.44%* in flat condition and *99.42%* in bending condition), repeatability and accuracy (within *1°* compared to the accelerometer) in deployment status. Additionally, the OLE has a compact size (*13mm×12mm×4mm*) and light weight (*10g*) which make it easy to attach on the glove. The way of using Velcro to attach OLEs also brings convenience for the OLE's replacement and maintenance.

3. Multi-point Sensing Method for SmartGlove

The multi-point sensing method for SmartGlove is developed based on the inverted design of the OLE (compared to the OLE for SmartSuit [34]) and the five natural arches in human hand. Multiple OLEs chained by a flat strip are placed on the 1st and 2nd knuckles of each finger to measure the flexion of MCP and PIP joints. The multi-point sensing principle is based on the simplified kinematic model so that it can only capture the FE motion of the finger joints now. It is compact in design and is verified to be effective on the SmartGlove. Moreover, the application of the multi-point sensing can be expanded into more areas (such as measuring the curvature of the spine or the deformation of the skin) rather than hand motion capture.

4. Effective Calibration Method

Calibration is critical to the accuracy of hand motion capture because different people come with different hand sizes. In this project, two methods are adopted for the calibration of SmartGlove. One is a commonly used method for roughly calibration. The other method uses a special designed calibration block to calibrate the OLEs one by one for precise calibration. The calibration verification tests show that both methods can improve the accuracy of the result, and the second method proposed in this project is more effective.

8.2. Future Work

Although the basic issues relating to the development of the SmartGlove have been addressed and initially solved, there are still several unexplored aspects in this area.

1. Abduction/Adduction Motion Tracking

In the first prototype, only the flexion/extension movement of the joint is captured. However, as introduced in the hand bio-mechanism, our hand is so highly articulated that only the FE motion cannot produce lifelike simulation of the real whole hand movements. Consequently, the abduction/adduction motion is critical for the vivid whole hand motion capture. Some of the other data gloves can provide the measurement of joint's AA motion using strain gauges (CyberGlove [8]) and fibre optics (ShapeHand [7]). In this project, as the optical mouse sensor ADNS-3530 is capable to do the 2D tracking, it is possible to improve the design of the OLE in order to make it able to measure the AA motion while no additional sensors are adopted.

2. Robustness in Design

Because of the hand's complex structure and deformable skin, a robust design becomes very important, which includes issues like: find a better way to firmly attach the OLEs and straps to the glove so that the influence of skin deformation can be minimized; re-design the strap to increase toughness and reduce friction and kinks. All of these can contribute to increase the robustness of the system, and further increase the accuracy of the measurement.

3. Integration with Other Sensors

Hand motion capture is the major function of the SmartGlove, but will not be the only one because there are a number of other glove products competent for it. The integration with other sensors can enormously expend the usage. For example, add touch sensors on the finger tip to sense the contact between fingers and other objects; apply force sensors to measure the bending force of the finger; use accelerometers to

track the gesture of the palm. Different sensors can be adopted based on different application, which can make our glove-based hand motion capture device exceptional.

4. Packaging Design

Our final goal is to develop a low cost, high performance, glove-based, un-tethered wearable full hand motion capture device with ergonomics and durability. Thus, the aim of packaging design is to make the SmartGlove unit, durable, comfortable to wear, and easy to use. OLEs will be packaged with cloth and still be able to be removed; the microcontroller will be sealed in small box; cables and wires will be hidden; and the glove will be designed easily to wear and remove.

REFERENCES

[1] G. Welch, E. Foxlin, "Motion Tracking: No Silver Bullet, but a Respectable Arsenal," *IEEE Computer Graphics and Applications*, Vol. 22, No. 6, pp. 24-38, 2002.

[2] V. Medved, "Measurement of Human Locomotion", *CRC Press*, 2001

[3] W. Goebl and C. Palmer, "Anticipatory Motion in Piano Performance", *Journal of the Acoustical Society of America*, Vol.120, Issue5, pp.3004, November 2006.

[4] K. Mitobe, T. Kaiga, T. Yukawa, T. Miura, H. Tamamoto, A. Rodger and N. Yoshimura, "Development of a motion capture system for a hand using a magnetic three-dimensional position sensor", *ACM SIGGRAPH Research posters: motion capture and editing*, Boston, Massachusetts, USA, 2006.

[5] Power Glove User Guide, Mattel Inc., September, 2007.

[6] 5DT Data Glove User Manual, Fifth Dimension Technologies, September, 2007.

[7] ShapeHand User Manual, Measurand Inc., September, 2007.

[8] CyberGlove Reference Manual, Immersion Corporation, September, 2007.

[9] Vhand User Guide, DGTech Inc., September, 2007.

[10] HumanGlove User Manual, Humanware S.R.L., May, 2008.

[11] T. Aaron, "A Novel Method for Joint Motion Sensing on a Wearable Computer", *Proceedings of the 2nd International Symposium on Wearable Computers,* pp. 158-159, October, 1998.

[12] N. Karlsson, B. Karlsson and P. Wide, "A Glove Equipped with Finger Flexion Sensors as a Command Generator Used in a Fuzzy Control System", *IEEE Transactions on Instrumentation and Measurement,* Vol.47, Issue 5, pp. 1330–1334, October 1998.

[13] L.H. Jose, K. Nicholas and W.L. Robert, "The AcceleGlove: a Whole-hand Input Device for Virtual Reality", *International Conference on Computer Graphics and Interactive Techniques, ACM SIGGRAPH*, pp.259, San Antonio, Texas, USA, 2002.

[14] T. Alessandro, C. Nicola, Z. Giuseppe and D.R. Danilo, "Characterization of a Movel Data Glove Based on Textile Integrated Sensors", *Proceedings of the 28th IEEE EMBS Annual International Conference.* pp.2510-2513, New York, USA, September 2006.

[15] M.N. Noaman, R.A. Ahmmad and A.I. Aula, "Design and Implementation of DHM Glove Using Variable Resistors Sensors", *Journal of Artificial Intelligence*, Vol.1, Issue 1, pp.44-52, 2008.

[16] D.J. Sturman and D. Zeltzer, "A Survey of Glove Input", *IEEE Computer Graphics & Applications*, Vol.14, Issue 1, pp.30-39, January 1994.

[17] D.L. Quam, "Gesture Recognition with a DataGlove", *Proceedings of the IEEE 1990 National on Aerospace and Electronics Conference,* Vol. 2, pp. 755-760, Dayton, Ohio, USA, 1990

[18] T. Kuroda, Y. Tabata, H. Ikuta and M. Murakami, "Consumer Price Data-glove for Sign Language Recognition", *Proceedings of the 5th International Conference on Disability, Virtual Reality & Assoc. Tech,* pp. 253-258, Oxford, UK, 2004.

[19] Cyber Glove Applications, Immersion Corporation, September, 2007.

[20] Poared Hand Exoskeleton, Department of Computer Science, TU Berlin, March, 2008.

[21] T.G. Zimmerman, J. Lanier, C. Blanchard, S. Bryson, Y. Harvill, "A Hand Gesture Interface Device", *Proceedings of the SIGCHI/GI conference on Human factors in computing systems and graphics interface*, pp. 189-192, Toronto, Ontario, Canada, April 1987.

[22] W.-C. Lam, F. Zou and T. Komura, "Motion Editing with Data Glove", *Proceedings of the ACM SIGCHI International Conference on Advances in computer entertainment technology,* Vol. 74. pp. 337-342, Singapore, 2004.

[23] L. Dipietro, A. M. Sabatini and P. Dario, "Evaluation of an Instrumented Glove for Hand Movement Acquisition", *Journal of Rehabilitation Research and Development,* Vol.40, Issue 2, pp.179-190, March 2003.

[24] Y. Yasumuro, Q. Chen and K. Chihara, "Three-dimensional Modelling of the Human Hand with Motion Constraints", *Image and Vision Computing,* Vol.17, Issue 2, pp. 149-156, February 1999.

[25] Y. Wu and T.S. Huang, "Human Hand Modelling, Analysis and Animation in the Context of HCI", *Proceedings of the International Conference on Image Processing.* Vol.3, pp. 6-10, 1999.

[26] T. Rhee, U. Neumann and J.P. Lewis, "Human Hand Modeling from Surface anatomy", *Proceedings of the 2006 symposium on interactive 3D graphics and games.* pp. 27-34, Redwood City, California, USA, 2006.

[27] W. Ying, T.S. Huang, "Hand Modelling, Analysis and Recognition", *Signal processing magazine, IEEE,* Vol. 18, Issue 3, pp.51-60, May 2001.

[28] J. Lee and T.L. Kunii, "Model-Based Analysis of Hand Posture", *Computer graphics and Applications, IEEE,* Vol.15 Issue 5, pp.77-86, September 1995.

[29] J. Lin, Y. Wu and T.S. Huang, "Modeling the Constraints of Human Hand Motion", *Proceedings of the Workshop on Human Motion, IEEE,* pp. 121-126, Los Alamitos, USA, 2000.

[30] J. J. Kuch and T.S. Huang, "Vision Based Hand Modeling and Tracking for Virtual Teleconferencing and Telecollaboration", *Proceedings of the Fifth International Conference on Computer Vision*, pp. 666-669, 1995.

[31] J. Denavit and R.S. Hartenberg, "A Kinematic Notation for Lower-pair Mechanisms Based on Matrices", *Journal of Applied Mechanics, ASME,* Vol.22, pp.215-221, June 1955.

[32] C.-C. Lien, "A Scalable Model-based Hand Posture Analysis System", *Journal of Machine Vision and Applications*, Vol.16. Issue 3, pp. 157-169, May 2005.

[33] M. Veber and T. Bajd, " Assessment of Human Hand Kinematics", *Proceedings of the 2006 IEEE International Conference on Robotics and Automation*, pp. 2966-2971, Orlando, USA, May 2006.

[34] K. Y. Lim, Y. K. Goh, W. Dong, K. D. Nguyen, I.-M. Chen, S. H. Yeo, H. B. L. Duh, and C. G. Kim, "A Wearable, Self-Calibrating, Wireless Sensor Network for Body Motion Processing", *IEEE International Conference on Robotics and Automation (ICRA 2008)*, pp. 1017-1022, Pasadena, California, May 2008.

[35] H.-L. Yu, R. A. Chase and B. Strauch, "Atlas of Hand Anatomy and Clinical Implications", *Mosby*, 2004.

[36] Datasheet of ADNS-3530, Avago Technologies, November, 2007.

[37] Arduino Diecimila User Guide, Arduino SmartProject, March, 2008.

[38] SPI Block Guide, Freescale Semiconductor, March, 2008

[39] M. Sama, V. Pacella, E. Farella, L. Benini and B. Ricco, "3dID: a Low-power, Low-cost Hand Motion Capture Device", *Proceedings of the conference on Design, automation and test in Europe,* Vol.2, pp.136-141, Munich, Germany, 2006.

[40] M. Fischer, P. Van de Smagt and G. Hirzinger, "Learning techniques in a dataglove based telemanipulation system for the DLR hand", *International Conference on Robotics and Automation*, pp.1603-1608, Leuven, Belgium, 1998.

[41] T.-S. Chou, A. Gadd, D. Knott, "Hand-eye: A Vision Based Approach to Data Glove Calibration", *Proceedings of Human Interface Technology*, 2000.

[42] W.B. Griffin, R.P. Findley, M.L. Turner, M.R. Cutkosky, "Calibration and Mapping of a Human Hand for Dexterous Telemanipulation", *ASME IMECE Conference Haptic Interfaces for Virtual Environments and Teleoperator Systems Symposium*, 2000.

[43] K. Rachid, M. Mounir, M. Marc, "Modeling of the Residual Capability for People with Severe Motor Disabilities: Analysis of Hand Posture", *International conference on user modelling,* Vol.3538, pp.231-235, Ediburgh, 2005.

[44] Datasheet of LIS3LV02DQ, ST Microelectronics, May, 2008

[45] W. Dong, K.Y. Lim, Y.K. Goh, K.D. Nguyen, I.-M. Chen, S.H. Yeo and B.L. Duh, "A Low-cost Motion Tracker and Its Error Analysis", *International Conference on Robotics and Automation*, pp.311-316, 19-23 May 2008.

[46] S. Wise, W. Gardner, E. Sabelman, E. Valainis, Y. Wong, K. Glass, J. Drace and J. Rosen, "Evaluation of a Fiber Optic Glove for Semi-automated Goniometric Measurements", *Journal of Rehabilitation Research and Development,* Vol.*27,* Issue 4, pp.411-24, 1990.

[47] N.W. Williams, J.M.T. Penrose, C.M. Caddy, E. Barnes, D.R. Hose and P. Harley, "A Goniometric Glove for Clinical Hand Assessment", *The Journal of Hand Surgery: Journal of the British Society for Surgery of the Hand,* Vol.25, Issue 2, pp.200-207, April 2000.

[48] L.K. Simone, N. Sundarrajan, X. Luo, Y.C. Jia and D.G. Kamper. "A Low Cost Instrumented Glove for Extended Monitoring and Functional Hand Assessment", *Journal of Neuroscience Methods,* Vol.160, Issue 2, pp.335-348, 2007.

[49] R. Gentner and J. Classen, "Development and Evaluation of a Low-cost Sensor Glove for Assessment of Human Finger Movements in Neurophysiological Settings", *Journal of Neuroscience Methods*, Vol.178, Issue 1, pp.138-147, March 2009.

[50] Koch, G. Gary, "Intraclass correlation coefficient" in "Encyclopedia of Statistical Sciences", S. Kotz and N. L. Johnson, *John Wiley & Sons*, New York, 1982.

Appendix A: OLE Circuit Board Design

Schematics design

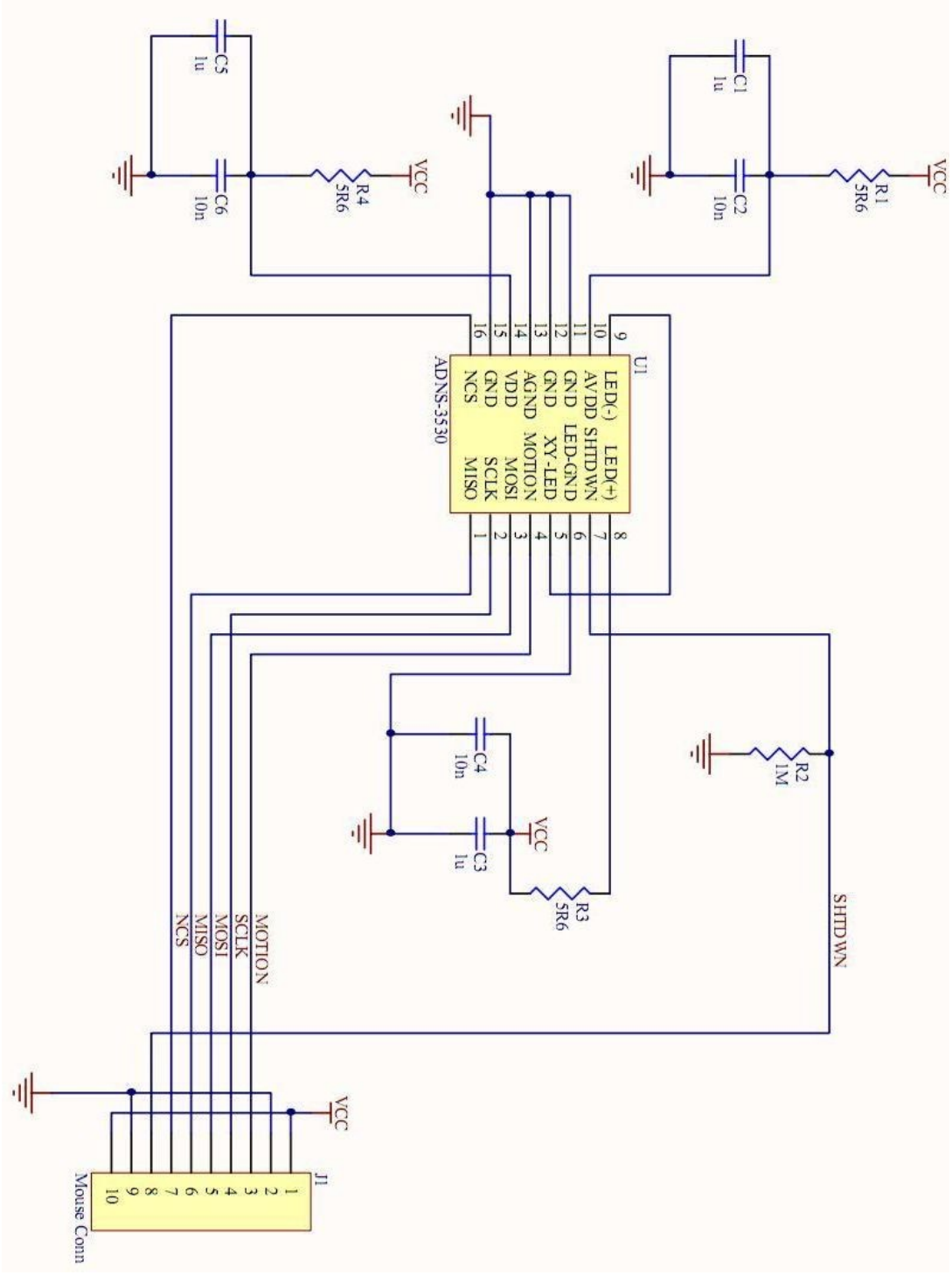

PCB layout

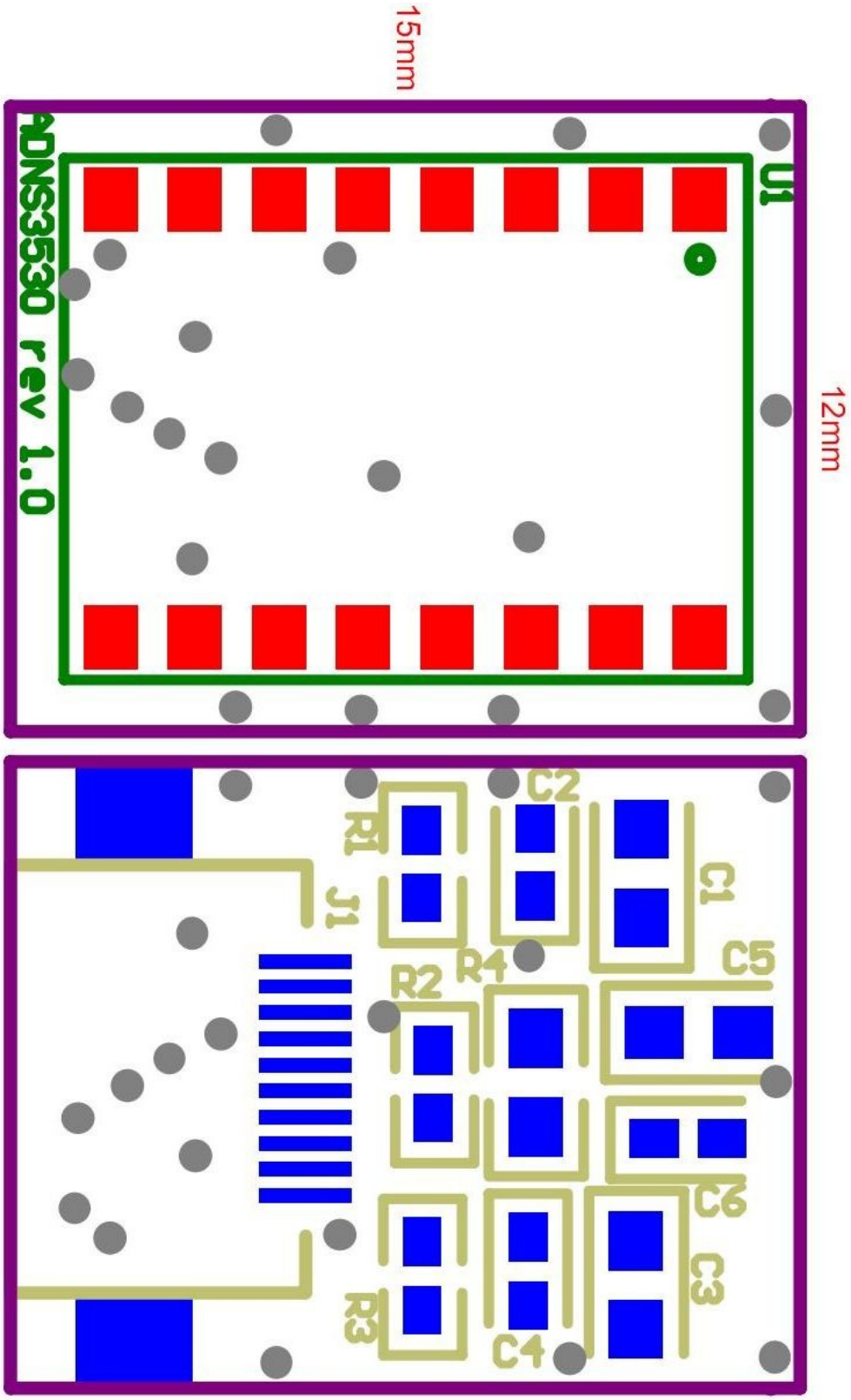

Considerations of PCB assembly

① Surface mount the sensor and all other electrical components into PCB;

② Reflow the entire assembly in a no-wash solder process;

③ Place the lens onto the base plate. Care must be taken to avoid contaminating or staining the lens.

④ Remove the protective kapton tape from optical aperture of the sensor and LED. Care must be taken to keep contaminants from entering the aperture. Recommend not placing the PCB facing up during the entire assembly process and holding the PCB first vertically for the kapton removal process.

⑤ Insert PCB assembly over the lens onto the base plate aligning post to retain PCB assembly. The lens piece has alignment posts to retain PCB assembly. The lens piece has alignment posts which will mate with the alignment holes on the sensor aperture.

⑥ The optical position reference for the PCB is set by the base plate and lens. Note that the PCB motion due to button presses must be minimized to maintain optical alignment.

Appendix B: OLE Housing Design

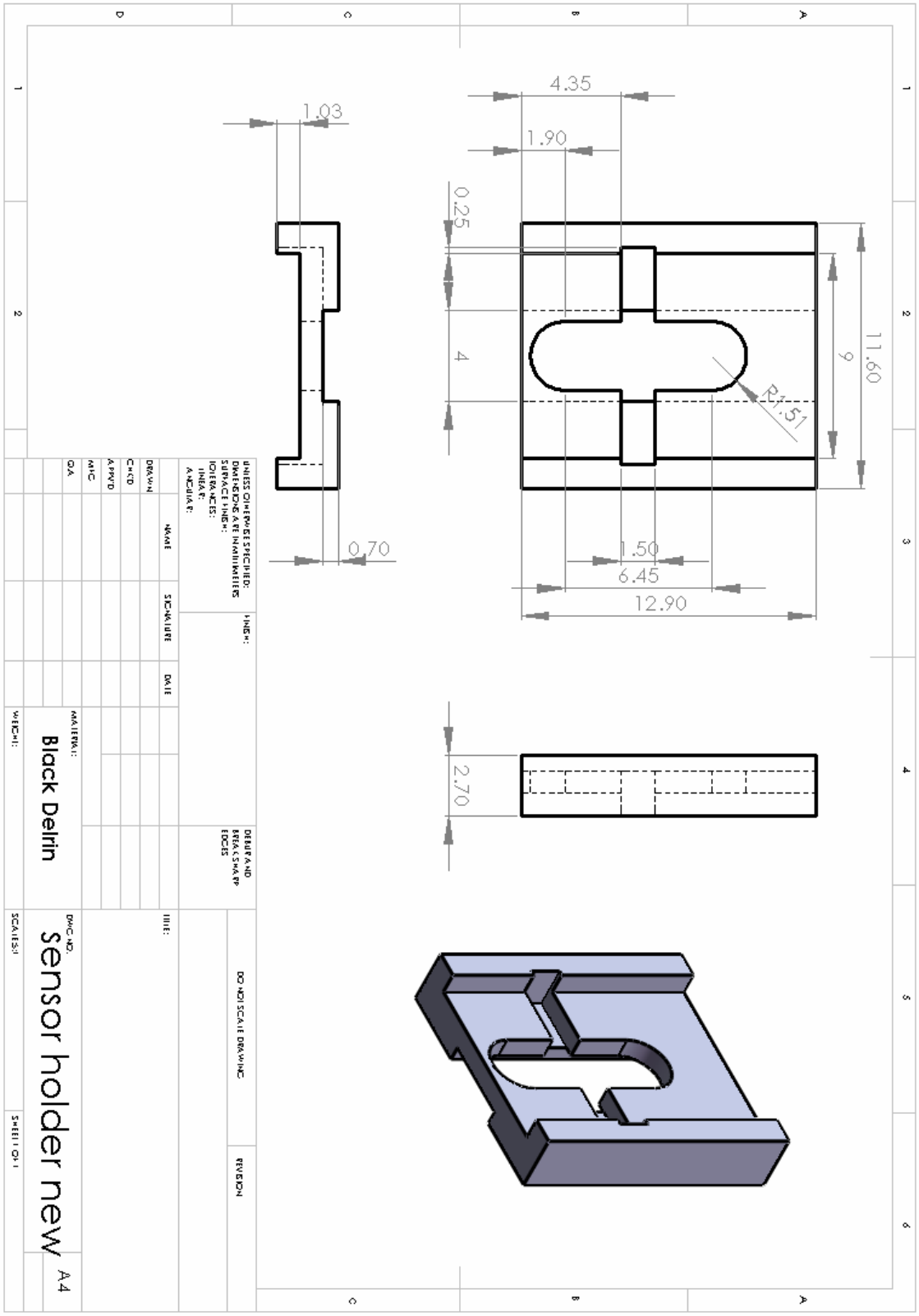

Appendix C: OLE Assembly

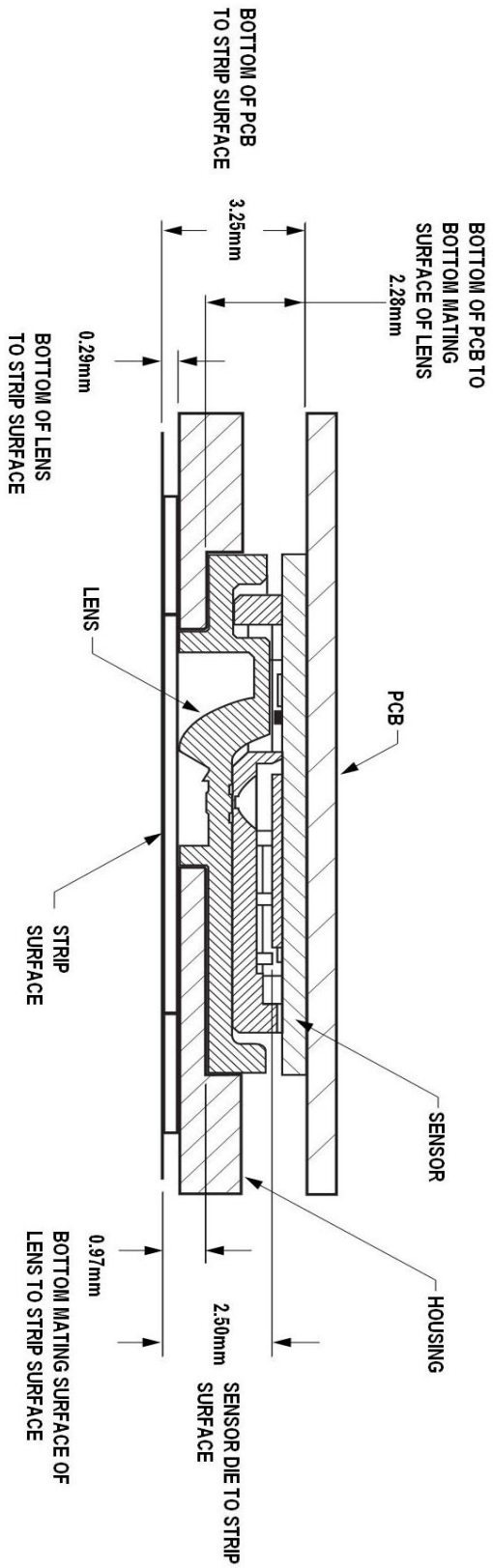

Appendix D: Interface Board Design

Schematics design

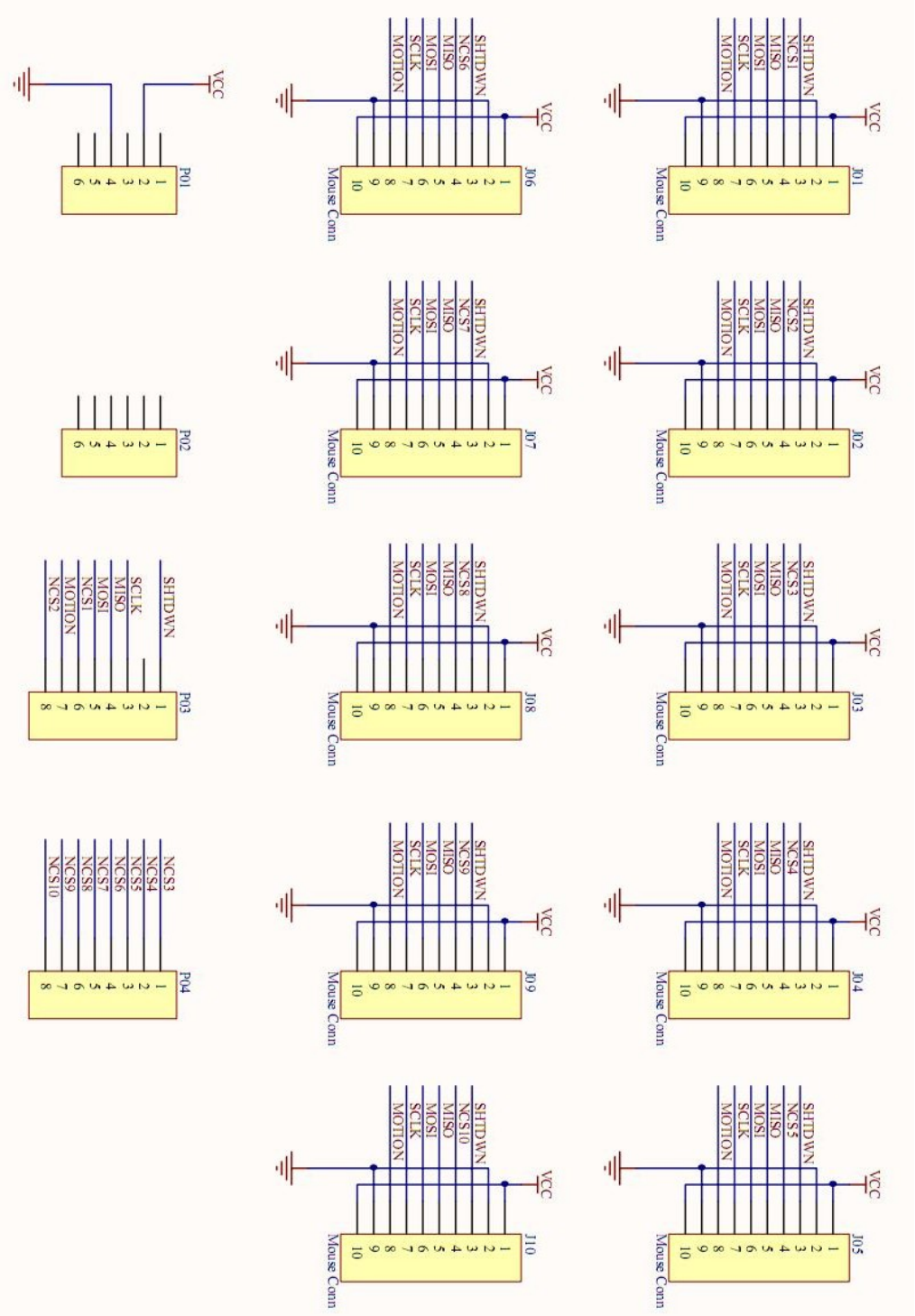

PCB layout

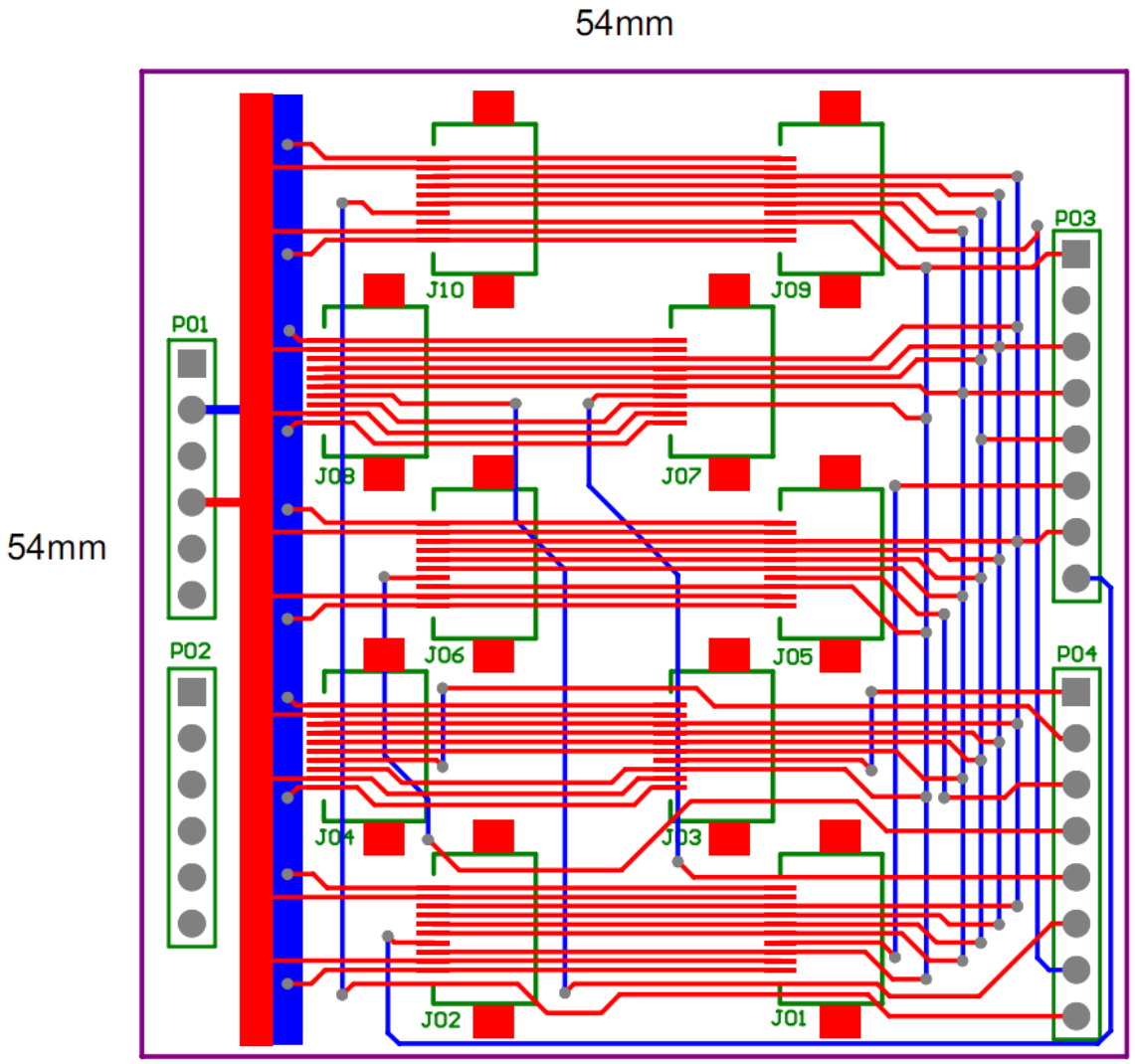

Appendix E: Calibration Block